DYNAMIC ANALYSES OF LOW STRENGTH MASONRY HOUSES BASED ON SITE SPECIFIC EARTHQUAKE GROUND MOTIONS

March 2009

Hari Ram Parajuli

ABSTRACT

Three thrust fault systems which pass throughout the length of Nepal and many small faults near Kathmandu show high seismicity in the region. Available earthquake data is not sufficient to justify the current slip rate of Himalaya. As an alternate approach, magnitude frequency relation is developed using available earthquake data, then taking slope of the fit as constant, other coefficient is calculated considering 50% slip rate which closely satisfies the rate of occurrences of complete big events and small events. A suitable attenuation equation developed for similar tectonic region based on worldwide earthquake data is selected. Two different approaches; one dividing the whole region into small area sources and other using Bayesian approach to combine the occurrences from directly historical earthquake data and digitized faults, are utilized. Assuming the occurrences of earthquakes as Poisson's process, mean rate of exceedences of horizontal ground acceleration and spectral acceleration at various natural periods are obtained. Probabilistic response spectra for two major cities, Kathmandu and Pokhara, corresponding to three return periods are plotted. Significant earthquakes for the two cities are estimated on basis of deaggregation of hazard for peak ground acceleration. Typically, for Pokhara city, significant durations calculated for various distances and magnitudes are multiplied by weights of corresponding deaggregation and weighted average duration for specific return period was estimated. For the city, design earthquake ground motions for three probabilities of exceedences- 40%, 10% and 5% probability of exceedences in 50 years are simulated. Since, there are no records of historical earthquake accelerograms for the region, random waves were generated based on probability density function developed from envelope function for earthquake duration. These waves were modified until the simulated and target spectrums were in good agreement. These earthquake ground motions can be useful for design of new structures and retrofit of existing structures.

In the next part of the study, performances of low strength masonry houses especially stone houses are evaluated through non linear dynamic analyses. Stone masonry houses are the most common type of construction in the Alpine Himalayan Belt across Pakistan, India and Nepal. However, the seismic resistance of these houses is highly questionable if constructed without any form of lateral support. Thus, effectiveness of wooden bond beams as a retrofit solution has been examined. Dry stone masonry houses have been modeled by finite element method considering

stones as linear solid and interfaces as joint elements. The joints are allowed to open and slide satisfying the Mohr-Coulomb criteria. To calibrate the values used in the numerical modeling, an experiment using a small scale wall made of wooden blocks was shaken in small custom made table. The corresponding parameters which showed good agreement with experimental results were taken as inputs for the non linear dynamic analyses of various model houses. The results showed that wooden bond beams can be an effective technique for upgrading low strength masonry houses in low seismicity regions. Thus, two typical types of mud bonded stone masonry houses were modeled by finite element method considering discontinuities between the equivalent stone elements as considered as in dry stone masonry houses. Then, dynamic analyses of those mud bonded stone masonry houses were done under simulated site specific earthquake ground motions. Parameters such as damping and friction were investigated from shaking table tests and the stiffness constants calculated from theoretical formulae. The stiffness constants depend upon the modulus of elasticity of wall and units. The model houses performed very poor even in 98 years return period earthquakes. As a mitigation measure, modified model houses by adding wooden bond beams were run under same earthquake ground motion as they were run before. Analyses show locally available wooden bond beams can be good mitigation measure for houses in low seismicity regions.

ACKNOWLEDGEMENTS

The research was carried out in Department of Urban Management, Graduate School of Engineering, Kyoto University, Japan. I am very grateful to the University. I wish to express my profound gratitude to the members of dissertation committee, namely, Professors Hiroyasu Ohtsu, Junji Kiyono and Akira Igarashi for their invaluable comments and suggestions.

I am extremely grateful to my academic advisor, Professor Junji Kiyono for advising me through my doctoral study and providing me necessary guidance and training to successfully finish my study at Kyoto University. I am very pleased to thank to Professor Charles Scawthorn, former advisor, to encouraging and giving me various advises to work in low strength masonry structures during initial two years of my study. His in-depth knowledge, wide range of experience and sense of humor has been a source of inspiration me.

It has been a great pleasure to work with Dr. Yusuke Ono, Assistant Professor. His continuous and ever-present support contributed significantly to my understanding about the subject matter. My discussion with him have enhanced my understanding of programming and greatly influenced my research work. I thank him very much.

I am very grateful to Mayumi Wada for providing me valuable supports from beginning of my stay in Japan. Without her support my stay would have been very difficult. Thanks to Eri Miyamoto for providing me various helps in administrative procedures.

Thanks to all of the students associated with Earthquake Disaster Prevention Systems Lab. The academic environment and friendliness among students played a big role in my productivity and enjoyment. I also thank to all of the students, staff and faculty of Structural Dynamics and Dynamics of Foundation and Structures lab. In particular, Masaaki Kobayashi, Yuu Sigetomi and Fumiko Taya have provided valuable support to do experiments.

I also thank to Professors Prem Nath Maskey and Hikmat Raj Joshi, Institute of Engineering, Tribhuwan University, Nepal, for encouraging for the study. I am very grateful to Emily So, Director, Cambridge, United Kingdom.

Table of Contents

List of Figures

List of Tables

Chapter 1

INTRODUCTION

1.1 Background

Masonry is the oldest construction material in the history of mankind. It has been used in various forms of construction materials for residential and public buildings for the past several thousand years. Adobe or mud masonry, unreinforced masonry and stone masonry are the typical types of vernacular masonry houses and are spread all over the world. They are very weak to take lateral forces and termed as low strength masonry (LSM). LSM is one the most important and widely used type of construction materials and is expected to continue to provide housing in rural areas because of its inherent advantages such as aesthetics, architectural appearances, effective heat and sound insulation, and fire resistances. Moreover, masonry materials are locally available and economical also, which has made them as prime construction material. There is large inventory of LSM buildings in the world. Most of them were built a little or no seismic loading requirements, and are not capable of dissipating energy through inelastic deformation during earthquakes and thus, they have been the prime cause of claming lives during earthquakes. Although they are recognized to be very weak and seismically vulnerable, strengthening of these houses is very difficult task due to various reasons such as diversities in construction and cost of strengthening.

Frequent natural disasters are major issues for development progress in developing countries such as Nepal and its neighbors. Out of many disasters, earthquakes have been the major cause of deaths and destructions. Despite, there is rising construction of houses by steel and concrete in urban areas, LSM is the most important construction in rural and periphery of urban area of Nepal. Two thirds of its population is living in masonry houses. It has been used for past several thousand years. Great numbers of national heritage structures such as temples and royal palaces had made of LSM and some of them have survived in past earthquakes also. However, some specific features have been invented during the course of time that improve the seismic behaviour of masonry buildings such as appropriate layout of masonry units, efficient planning of rooms and walls in the buildings etc., masonry constructions, today, remains most vulnerable part of building stocks

(Tomazevic 1999). Discontinuities present in the masonry wall substantially decrease the wall strength, start cracking through joints and make them very vulnerable to earthquakes.

In the last few decades, significant researches on the behaviour of masonry walls and buildings subjected to earthquake loads have been carried out in many countries. Use of high strength mortar, added reinforcements, improved detailing, introduction of anchorages between floors, roofs and corners of walls are common methods to increase the strength of walls and buildings. Beside these techniques, recently, various types of fiber reinforced polymers (FRP) and polypropylene (PP) bands in different patterns and base isolation method have been investigated as good strengthening techniques. Majority of LSM houses stack are in rural areas of the world. They have been shelter of poor people. On the one hand, people can not afford expensive material and on the other hand, costs of retrofitting material would be even more than the cost of original house. Locally available material might be cheap but might not withstand the design load. So choosing appropriate material is also a difficult. On the basis of local availability various materials like bamboo, burlap, rice and wheat straw, plastic sheets, steel rods and wires, rubber, polypropylene bands and fiber reinforced polymer have been used for strengthening the masonry structures in the form of strip, grids and fabrics. Strengthening of these houses is not impossible; however, economical solution is most important issue.

1.2 Objective of the study

Overall objective of this study is to suggest cost effective measure for upgrading of LSM houses. Particularly here, stone masonry houses built in Nepal and its neighbors are focused. It requires dynamic analysis of these houses giving earthquake ground motions as input. Thus, input motions are simulated for Nepal. Applying these simulated ground motions, effectiveness of locally available wooden bond beams are investigated as cost effective solution. The specific objectives are

i. Seismic hazard analysis
ii. Simulation of design earthquakes
iii. Formulation of numerical model for LSM houses
iv. Evaluation of effectives wood bond beams in LSM houses
v. Identification of most economical solution

1.3 Outline

The introductory chapter, Chapter 1, mentions the importance and objectives of the study. The overall study includes two parts; seismic input simulation and application of simulated seismic input for evaluation of LSM houses. Former includes chapters 2 and 3, and later includes chapters 4 -6. In chapter 2, detailed seismic hazard analyses for Kathmandu city has been carried out. Short coming of past estimate has been pointed out. Three different components faults, historical earthquakes and intra-plate slip dominating the hazard will be employed by kernel estimation techniques. The hazard estimation method developed for Katmandu is applied for whole country. For two major cities, Kathmandu and Pokhara, peak ground acceleration has been deaggregated and significant earthquakes are identified. In chapter 3, design earthquake ground motions for three different probabilities of exceedences are simulated for Pokhara city.

In chapter 4, general overviews about historical characteristics and methodologies of strengthening techniques are summarized. Various methods regarding numerical and experimental which were employed in the past for enhancing LSM houses have been described. In chapter 5, numerical methodology to analyze LSM is formulated and effectiveness of wooden bond beams is evaluated. In chapter 6, two typical types of Nepalese houses are evaluated applying site specific earthquakes ground motions simulated in chapter 3. Application of wooden bond beams for mitigation is concluded as cost effective solution. At last, summary and conclusion of overall work are presented in chapter 7.

Chapter 2

SEISMIC HAZARD ASSESSMENT

2.1 Introduction

Estimation of seismic intensity consist of collection of historical earthquake data, allocation of earthquake data into the faults, development of magnitude frequency relationship, estimation of mean rate of exceedences of specified value of hazard and calculation of acceleration for certain probability of exceedences in specified period. Since Cornell (1968), probabilistic seismic hazard analysis has been well known and widely accepted tool for estimating hazard. Poisson recurrence model and ground motion attenuation equations are coupled to estimate expected ground motion exceedences. To estimate the hazard, Kathmandu city of Himalayan country Nepal has been taken.

Kathmandu is the capital city of Nepal and lies in the Himalayan range, one of the most visible consequences of plate tectonics (Molnar 1984). Running east to west throughout the length of Nepal (Fig. 2.1) are three fault systems, Main Central Thrust (MCT), Main Boundary Thrust (MBT) and Himalayan Frontal Thrust (HFT), as well as many smaller faults (Fig. 2.2). Kathmandu is located in the Lesser Himalayan region in between MBT and MCT (Fig. 2.1). Most of these faults might have formed during the past 10 million years and lie at the interface of the Indian and Tibetan plates. The convergence of these two plates has resulted many earthquakes larger than moment magnitude M8 (Molnar, 1984, Ambraseys and Douglas, 2004; hereafter M stands for moment magnitude unless stated otherwise). Three earthquakes, in 1833 with M7.7 (Bilham 1995), in 1934 with M8.1 (Molnar 1984 and Ambraseys and Douglas 2004) and in 1988 with M6.6 (BECA 1993) have been observed in the vicinity of Kathmandu, which have caused significant death and destruction.

All of the faults identified in the Seismic Hazard Mapping and Risk Assessment of Nepal (BECA, 1993) were formed in the early Tertiary period whereas historical earthquake records exist for only a short recent period of time. Estimation of the seismic intensity based on limited earthquake data over a very short period of time as compared to the tectonic history is a difficult task. In this study, seismic hazard is estimated using two approaches, one fully probabilistic method

which divides the study area into small area sources, and the other taking directly available earthquake data and faults, details of which are described latter.

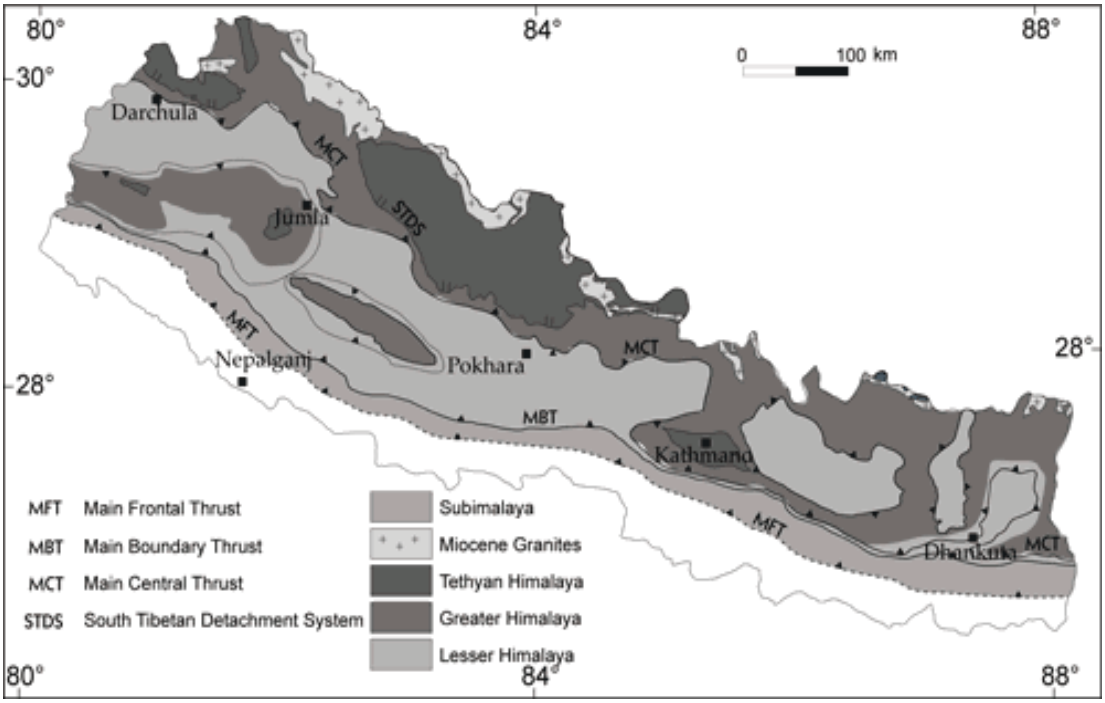

Fig. 2.1a. Geological map of Nepal

(Source: http://www.geocities.com/geologyofnepal/geology.html)

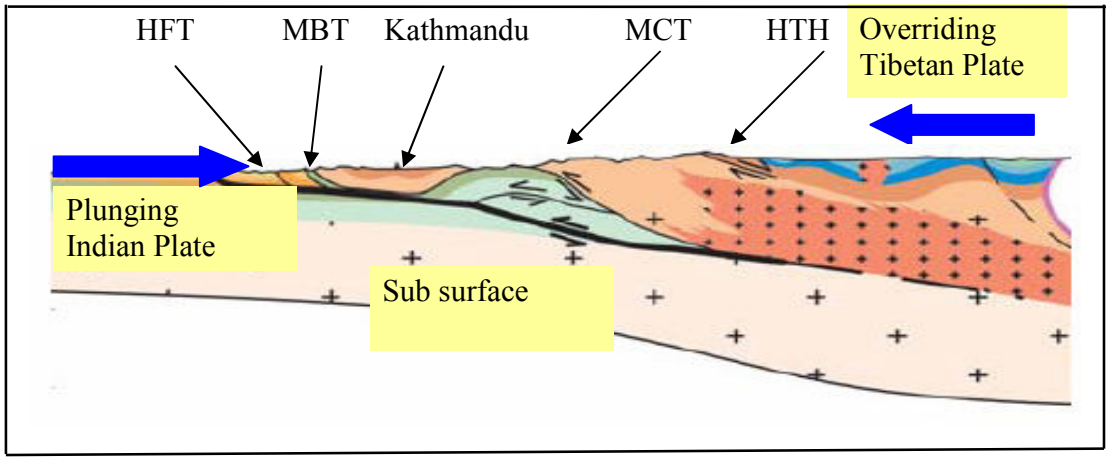

Fig. 2.1b. North-South cross section of Nepal through Kathmandu showing depth and faulting systems (after Avouac, J.P. 2003)

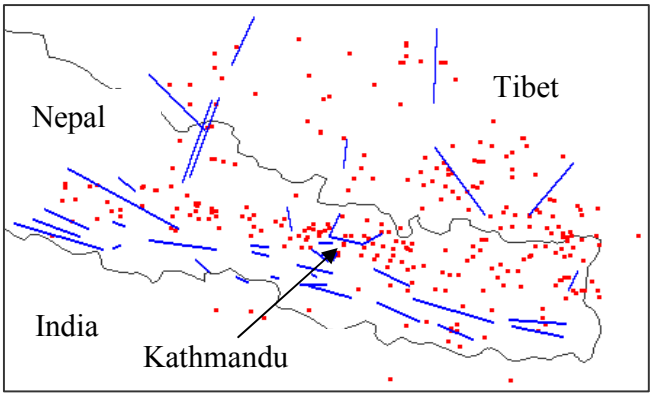

Fig. 2.2 Faults (line) and historical earthquakes (points) around Kathmandu

2.2 Review of regional hazard estimate

Various investigators have addressed the problem of estimating the seismic hazard in the Himalayan region. Seismicity map were produced for the Indian subcontinent (Imtiyaz and Avadh 1999) dividing it into various regions, considering four different occurrence models (Lognormal, Weibull, Gamma and Exponential) to estimate the future probability of earthquakes with magnitude M6-M7. A seismic hazard mapping has been performed (Nath et al 2005) of the Sikkim (India) Himalaya, a sector of the greater Himalaya between eastern Nepal and Bhutan in Sikkim, in terms of peak horizontal acceleration, and scenario earthquakes have been identified for 10% probability of exceedance in 50 years. Das et al. (2006) developed an attenuation law to estimate spectral velocity using records obtained from major Indian earthquakes. Probabilistic seismic hazard estimation of peninsular India (Jaiswal and Sinha 2007) has been performed considering four different types of seismicity (uniform seismicity, geo-based seismicity, reservoir induced seismicity and background seismicity) assigning different weights to each. Hazard curves and risk consistent response spectra were obtained (Maskey and Datta 2004) for a typical location in the Kathmandu valley. Free field peak ground acceleration was obtained considering the soil non linearity. As a part of the preparation of a building code, seismic hazard mapping and risk assessment for Nepal (BECA 1993) was performed, which is the most specific document addressing the hazard situation of Nepal. The BECA study identified 92 faults within and around Nepal. The whole area was divided into three sub zones depending on seismicity obtained from available data, although details are not provided on how the earthquake data were considered. Seismic hazard was then assessed

considering both historical data and assigned characteristic earthquakes after subdividing Nepal into 21 small zones. They assigned different magnitude frequency relations to the 92 identified faults, though details are not provided. BECA further divided the whole study area into small area sources, assigning different maximum magnitudes for each region, although no area had a maximum magnitude greater than M8, whereas three earthquakes larger than M8 have occurred (one of which is included in their catalogue).

Three major earthquakes with magnitude greater than M8 have occurred in the periphery of Kathmandu since 1100AD. The current accumulated slip deficit also shows that a great quake might be overdue. The 1934 Nepal-Bihar M8.1 earthquake claimed 10,700 lives (USGS) in Nepal and India. Since that time, the population has doubled, and the construction of low quality building has substantially added to the vulnerable stock of existing masonry structures. The damages and deaths caused by the Pakistan earthquake (Naeem at al. 2005) are sufficient to imagine a future scenario of damage if a similar quake strikes Nepal.

2.3 Attenuation of ground motion

Prediction of ground motion plays an important role in assessment of seismic hazard. In the past decades, important progress in ground motion estimation has been made in seismological and engineering fields. Attenuation relations are empirically developed by regression analyses. Ground motion attenuation relations can generally be categorized into four groups, shallow crustal earthquakes in active regions (Campbell 1997, Campbell and Bozorgnia 2003, Abrahamson and Silva 1997 and Boore et al 1997), shallow crustal earthquakes in stable regions (Campbell 2003 and Atkinson and Boore 1997), subduction zones (Crouse 1991 Young et al. 1997 and Molas and Yamazaki 1995), and extensional tectonic regimes (Spudich et al. 1997). Because no earthquake attenuation relations have been developed specific to the Himalayan region, we employ an attenuation equation already developed for tectonics, geology and faulting systems similar to the Himalaya region. Mishra (2004) did a comparative study regarding the suitability of attenuation equations for the Himalaya. He collected many attenuation equations including the attenuation equations used in BECA 1993, calculated the hazard, compared the results with the intensity recorded in 1934 M8.1 Nepal-Bihar earthquake and found the Youngs et al. (1997) and Crouse (1991) relations were the most suitable for Nepal. These attenuation equations are for subduction

zones which could be applicable in Himalayan region where the Indian subcontinent plunges beneath the Eurasian-Tibetan subcontinent. Atkinson and Boore (2003) extended the databases of both Youngs and Crouse, added recent earthquakes data from Japan through 2001, forming a subduction zone event database four times larger, and developed a new ground motion relation. As the Atkinson and Boore (2003) equation is the most recent, and includes all types of earthquakes, it is selected for this study. The functional form of their equation is given by

$$\log Y = c_1 + c_2 M + c_3 h + c_4 R - g \log R + c_5 slS_C + c_6 slS_D + c_7 slS_E \quad 2.1$$

$$R = \sqrt{D_{fault}^2 + \Delta^2} \quad 2.2$$

$$\Delta = 0.00724 * 10^{0.507M} \quad 2.3$$

$$g = 10^{(1.2-0.18M)} \text{ for interface events} \quad 2.4a$$

$$g = 10^{(0.301-0.01M)} \text{ for in-slab events} \quad 2.4b$$

where, Y is peak horizontal acceleration (gal), M is moment magnitude, h is focal depth (km) and D_{fault} closest distance to fault surface (km), Δ is near surface saturation factor which accounts for fault geometry, c_1-c_7 are coefficients and sl is factor for amplification corresponds to soil types, S_C, S_D and S_E (NEHRP classification, Dobry et al. 2000) are the factor equal to 1 for desired soil condition and 0 for others. The coefficients (c_1-c_7) are different for interface and in-slab events. In order to identify the event type, all historical data and faults are plotted (Fig.2.2). All the events around the normal faults in Higher Tibetan Himalayas are taken as in-slab events and these normal faults are taken to generate in-slab events. Other events correspond to the thrust faulting (MFT, MBT, MCT) region, and thrust mechanisms are assumed to represent in-slab events if the events occur at depths greater than 50 km. This study combines the occurrences of earthquakes from both fault models and direct earthquake data. Because it is not possible to predict at what depth the next earthquakes will occur, a magnitude dependent depth value delta (Δ) is assumed in the analysis.

2.4 Historical seismicity and intra-plate slip

All historical earthquake data within 300 km radius including events since 1100 to 2006 have been collected by merging data from U.S. Geological Survey, National earthquake Information Centre (NEIC), BECA, 1993, Ambraseys and Douglas (2004) and Lave et.al (2005). Because the earthquake data have been reported in different magnitudes and intensity scales, all data were

converted to moment magnitude (Hank and Kanamori, 1979) using various relationships (McGuire, 2004) and scaling relationship for Himalayan region (Ambraseys and Douglas, 2004). The total 197earthquake events with magnitude greater than M4 are grouped as shown in table 2.1. The data are not uniformly distributed temporally, with only a few records for early periods. Analysis for temporal completeness was performed (Stepp, 1972), with events grouped into small intervals of time. If k_1, k_2, k_3, …k_n, are the number of quakes per unit time interval, then an unbiased estimate of the mean rate of earthquakes per unit time interval of the sample exceeding each magnitude is given by Eq. 2.5.

$$rate_M = \frac{1}{n}\sum_{i=1}^{n} k_i \qquad 2.5$$

Table 2.1. Arrangement of earthquake events

Year		Magnitude					Total events
Start	End	4.0-4.9	5.0-5.9	6.0-6.9	7.0-7.9	8.0-8.9	
1100	1931	1	2	5	5	2	**15**
1932	1936	1	2	1	1	1	**6**
1937	1941		2				**2**
1942	1946		1				**1**
1947	1951		1				**1**
1952	1956		4	2			**6**
1957	1961		2				**2**
1962	1966	7	5	1			**13**
1967	1971	11	3	1			**15**
1972	1976	13	3				**16**
1977	1981	12					**12**
1982	1986	14					**14**
1987	1991	29	2	1			**32**
1992	1996	19	1	1			**21**
1997	2001	23	2				**25**
2002	2006	16					**16**
Total events		**146**	**30**	**12**	**6**	**3**	**197**

The rate of earthquakes exceeding each magnitude using Eq.2.5 are calculated (Table 2.2) and plotted in semi log scale (Fig.2.3). The magnitude frequency relationship is represented by Eq. 2.6.

Table 2.2 Rearrangement of earthquakes for estimating annual rate (end year 2006)

Year		M4		M5		Year		M6		M7		M8	
Start	T	N	N/T	N	N/T	Start	T	N	N/T	N	N/T	N	N/T
2002	5	16	3.20	0	0.00	1957	50	4	0.08	0	0.000	0	0.000
1997	10	41	4.10	2	0.20	1907	100	9	0.09	2	0.020	1	0.010
1992	15	62	4.13	4	0.27	1857	150	10	0.07	2	0.013	1	0.007
1987	20	94	4.70	7	0.35	1807	200	16	0.08	5	0.025	1	0.005
1982	25	108	4.32	7	0.28	1757	250	16	0.06	5	0.020	1	0.004
1977	30	120	4.00	7	0.23	1707	300	16	0.05	5	0.017	1	0.003
1972	35	136	3.89	10	0.29	1657	350	17	0.05	5	0.014	1	0.003
1967	40	151	3.78	15	0.38	1607	400			5	0.013	1	0.003
1962	45	164	3.64	22	0.49	1557	450			5	0.011	1	0.002
1957	50			24	0.48	1507	500			5	0.010	1	0.002
1952	55			30	0.55	1457	550			6	0.011	2	0.004
1947	60			31	0.52	1407	600			6	0.010	2	0.003
1942	65			32	0.49	1357	650			7	0.011	2	0.003
1937	70			34	0.49	1307	700			7	0.010	2	0.003
1932	75			37	0.49	1255	752			8	0.011	2	0.003
						1205	802					2	0.002
						1155	852					2	0.002
						1100	906					3	0.003
Rate			3.97		0.37	Rate			0.069		0.013		0.003

$$Log(N/Y) = 3.47 - 0.76M \qquad 2.6$$

The slope of magnitude frequency relationship (Eq.2.6) is lower than 1 and shows high rate of occurrences of larger magnitude earthquakes. Though historical earthquakes in Nepal have been documented since 1100 AD, various researchers (Bilham et al 2007, Feldl and Bilham 2006, Bilham and Ambrasseys 2005, and Jouanne et al. 2004) have pointed out that an intra-plate slip

deficit exists in the Himalayan region. The slip velocity between India and southern Tibet as measured by GPS measurement is 16-18 mm/year (Bilham et al. 1997) and the slip velocity of central and eastern Nepal is 19mm/year (Jouanne et al. 2004). The slip rate estimate (Bilham and Ambraseys 2005) based on 500 years of earthquake data accounts for only one third of the total seismic rate of the region, and the remaining slip deficit is equivalent to five earthquakes greater than M8.5.

The question therefore arises of whether this fit is sufficient to represent the seismicity of the region when a large slip deficit exists and the faults are sufficiently mature to sustain renewed rupture (Feldl and Bilham 2006) – effectively, there is the possibility of a mega thrust event with 600km by 80km rupture area and more than 9m slip (Bilham and Ambraseys 2005). Slip rate ($\dot{s}$) can be obtained from moment rate ($\dot{M}_0$), shear modulus (μ) and fault area (A_f) using equations 2.7-2.11 (McGuire 2004).

$$\dot{s} = \frac{\dot{M}_0}{\mu A_f} \tag{2.7}$$

$$\dot{M}_0 = \frac{\nu_{M_{\min}} k\beta \exp\left[\beta\left(M_{\min} + 16.05/1.5\right)\right]}{\gamma - \beta}\left(M_{0_{\max}}^{1-\beta/\gamma} - M_{0_{\min}}^{1-\beta/\gamma}\right) \tag{2.8}$$

$$k = \left[1 - e^{-\beta(M_{\max} - M_{\min})}\right]^{-1} \tag{2.9}$$

$$\nu_{M_{\min}} = 10^{(a - bM_{\min})} \tag{2.10}$$

Where $\gamma = 3.454$ and $\beta = 2.303b$, and $M_{0_{\max}}$ and $M_{0_{\min}}$ are maximum and minimum moments corresponding to maximum and minimum magnitudes, calculated using Eq. 2.11 (Hank and Kanamori, 1979).

$$\log_{10} M_0 = 1.5M + 16.05 \tag{2.11}$$

Considering the lower threshold magnitude M5 and maximum magnitude M8.8 (Lave et al 2005), fault area 600km by 80km, a and b (coefficients) values from Eq. 2.6 and μ=3.3E11dyne/cm^2, the slip rate is 37% of total slip (1.9cm/year). Alternative explanations are possible for the apparent contradiction between observed data and slip velocity. Earthquake data may be missing, the magnitude value of the events may have been underestimated, the slip may be aseismic creep, or the current study period may not be long enough compared to the recurrence rate of great earthquakes.

Efforts have been made to find missing data – for example, recently an earthquake in 1100 AD has been identified in eastern part of Nepal (Lave et al 2005) and another one in Garhwal Himalaya (Kumar et al 2006).

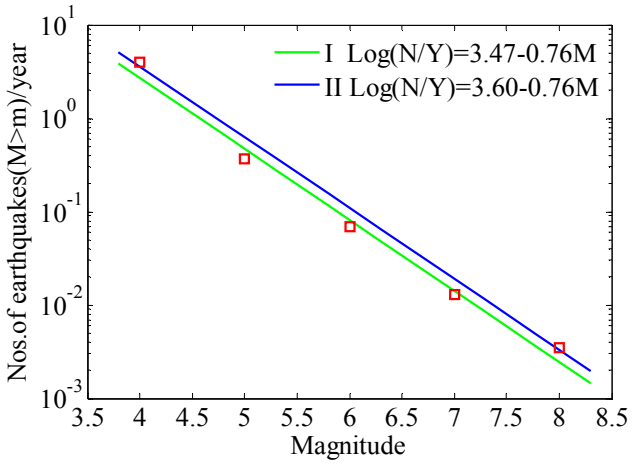

Fig. 2.3, Magnitude frequency relationship

Observing Eq. 2.6, slip depends upon a, b values, area of fault and maximum magnitude. The main shortcoming of this magnitude frequency fit is that it is based on relatively few data. However, earthquake data are almost complete at magnitude M4, and the period of study since 1100 AD may not be sufficient for events greater than M8. As three earthquakes greater than M8 have been identified and the return period for these events is nearly 500 years (Feldl and Bilham, 2006), the seismic hazard assessment should be based on the rates of these events. In that sense, considering the slope (b value) of the magnitude frequency relation and maximum magnitude are constant, and taking the same area as Bilham and Ambraseys (2005), an increased slip rate to 50% yields a (coefficient of magnitude frequency relation) value of 3.60, which closely matches the rate of occurrence of events greater than M8 and complete M4 (Fig. 2.3, blue line), so that the magnitude frequency relation can be represented by Eq. 2.12.

$$Log(N/Y) = 3.60 - 0.76M \qquad 2.12$$

A seismic hazard analysis for the region (BECA 1993) also assumes some data "A review of the tectonics of the Himalayan arc, developed for the project, and the historic seismicity recurrence data for the entire Nepal study region suggests that the total rate of earthquake activity for the Nepal study region may be in the order of 500 M6 or greater earthquakes per 1000 years", however, details are not well explained. Though adding or subtracting a fixed number of data is difficult to

justify, that hazard analysis (BECA 1993) also agrees that current historical data are insufficient and an alternate method should be sought for better estimation of the hazard. Thus, this study presents two hazard estimates using Eqs. 2.6, and 2.12, and discusses the difference in the results.

2.5 Seismic hazard estimate methods

To estimate the seismic hazard of Kathmandu, two different approaches are employed; one is a fully probabilistic seismic hazard analysis dividing the whole study area into small area sources, while the other combines historical earthquake data and the maximum magnitude of faults.

2.5.1 Approach I: Probabilistic seismic hazard assessment (PSHA)

Seismic hazard curves can be obtained for individual source zones and combined to estimate the total hazard at a particular site. Let N_s be the numbers of sources in the region, then the total average exceedance rate (Kramer 1996) for the region is given by Eq. 2.13.

$$\nu_{y^*} = \sum_{i=1}^{N_s} \nu_{i_{M\min}} \int\int P\left[Y > y^* \mid m, r\right] f_{Mi}(m) f_{Ri}(r) dm dr \qquad 2.13$$

Where, $\nu_{i_{M\min}} = \exp(\alpha_i - \beta_i m_{\min})$ is the total rate of exceedence of the threshold magnitude (M=5.0 is taken in this study), with $\alpha = 2.303a, \beta = 2.303b$. $P\left[Y > y^* \mid m, r\right]$ is the conditional probability that the chosen acceleration is exceeded for a given magnitude (M) and distance (R), and $f_{Mi}(m)$ and $f_{Ri}(r)$ are probability density functions for magnitude and distance respectively. The probability density function for the Gutenberg-Richter law with lower and upper bound magnitude is expressed in Eq. 2.14.

$$f_M(m) = \frac{\beta \exp\left[-\beta(m - m_{\min})\right]}{1 - \exp\left[-\beta(m_{\max} - m_{\min})\right]} \qquad 2.14$$

An area of 600 km by 600 km around Kathmandu (27.7N, 85.2E) is divided into 120 by 120 cells. Distances between center of cells and the site are calculated. The recurrence equation is applicable for the whole region, but the earthquake data are not uniformly distributed over the entire area (Fig. 2.2). A higher concentration exists in the narrow zone along MCT, MBT than Tibetan Himalayan and the lowest concentration is in the southern alluvium. Thus, separate earthquake densities for each cell are considered using Kernel estimation methods (Woo 1996). The mean activity

rate $\lambda(m,x)$, at a cell *x* is taken as a kernel estimation sum considering the contribution of N events, inversely weighted by its effective return period which satisfies the condition (Eq. 2.15), can be obtained from equations 2.16-2.18.

$$r \le h(m_j) \tag{2.15}$$

$$\lambda(m,x)_i = \sum_{j=1}^{N} \frac{K(m_j, r_j)}{T(r_j)} \tag{2.16}$$

$$K(m,r)_j = \left[\frac{D}{2\pi h(m_j)}\right]\left\{\frac{h(m_j)}{r_j}\right\}^{2-D} \tag{2.17}$$

$$h(m_j) = H\exp(Cm_j) \tag{2.18}$$

where, $K(m,x)$ is a kernel function, $T(r)$ is the return period of the event located at distance from *r*, $h(m)$ is the kernel band width scaling parameter shorter for smaller magnitude and vice vice-versa, which may be regarded as fault length (Chen et. al. 1998) and *D* is a fractal dimension, taken as 1.7. *H* and *C* are constants equal to 1.45 and 0.64 respectively. From Fig. 2.2, we can see that the distribution of earthquakes is not only uneven but no data exists near some faults. The faults are geological evidence of sources of earthquakes even though earthquakes may not have occurred in the short time span of the available data. The activity rate may be based partly on geological and partly on historical data (Woo 1996) and are calculated considering all earthquake data and considering the maximum magnitude of small digitized faults (Table 3.3) at the centre of its length. Now, the density of each cell is calculated from Eq. 2.19.

$$\rho_i = \frac{\lambda(m,x)_i}{\sum_{i=1}^{N_s} \lambda(m,x)_i} \tag{2.19}$$

Magnitude is divided into 0.5M and distance into 5 km intervals. N_m and N_r are the total numbers of magnitude and distance bins and the mean rate of occurrence can be obtained by Eq. 2.20.

$$\nu_{y^*} = \sum_{i=1}^{N_s}\sum_{j=1}^{N_r}\sum_{k=1}^{N_m} \nu_{i_{M\min}} \rho_i P[Y > y^* \mid m,r] P[M = m] P[R = r] \Delta m \Delta r \tag{2.20}$$

Using the Atkinson and Boore (2003) attenuation equation, peak ground acceleration and coefficients at various natural periods for spectral acceleration are obtained and plotted (Figs. 2.5 and 2.6)

2.5.2 Approach II: Combination of historical data and faults

In this method the mean rate of exceedences for each accelerations are calculated from historical data directly, and from ratio of moment rate and maximum moment of fault, and are combined using a Bayesian approach.

2.5.2.1 Historical data

Considering N_h historical earthquake, the occurrence rate over period of T years in a region is defined as in Eq. 2.21 (Toki et al 1991, Kiyono and Sato 1991, and Portugal et al. 1995):

$$\nu_h = P\left(Y > y^*\right)\nu_h' \qquad 2.21$$

where, $P\left(Y > y^*\right)$ is the probability of occurrence of acceleration Y exceeding specified value of acceleration y^* at the site, found from an attenuation relation, and ν_h' is the average rate of earthquake occurrence in that region, found from the number of historical earthquake events dividing by the occurrence time interval of these events (Eqs. 2.6 and 2.12). The probability of exceedance of acceleration Y over y^* given specific magnitude, M_i and distance, R_i over a certain period of time due to the i^{th} event and summing over all events, the rate of occurrence can be obtained by Eq. 2.22.

$$\nu_h = \sum_{i=1}^{N_h} \frac{P_i\left(Y > y^*\right)}{N_h} x \nu_h' \qquad 2.22$$

2.5.2.2 Fault data

All faults (Table 2.3) within 300 km radius from the site (BECA 1993), have been considered for the study. The 'U' shaped fault (Gosaikunda) is digitized into three linear faults. A total of forty six linear faults have been considered. The rate (ν_{fi}) of earthquake occurrence from the faults based on maximum magnitude model (Wesnousky et al. 1983) is the ratio of moment rate to the maximum moment of geologically permissible earthquake on the fault (Eq. 2.23).

$$\nu_{fi} = \frac{\dot{M}_0}{M_0^{\max}} = \frac{\mu A_f \dot{s}}{M_0^{\max}} \qquad 2.23$$

The fault rupture area (A_f) and maximum magnitude (M_{max}) are calculated from the Wells and Coppersmith (1994) empirical relationship. Slip rate ($\dot{s}$), a fraction (37% and 50%) of the 19mm/year is distributed to all faults considering the maximum magnitude and density of

earthquakes near the faults using the kernel estimation method explained above. Maximum moment ($M_0^{\max}$) is calculated using Eq. 2.11. Earthquake occurrence rate ($\hat{\nu}_{fi}$) of i[th] fault with an acceleration Y which exceeds specified level of acceleration y^* can be written as the conditional probability of occurrence $P\left(Y > y^* \mid M_i, R_i\right)$ given M_i and distance R_i multiplied by occurrence rate (ν_{fi}) (Toki et al. 1991 and, Kiyono and Sato 1991) obtained by Eq. 2.24 and summed over total faults N_f (Eq. 2.25).

Table 2.3. Faults considered in the study[1]

S.N.	Fault ID	Name of Fault	Type	Length (KM)	M_{max}
1	HFF-1.5	Rapti	R	55	7.1
2	HFF-1.6	Koilabas	R	110	7.5
3	HFF-1.7	Patharkot	R	9	6.2
4	HFF-1.8	Baraghat	R	22	6.6
5	HFF-1.9	Raghia	R	15	6.4
6	HFF-1.10	Narayani River	R	18	6.5
7	HFF-1.11	Chitwan	R	8	6.1
8	HFF-1.12	Hetauda	R	7	6.0
9	HFF-1.13	Amlekhganj	R	30	6.8
10	HFF-1.14	Bagmati	R	49	7.1
11	HFF-1.15	Dhalkebar	R	52	7.1
12	HFF-1.16	Bhatibalan	R	50	7.1
13	HFF-1.17	Dharan Madhumalla	R	112	7.5
14	MBT-2.2.4	Dang	O	55	7.1
15	MBT-2.3	Arun Khola	R	75	7.3
16	MBT-2.4	Narayani	R	20	6.6
17	MBT-2.5	Hetauda	R	40	7.0

[1] HFF: Himalayan Frontal Fault, MBT: Main Boundary Thrust, MCT: Main Central Thrust, LH: Lesser Himalaya, HTH: Higher Tibetan Himalaya, SS: Strike Slip, N: Normal, R: Reverse, O: Oblique, RL: Right lateral strike slip, DS: Dip slip

18	MBT-2.6	Udaipur-Sunkoshi	R	95	7.4
19	MBT-2.7	Saptakoshi-Deomai	R	62	7.2
20	MCT-3.2.3	Tibrikot	RL	34	6.9
21	MCT-3.2.4	Dhaulagiri	N	24	6.7
22	MCT-3.3	Gosaikunda	R	110	6.9
23	LH-4.5.1	Badigad	RL	150	7.6
24	LH-4.5.2	Dhorpatan	RL	25	6.7
25	LH-4.6	Jhimrukkhola	RL	15	6.5
26	LH-4.7	Budhigandaki	N	30	6.8
27	LH-4.8.1	Kalphu	N	14	6.4
28	LH-4.8.2	Kulekhani	N	22	6.6
29	LH-4.8.3	Chitlang	N	6	5.9
30	LH-4.9.1	Bungmati	RL	6.1	6.0
31	LH-4.9.2	Bagmati	N	3.1	5.5
32	LH-4.9.3	Thankot	N	8	6.1
33	LH-4.9.4	Basigaon-Panga	R	3	5.6
34	LH-4.9.5	Kirtipur	N	8	6.1
35	LH-4.10	Sunkoshi-Rosikhola	RL	45	7.0
36	LH-4.11	Taplejung	DS	25	6.7
37	HTH-5.6	A-Mu-Chun	N	150	7.7
38	HTH-5.7.1	Thakkhola Graban East	N	125	7.6
39	HTH-5.7.1	Thakkhola Graban West	N	115	7.6
40	HTH-5.7.2	Tagar	N	95	7.5
41	HTH-5.8	Puriko Co-Gyiong	N	38	6.9
42	HTH-5.9	Kung Co-Tingri	N	105	7.5
43	HTH-5.10	Xuru Co	N	100	7.5
44	HTH-5.11	Pum Qu-Dinggya(A. R.)	N	90	7.4

$$\hat{\nu}_{fi} = P\left(Y > y^* \mid M_i, R_i\right)\nu_{fi} \qquad 2.24$$

$$\nu_f = \sum_{i=1}^{N_f} \hat{\nu}_{fi} \qquad 2.25$$

The mean ($\hat{\nu}_f$) and variance ($\sigma_{\nu f}$) of earthquake occurrences (Toki et al. 1991) are calculated by Eqs. 2.26 and 2.27.

$$\hat{\nu}_f = \exp\left(\ln \nu_f + \frac{1}{2}\varsigma^2\right) \quad 2.26$$

$$\sigma_{\nu f} = e^{2\ln \nu_f}\left(e^{2\varsigma^2} - e^{\varsigma^2}\right), \quad 2.27$$

where $\varsigma = \ln 10^2$

2.5.2.3 Combined occurrence

Once the mean rate of occurrence from historical events and active faults data are obtained, both results are combined using a Bayesian approach (Benjamin and Cornell 1970). Bayes' theorem states that the posterior probability density $f''(\nu)$ is the product of the prior probability density $f'(\nu)$ and the likelihood function $L(\nu)$ times a constant k (Eqs. 2.28 and 2.30). The prior distribution (Eqs 2.31-2.33) is described by probability density function of earthquake occurrences in faults (Katayama 1982) and likelihood function (Eq. 2.29) is obtained from historical data (Toki et al. 1991).

$$f''(\nu) = kL(\nu)f'(\nu) \quad 2.28$$

$$L(\nu) = \frac{\nu}{\nu_h}\exp\left(-\frac{\nu}{\nu_h}\right) \quad 2.29$$

$$k = \left[\int_{-\infty}^{+\infty} L(\nu)f'(\nu)d\nu\right]^{-1} \quad 2.30$$

$$f'(\nu) = \frac{1}{\sqrt{2\pi}\xi\nu}\exp\left[-\frac{1}{2}\left(\frac{\ln\nu - \lambda}{\xi}\right)^2\right] \quad 2.31$$

$$\lambda = \ln\hat{\nu}_f - \frac{1}{2}\xi^2 \quad 2.32$$

$$\xi = \sqrt{\left[\ln\left\{1 + \left(\frac{\hat{\sigma}_{\nu f}}{\hat{\nu}_f}\right)^2\right\}\right]} \quad 2.33$$

where, $\hat{\nu}_f$ is the mean and $\hat{\sigma}_{\nu f}$ is the standard deviation.

Considering historical earthquakes and active faults, the combined mean rate of occurrences is given by Eq. 2.34.

$$\hat{\nu}_c = \int_0^\infty \nu f''(\nu) d\nu \qquad 2.34$$

After calculating the combined mean rate of exceedences, the probability of exceedance of at least one event and the return period of these events are calculated.

2.6 Probabilistic response spectra

The mean rate of exceedance of peak ground acceleration and spectral accelerations at various periods of vibration are obtained using both of the above approaches. The mean rate of exceedance of peak ground acceleration is plotted as shown in Fig. 2.4. Assuming earthquake occurrences obey Poisson's process, accelerations corresponding to "return periods" of 98 years (40% probability of exceedance in 50 years), 475years (10% probability of exceedance in 50 years) and 975 years (5% probability of exceedance in 50 years) are determined for peak ground acceleration and for various natural periods using Eq. 2.6 and 2.12. The corresponding probabilistic spectra are plotted in Figs. 2.5 and 2.6 respectively. Both spectra are for 5% damping and for soft soil condition. In Figs. 2.5 and 2.6, I and II stand for approach I and approach II, respectively. Both approaches yield similar result, with a small difference due to the lack of historical data and that none of the digitized faults has maximum magnitude greater than M7.7.

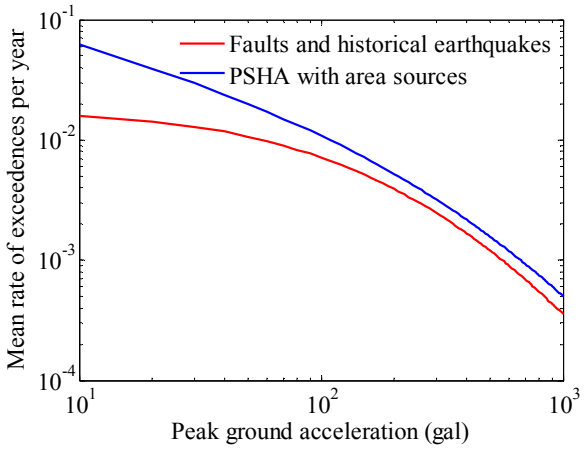

Fig. 2.4. Hazard curve for Kathmandu

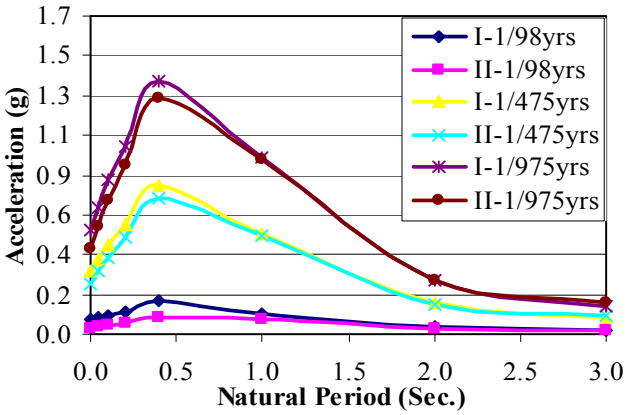

Fig. 2.5. Probabilistic response spectra (5% damping) for soft soil for Eq. 2.6

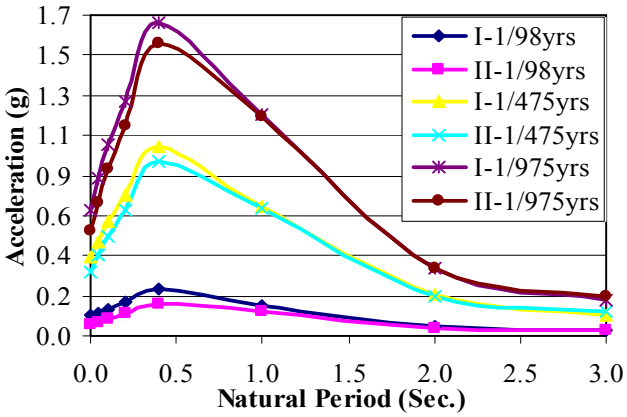

Fig. 2.6. Probabilistic response spectra (5% damping) for soft soil for Eq. 2.12

A greater difference between the two curves in Fig. 2.4 can be seen at lower accelerations than at higher accelerations. One of the reasons for this is the two different approaches. The smaller values of accelerations are more affected by lower magnitude earthquakes (e.g., M5-M6) which are missing on the catalogue. The locations of faults and their distances to the site also have an effect.

2.7 Comparison of results and sensitivity

Peak ground accelerations and spectral accelerations obtained for various return periods from approach I using Eqs. 2.6 and 2.12 are plotted against the BECA (1993) result (which uses

Kawashima, 1984, attenuation relation), Figs. 2.7-2.10. To compare the results the highest values (soil group 2) from BECA, 1993 among three types of soil conditions are used. The purpose of using "return period" 100 (39% probability of exceedance in 50 years), 475 (10% probability of exceedance in 50 years), 1000 (4.85% in 50 years) and 2000 (2.45% probability of exceedance in 50 years) years is for comparison with BECA (1993).

For 39% probability of exceedance in 50 years, the BECA (1993) estimates are higher than this study but, as the "return period" increases, the BECA (1993) estimates decrease, and the natural period of the peak values shift. The reason for this natural period shift is due to the two different attenuation laws. Atkinson and Boore 2003 takes the closest distance to the fault whereas Kawashima et.al. 1984 assumes epicentral distance.

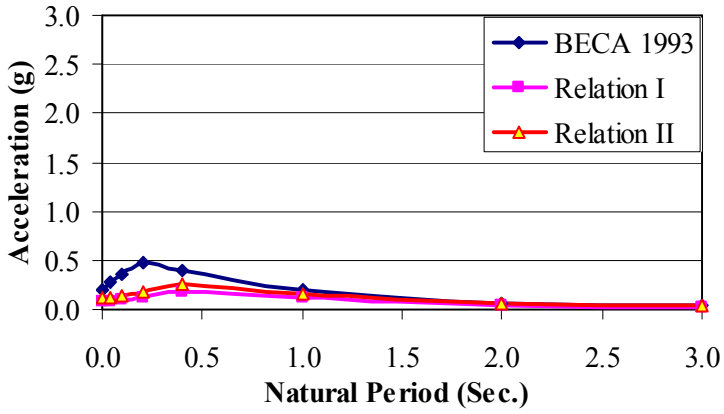

Fig. 2.7. Comparison of spectra for 5% damping and in 100 year return period

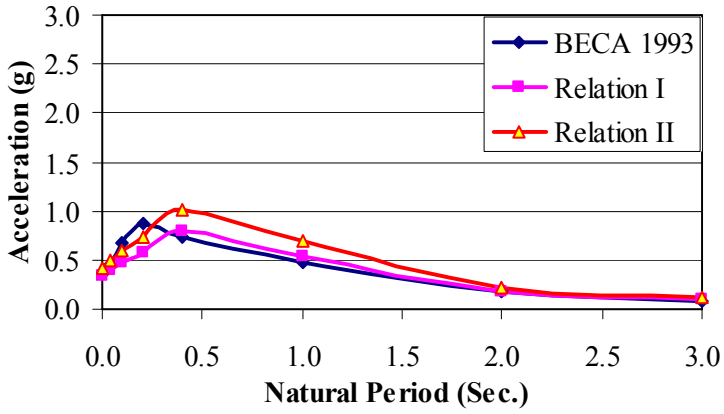

Fig. 2.8. Comparison of spectra for 5% damping and in 475 year return period

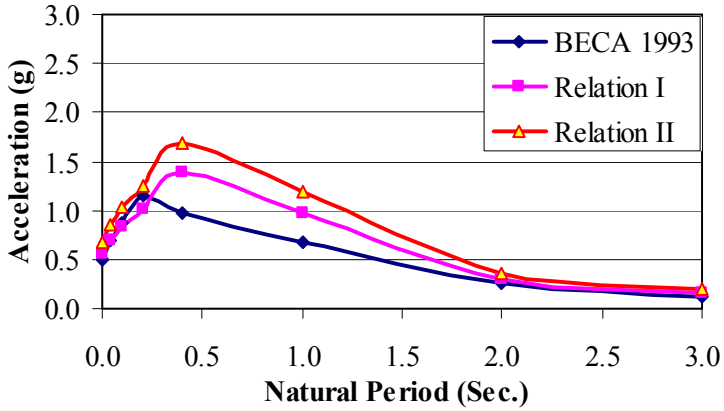

Fig. 2.9. Comparison of spectra for 5% damping and in 1000 year return period

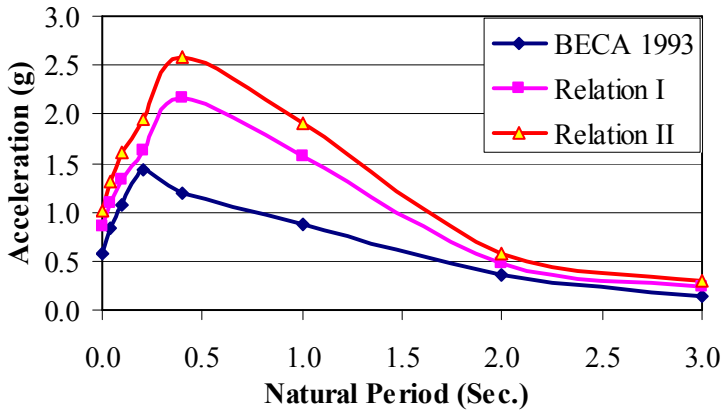

Fig. 2.10. Comparison of spectra for 5% damping and in 2000 year return period

Kawashima et al., 1984 considers earthquakes up to 50 km focal depth whereas Atkinson and Boore 2003, considers up to 100 km depth and provide separate coefficients for interface and intra-plate events. Site soil classifications also have a significant effect on the results. As the natural period increases the contributions of bigger events increases. BECA (1993) does not consider events greater than M8, which may be another reason for the natural period shift. The result is that BECA (1993) estimates low hazard for less frequent events. These results are dependent upon the coefficients of the magnitude frequency relations and maximum magnitude. The coefficients of magnitude frequency relations are generally justified from available data. Taking same magnitude frequency relationship, sensitivity of assumption made for maximum magnitude are examined considering maximum magnitudes M8.2, M8.5, M8.8 and M9 (Fig. 2.11). Results are insensitive to

changes in maximum magnitude for more frequent events but less so for less frequent events. The highest difference of acceleration for maximum magnitudes of M8.2 and M8.8 is 6%.

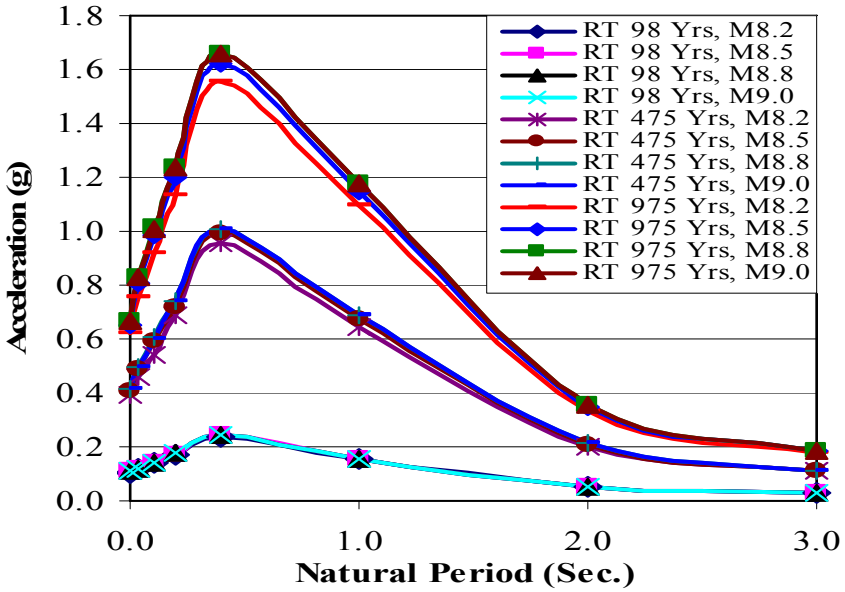

Fig. 2.11. Sensitivity of results changing maximum magnitude for 5% damping in soft soil

2.8 Hazard map

As discussed above, two different methods were applied to estimate the hazard. Sensitivity and usefulness of methods were discussed and approach I with extended magnitude frequency relationship satisfying the intra-plate slip was found reliable. Thus, this approach is extended to whole Nepal to plot hazard contours. All the historical earthquakes and faults around the region were collected and are plotted as shown in Fig 2.12. There are 92 faults and 1290 earthquake data in the boundary shown in Fig. 2.12.

Magnitude frequency relationship has been developed for eastern side (600km in length) Nepal's total length is approximately 1000km only. Thus, all earthquake data of 60% area has been already employed in estimating relationship presented in Fig. 2.3. Actually, the earthquake data has been employed to estimate only the slope of the magnitude frequency relationship (Fig. 2.3) and other coefficient for the line was estimated from intra-plate slip. This slip is not changed in few

kilometers and equally applicable for central part of great Himalaya which includes whole Nepal. Thus the same relationship is applicable for whole Nepal. Study area located from 80E to 88E in longitude and 26N to 30.5N in latitude was selected. Longitude was divided into 0.50^0 intervals and latitude was in 0.25^0 intervals. Sine the magnitude frequency relationship (Fig. 2.3) was developed for 300km radius, from each site, circle with 300km was drawn and all the faults and historical earthquakes were taken into account.

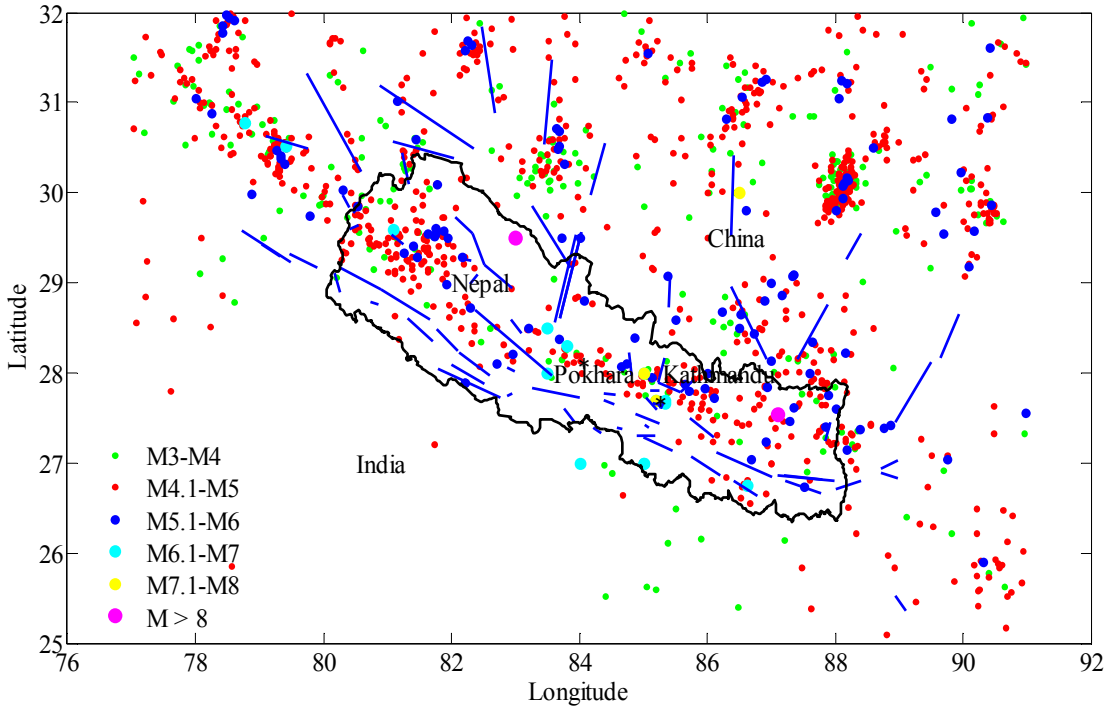

Fig. 2.12 Historical earthquakes and faults in and around Nepal

As the same procedure done above, the area encircled with in the radius was divided into small shells with 5km x 5km size. Centre of each shell was considered as source. Earthquake density at each sources were calculated using equations 2.15-2.18. Maximum magnitudes (Wells and Coppersmith 1994) for all faults were calculated. Considering maximum magnitude as one equivalent earthquake, they were added in earthquake data base in order to ensure faults hold at least one earthquake. Taking the data base, density of each shell with in 300Km radius around the site were estimated form Eqs. 2.15 to 2.19. Considering Eqs. 2.12 and 2.20, mean rate of exceedences and corresponding response accelerations for 40%, 10% and 5% probability of

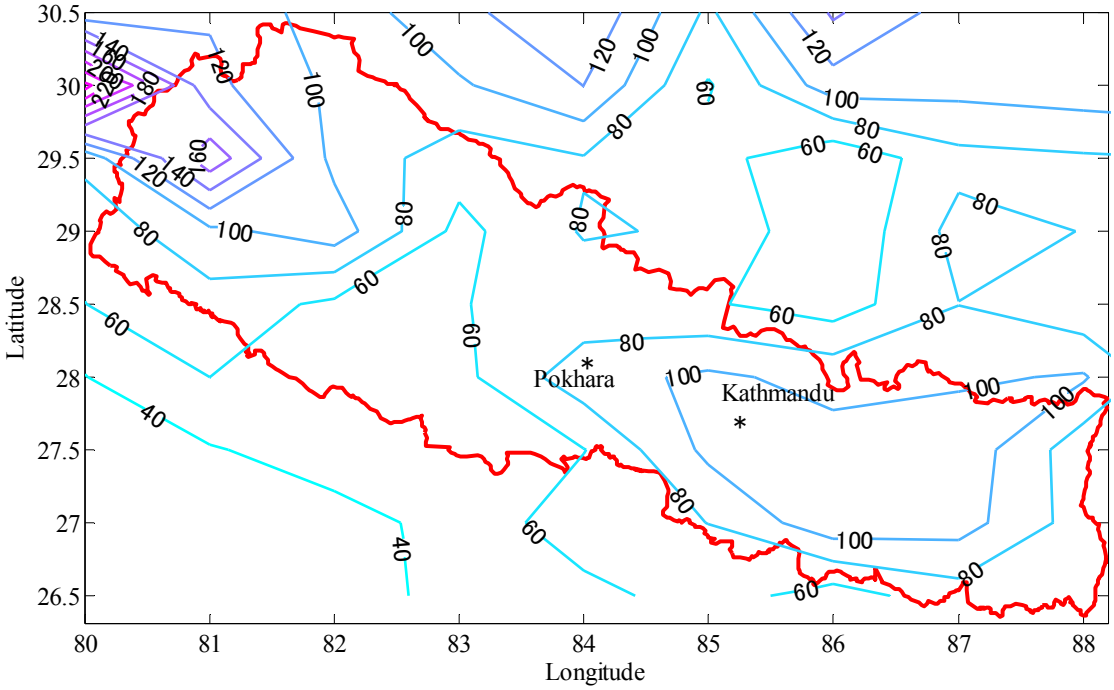

Fig. 2.13 Peak ground acceleration for 40% probability in 50 years (soft soil)

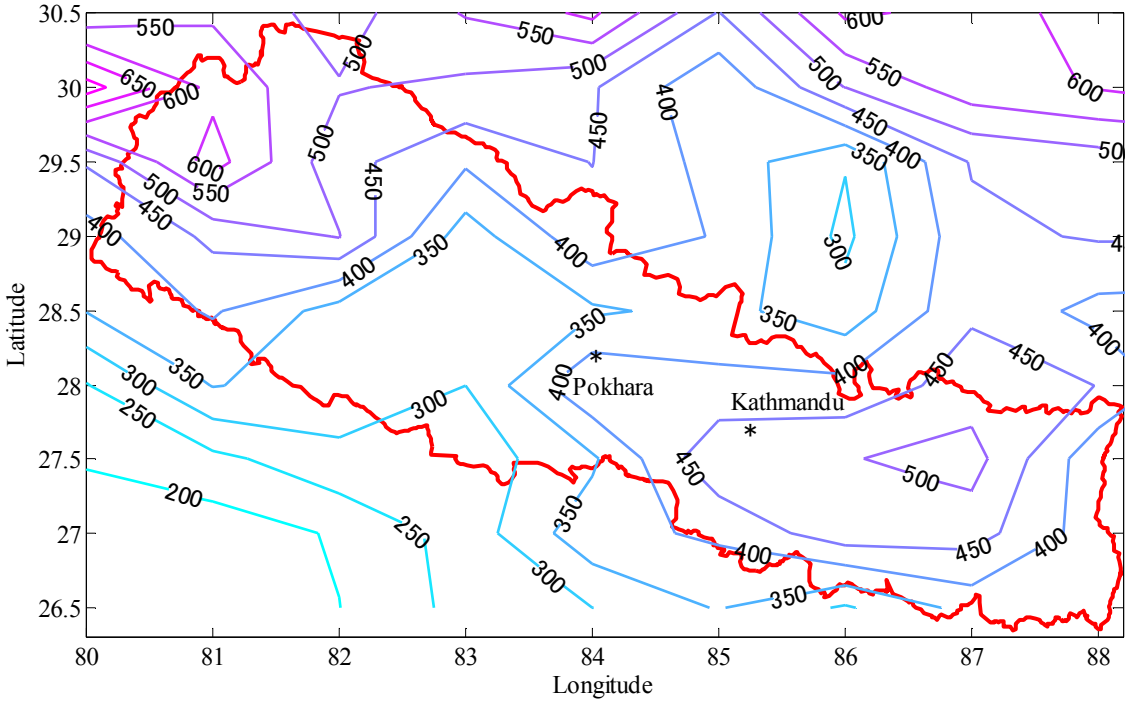

Fig. 2.14 Peak ground acceleration for 10% probability in 50 years (soft soil)

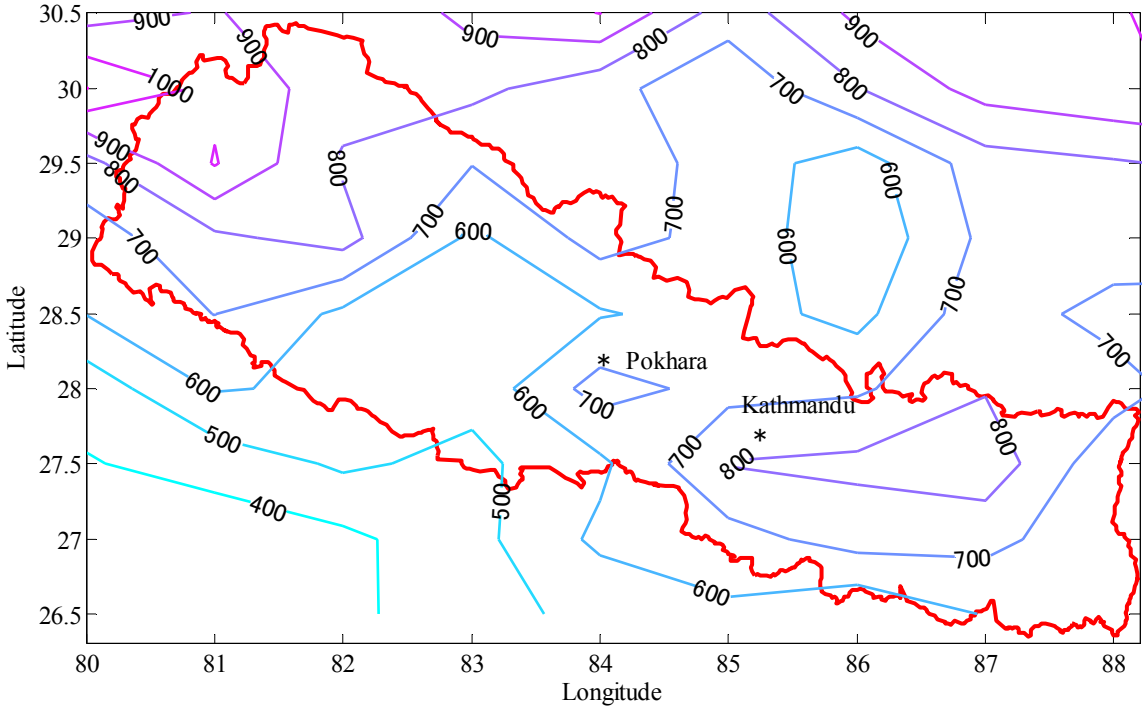

Fig 2.15 Peak ground acceleration for 5% probability in 50 years (soft soil)

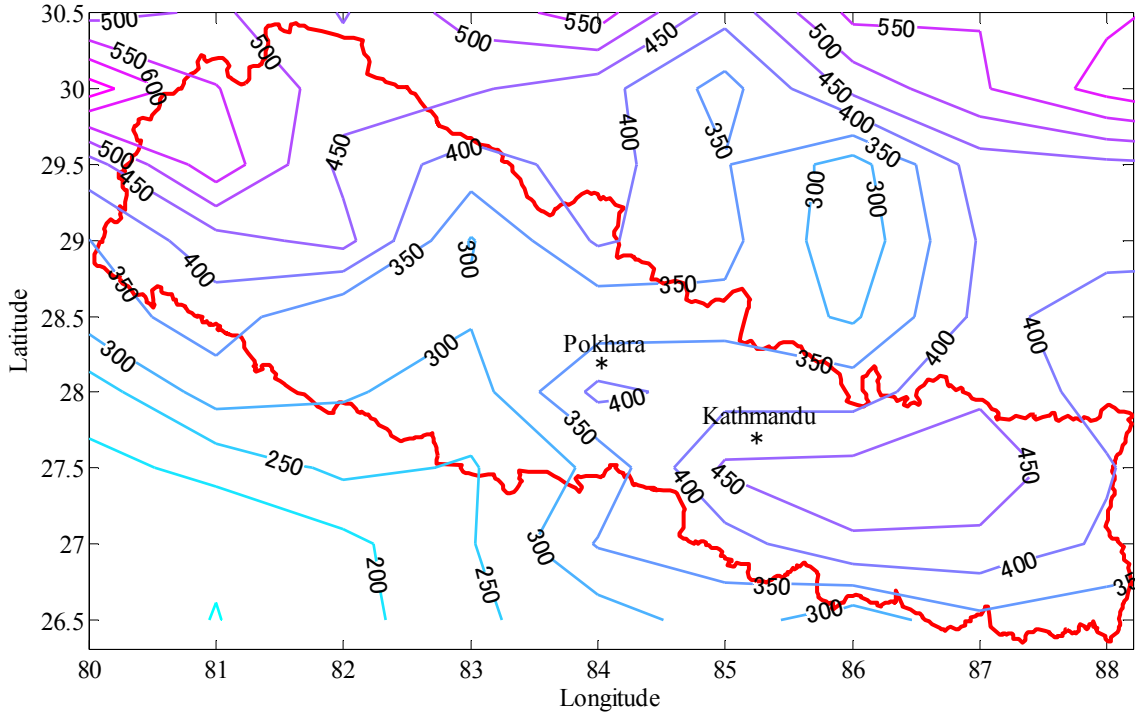

Fig 2.16 Peak ground acceleration for 10% probability in 50 years (medium soil)

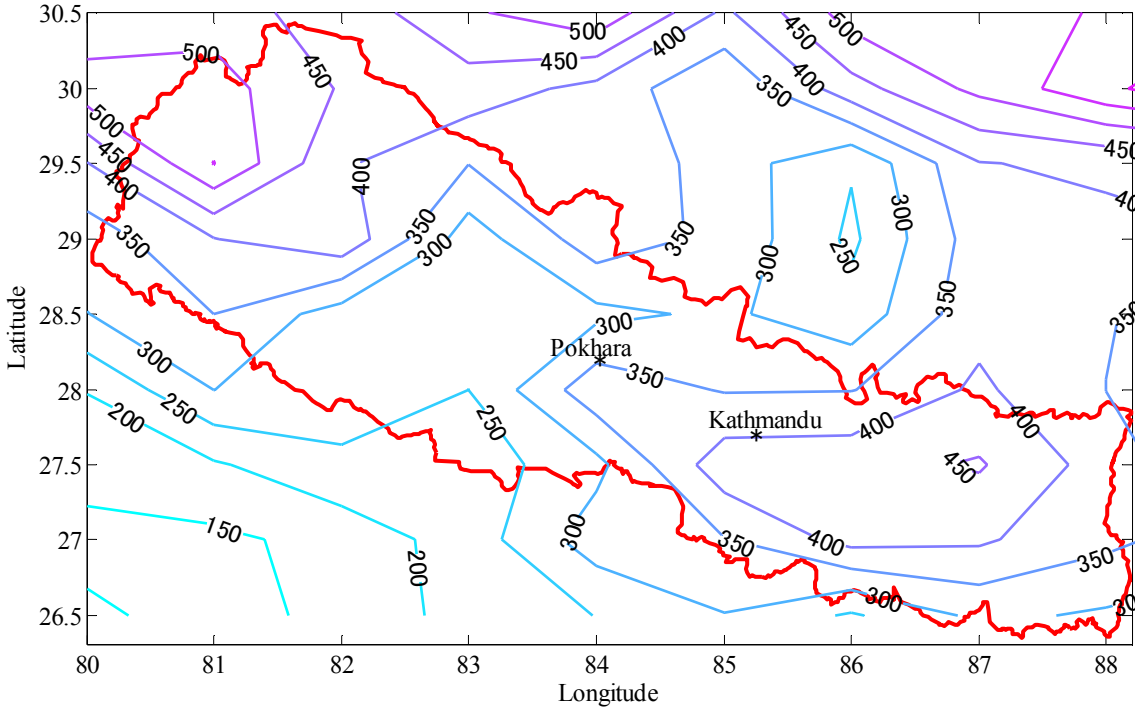

Fig. 2.17 Peak ground acceleration for 10% probability in 50 years (hard soil)

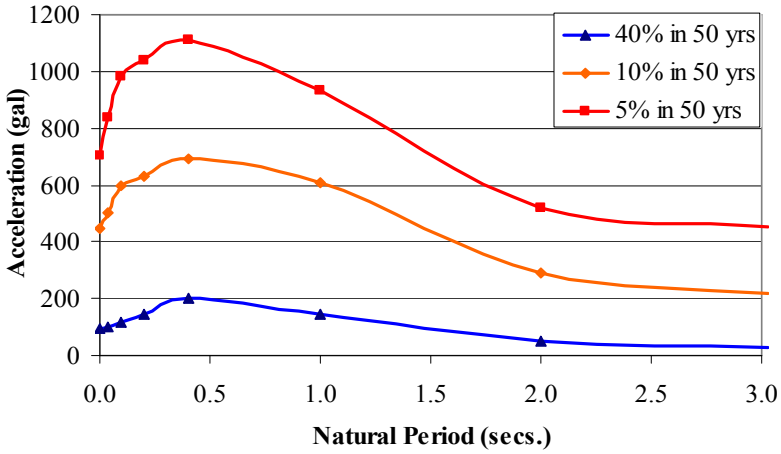

Fig. 2.18 Response spectra (5% damping) at Pokhara (soft soil)

exceedences in 50 years were calculated and plotted in Figs. 2.13 – 2.17. The figs. show that eastern and far western regions may experience bigger peak ground accelerations than in central regions. Two big (greater than M8) earthquake have occurred and lower magnitude historical earthquakes

(Fig.2.12) are also densely populated in these regions than in central region. Long faults are also in western and eastern side, however, small faults are in central part. As a typical example, for Pokhara city, latitude 28.2N and longitude 83.98E, peak ground accelerations and spectral accelerations at various periods for soft soil condition are obtained and plotted (Fig. 2.18).

2.9 Deaggregation and significant earthquakes

The main advantage of probabilistic seismic hazard analysis over other representations of earthquakes threat is it integrates over all possible earthquake occurrences and ground motions to calculate a combined probability of exceedence that incorporate relative frequencies of occurrence of different earthquakes. A disadvantage of PSHA is that the concept of a design earthquake is lost. There is no single event in terms of magnitude and distance that can be identified as dominating the hazard. Various researchers (Mcguire 1995, Chapman 1995, Harmsen et al. 1999, Bazzurro and Cornell 1999, Harmsen 2001) have developed the model for deaggregation of hazard and calculated mean and modal magnitudes and distances. The mean rate of exceedence corresponding to particular value of response acceleration at specified probability of exceedences specified period of years (e.g. 10% in 50 years) is sum of all contributions of mean rate of exceedences from various earthquakes having different magnitudes and distances.

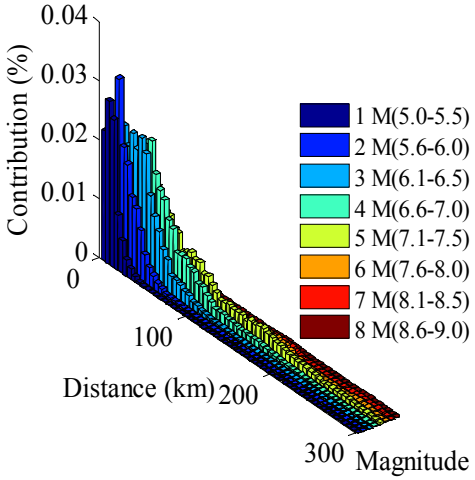

Fig. 2.19 Deaggregation of peak ground acceleration of 10% in 50 years (soft soil at Kathmandu - approach I)

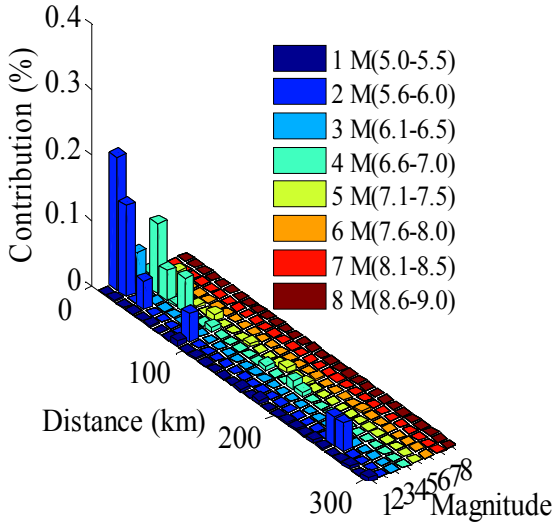

Fig. 2.20 Deaggregation of peak ground acceleration of 10% in 50 years (soft soil at Kathmandu - approach II)

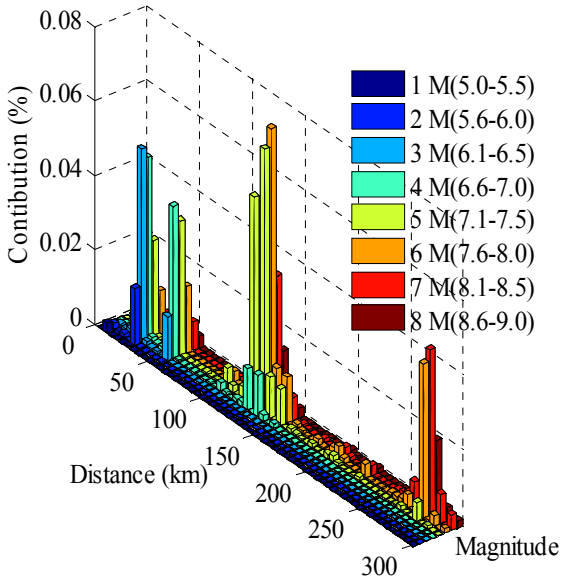

Fig. 2.21 Deaggregation for peak ground acceleration of 40% in 50 years (soft soil at Pokhara)

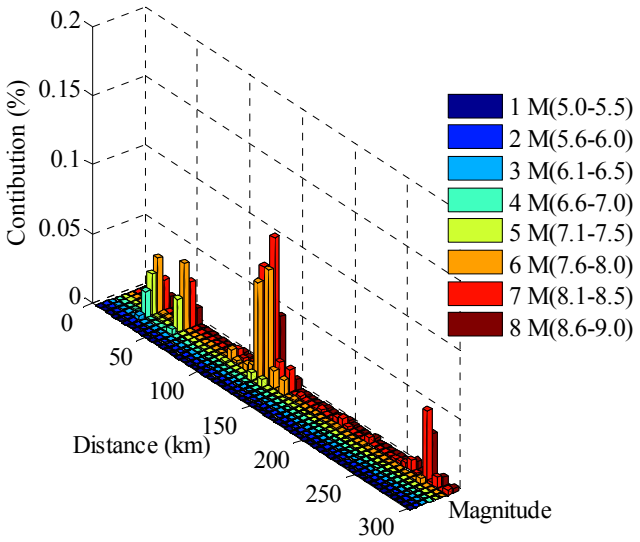

Fig. 2.22 Deaggregation for peak ground acceleration of 10% in 50 years (soft soil at Pokhara)

This mean can be deaggregated with respect to magnitudes and distances' contribution which gives deggregated plot as shown in Figs. 2.19-2.22. In order to find the most dominant event for Kathmandu, a mean rate of exceedance corresponding to peak ground acceleration with 10% probability of exceedance in 50 years (return period 475 years) is deaggregated into distances and magnitudes bins. The contribution of each magnitude and distance cells are plotted in Figs. 2.19 and 2.20. Seismic hazard at Kathmandu has the most contribution from magnitude M5.6-M6.0 and distance 5-15km. Similarly, for Pokhara city also, mean rate of exceedences for 40% and 10% in 50 years were deaggregated into various magnitudes and distances bins. They are plotted in Figs. 2.21 and 2.22 respectively. Earthquakes if occurred at distance 100 to 150 KM exceeding magnitude M8 will be dominant at Pokhara.

2.10 Conclusion

Available historical data are insufficient to estimate the seismic hazard of Kathmandu and the region around it. Considering the slope of magnitude frequency relationship developed from available data, and intra-plate slip rate 50% yields a magnitude frequency relationship which closely satisfies the rate of occurrences of big and small events which are complete. In order to better estimate the hazard, two different approaches were employed, with similar results. This hazard estimates are significantly higher than estimates from the only important previous study for the

region, (BECA 1993), which is also the basis for the seismic code for Nepal. Because of limited information regarding earthquake data and faults, the hazard may be under or overestimated and still may require further study.

Probabilistic seismic hazard estimate for a region where earthquakes data are missing has been done. There are many small faults around the big Himalayan thrust. But sufficient historical data are not available and available earthquake data does not satisfy the current intra-plate slip. Many of the faults are empty of historical earthquakes. However, they are the surface evidences of rupture occurred in its history. The method employed here combines three parts; historical earthquakes, faults and intra plate slip and estimate the probable hazard for the region. The density of earthquakes (Fig. 2.12) and contour plot (Fig.2.13-2.17) shows that the eastern and western part may experience larger accelerations than the central part. Then, probabilistic spectra for the city Pokhara has been plotted (Fig. 2.18). In the City, the structures having long natural period experience higher acceleration than in Kathmandu. Kathmandu is surrounded by many small faults and would experience severe if near source earthquakes, however, Pokhara may experience severe damages if distant big earthquakes like subduction zone events occur.

Most of the existing masonry buildings, and even reinforced concrete buildings, in Kathmandu, Pokhara and other cities have been constructed for vertical loads only and this trend of construction without considering seismic requirements has accelerated recently. Many strong earthquakes have already occurred in the region, and the accumulated slip deficit is likely to produce even greater earthquakes in the future. As the geology and construction pattern of houses of Nepal, India and Pakistan are very similar, the evidence from the 2005 Pakistan (Naeem et al 2005) and Bhuj (Jagadish et al 2001) events are sufficient to say a future Kathmandu earthquake could be catastrophic.

Chapter 3

DESIGN EARTHQUAKE GROUND MOTIONS

3.1 Introduction

Nepal takes approximately half length of greater Himalaya, which is part of the trans-alpine belt, regarded as one of the main earthquake prone zones of the world. Because of tectonic movement, many earthquakes have occurred in this region in its history. Records noted on some Nepalese religious tracts indicate that a big earthquake hit Kathmandu in June 1255 AD. The quake killed approximately one-third of its population at that time. Since then severe earthquakes have been reported which occurred in 1405, 1408, 1681, 1810, 1833, 1866 and 1934 AD (BECA 1993, Ambraseys and Douglas 2004). Evidences of big earthquake in central part of Nepal occurred in the period from 700 to 1100 AD have been published recently but exact occurred date has not conformed yet (Lave et al. 2005). Historical records show that at least as far back as the early 18^{th} century, damaging earthquakes have occurred in the Himalayan region in every few decades. But since 1950, the damaging earthquakes have not been reported in the region and in some areas. From recent studies depending upon the various analyses and GIS data, slip rate of Indian and Tibetan plates is 19 mm per year (Jouanne et al. 2004). But the calculated slip for whole Himalyan-arc from occurred earthquakes is only one third of the observed slip (Bilham and Ambrasseys 2005). It shows that either the earthquake records are missing or severe earthquakes may be overdue. Many earthquakes struck greater Himalayan region in the past but the worst may be yet to come and it may occur in or near Nepal. According to the new analysis by Bilham and Ambrssseys 2005, one or more massive earthquakes measuring greater than M8 on Richter scale may be overdue in the Himalaya, threatening the millions of people that live in the region.

More than ten thousand people were killed in 1934 earthquake. Since then, Nepal's population has doubled and urban population has increased by a factor of more than ten since last great earthquake. In urban, most of the people live in poorly constructed houses without considering the seismic codes. In rural area almost all people live in low strength masonry houses constructed by mainly by stones and bricks which have been proved the major cause of live loss in earthquakes. Considering past human tolls from earthquakes, population increases that have occurred since then

and the added low quality houses, the future scenario of deaths and damages could be worse than 2005 Pakistan earthquake. Previous seismic hazard estimate (BECA 1993) is based on uniform distribution of assumed earthquakes data over big area without well explained details. That study does not consider the earthquakes greater than magnitude 8 whereas their catalogue also has earthquakes greater than that magnitude. In previous chapters, revising all earthquake data, selecting suitable attenuation law, peak ground and spectral accelerations for various probabilities of exceedences were estimated and contours were plotted for the region. For a particular site such as Kathmandu and Pokhara, contribution to particular value of acceleration by various magnitudes and distances were disaggregated. Though, there is long history of earthquakes, no acceleration histories have been recorded. For dynamic analyses, acceleration is essential. Now, in this chapter, earthquake ground motion histories for Pokhara City for various probabilities of exceedences are estimated for the weighted average duration. To get weighted average duration, first, significant durations for all bins corresponding to deaggregated magnitude and distances are calculated. Weighted average duration and envelope function are obtained by multiplying disaggregated hazard with significant duration. Design earthquake is estimated for calculated weighted average duration fitting with obtained probabilistic spectra. The whole procedure is shown in flow chart (Fig.3.1).

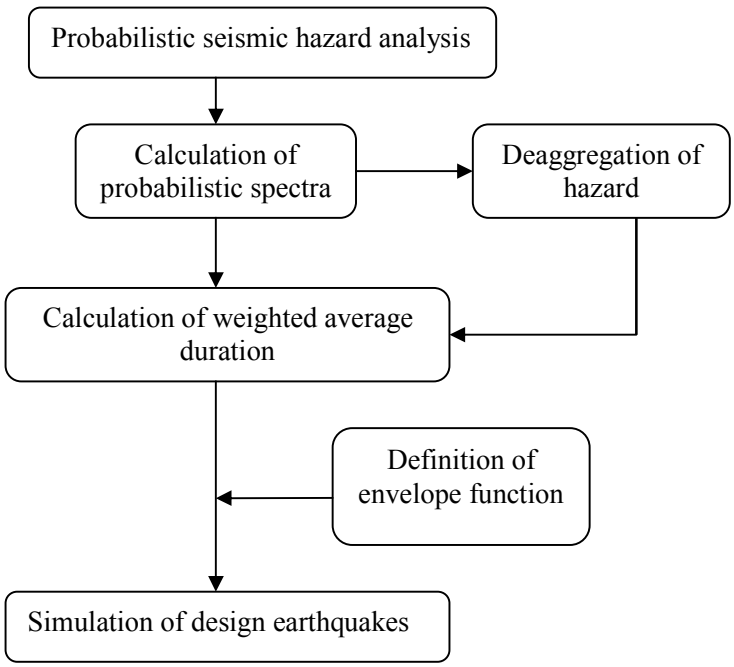

Fig.3.1 Flow chart for simulation process

3.2 Duration and envelope function

Duration of earthquake is function of magnitude and epicentral distance, thus each earthquake has separate duration. A probabilistic spectrum consists of many earthquakes. Even within duration span, acceleration amplitudes are not uniform. Thus total duration (T_D) is divided into three parts as shown in Fig.3.2. In the first part up to T_B acceleration will be ascending, between T_B to T_C, it is much effective and after T_C, it starts descending. T_B (Eq. 3.1) and T_C (Eq. 3.2) are calculated using equations following Osaki 1994 and T_D (Eq. 3.3) is calculated using equation following Kemption and Stewart 2005. It is significant duration which is defined as the time interval across which 5 to 95% of total energy is dissipated.

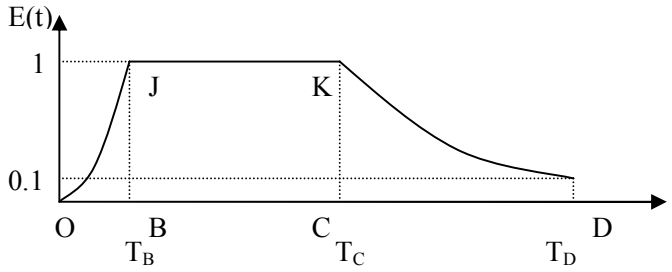

Fig. 3.2 Division of duration and envelope function

$$T_B = [0.12 - 0.04(M - 7)]T_D \tag{3.1}$$

$$T_c = [0.50 - 0.04(M - 7)]T_D \tag{3.2}$$

$$\ln T_D = \ln\left[\frac{\left(\frac{\exp(b_1 + b_2(M-6))}{10^{1.5M+16.05}}\right)^{-1/3}}{4.9.10^6\beta} + c_2 r + c_1 s\right] \tag{3.3}$$

where, b_1, b_2, c_1, c_2 are coefficients equal to 2.79, 0.82, 1.91, 0.15 respectively, β is shear wave velocity equal to 3.2km/sec. s is soil type and equal to 1 for soil, and zero for rock, M is magnitude of earthquake and r is epicentral distance. Envelope function E(t) is calculated using Eqs. 3.4 - 3.6.

$$0 \le t \le T_B:\ E(t) = \left(t/T_B\right)^2 \tag{3.4}$$

$$T_B \le t \le T_c:\ E(t) = 1 \tag{3.5}$$

$$0 \le t \le T_B:\ E(t) = \exp\left(\frac{\ln 0.1}{T_D - T_C}(t - T_C)\right) \tag{3.6}$$

In order to find out appropriate duration, all accelerations are disaggregated in terms of magnitudes and distances (Fig. 2.19 – 2.22). Disaggregated cells have separate magnitudes, distances and weights. Separate significant durations for all cells using Eqs. 3.1-3.3 were calculated, then, obtained durations are multiplied by corresponding cell's weight obtained from disaggregation and weighted durations are found summing up all bins' durations. We obtain duration for particular value of response acceleration corresponds to specific period. However, we need a single value applicable for all acceleration that fall in specified probability of exceedence in specified period of years. Thus, using similar procedure, durations for all accelerations are calculated. These calculated durations have combined effects of distance, magnitude and weight of deaggregation. For lower accelerations, contribution of lower magnitude earthquakes in hazard is significant but duration is short. For distant earthquakes duration is long but its contribution to hazard is low. For frequent earthquakes, smaller magnitude earthquake also contribute more but when probability decreases contribution of higher magnitude earthquake increases. In an average, the duration remains almost same for all earthquakes which fall in same return period. Thus, the weighted durations corresponding to same return period are in close margin. Then weighted average duration is calculated from all accelerations. For spectra shown in Fig. 2.18, durations are presented in Table 3.1.

Table 3.1 Weighted average duration for Pokhara

Durations	40% in 50 yrs	10% in 50 yrs	5% in 50 yrs
TD	30.0	45.0	51.0
TB	3.5	5.3	5.9
TC	15.0	23.0	26.0

3.3 Design earthquakes

Design earthquakes are simulated for calculated durations shown in Table 3.1. Total duration is first divided into small interval dividing by number N as shown in Eq. 3.7. Using incremental time, Fourier transform pair C_k and x_m are evaluated through Eqs. 3.8 - 3.11.

$$\Delta t = \frac{T_D}{N} \tag{3.7}$$

$$C_k = \frac{1}{N}\sum_{m=0}^{N-1} x_m \exp\left(-i\left(2\pi km/N\right)\right),\ \text{k=0, 1, 2, … , N-1} \tag{3.8}$$

$$x_m = \sum_{k=0}^{N-1} C_k \exp\left(i\left(2\pi km/N\right)\right),\ \text{m=0, 1, 2, … , N-1} \tag{3.9}$$

$$C_k = F_k\left(\cos\phi_k + i\sin\phi_k\right) \tag{3.10}$$

$$R_d = \frac{S_{ds}}{S_{dt}} \tag{3.11}$$

where F_k is Fourier amplitude,ϕ is phase angle, R_d, is ratio of simulated (S_{ds}) to target spectra (S_{dt}). Envelope plot (Fig. 3.2) was divided into small increments. Using Eqs. 3.4 - 3.6, value of envelope function E(t) was calculated. Cumulative value of E(t) was calculated at each interval and these all values are divided by final sum which give cumulative probability density function from zero to one. Considering total duration as three hundred sixty degree, phase angles for every time steps were determined randomly using probability density function. At first, Fourier amplitude F_k is assumed unity. From, Fast Fourier Transform (FFT), accelerations at each intervals were calculated. Accelerations were obtained from Inverse Fourier Transform. To make the simulated ground motion similar to natural earthquakes, the acceleration obtained from inverse Fourier transform were multiplied by envelope function. Using the calculated accelerations, response spectra was determined and compared with original spectra called target spectra. Ratio from simulated spectra to target spectra at each interval was obtained. New Fourier amplitude was then calculated multiplying old amplitude by obtained ratio. Again FFT were calculated and accelerations were determined. The process was repeated until the simulated spectra and target spectra fit well. The schematic diagram of whole process is shown in Fig. 3.3.

The accelerations histories obtained from this procedure for three probabilities of exceedences have been plotted in Fig. 3.4. From simulated acceleration histories, acceleration response spectra were calculated and plotted against target spectra (Fig. 3.5). In Fig. 3.5, for target peak ground accelerations are taken at zero period. But, for simulated spectra, plotting starts from 0.1 sec. for 975 and 475 years return periods and 0.05 sec. for 98 years return period. However, the spectra from simulated earthquake and originally calculated from attenuation law are in good agreement. In real earthquakes, accelerations start from zero, increase gradually, attains peak values and decrease

to zero finally. Simulated earthquakes also look similar to natural earthquakes. Amplitudes and nature of simulated ground motions are totally depend on target spectra.

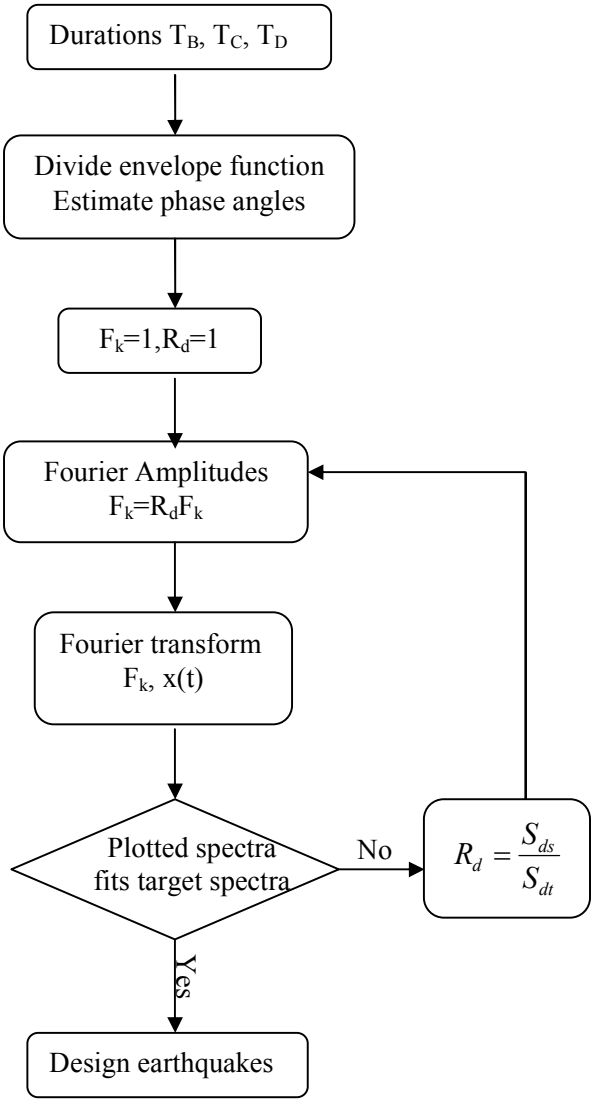

Fig. 3.3 Flow chart for generating acceleration histories

In order to see the differences of simulated ground motion from real earthquake and randomly occurred earthquake, a simulated earthquake ground motion for 5% probability of exceedence in 50 years has been shown in Fig. 3.4 (d). Input was given Kobe 1995 earthquake. When it is fitted with 5% probability of exceedences in 50 years, the original earthquake completely changes its shape

according to target spectrum. Thus, whatever is the input either real earthquake or randomly occurred wave, it follows the target spectrum. In random occurrences there are many possibilities, however the maximum amplitude of acceleration in both case are almost similar (Fig. 3.4 c-d).

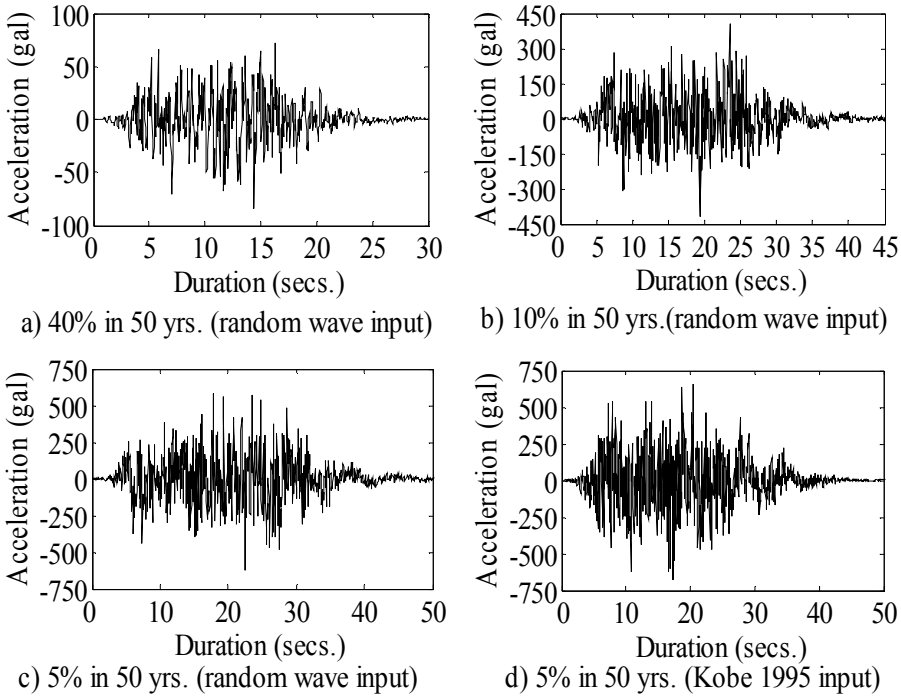

Fig. 3.4 Simulated acceleration histories for various return periods

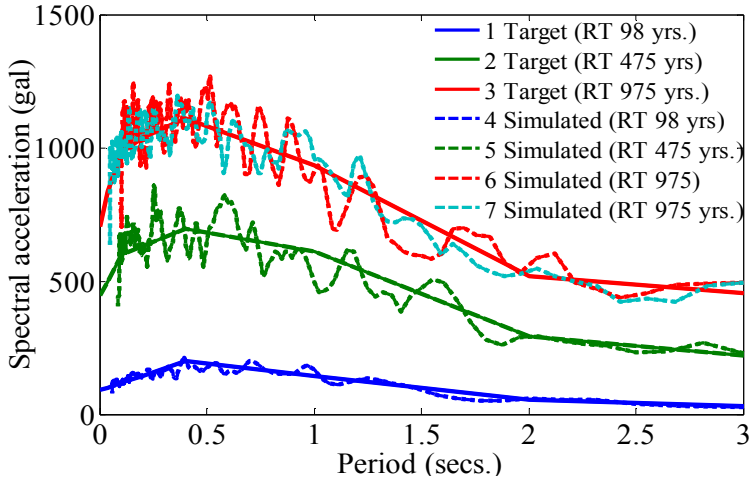

Fig. 3.5 Comparison of simulated and target spectra

3.4 Discussion

Probabilistic earthquake ground motions were obtained for weighted average duration which obtained from significant duration multiplied by weights of deaggregation and taken average for all durations corresponding to specified return period. Previous researchers have also given efforts to estimate risk consistent ground motion for example Kameda and Nojima 1988. Simulation of ground motion has been carried out focusing the characteristic or significant earthquakes. The method employed here through deaggregation is different than others. If we look at the deaggregation plot (Fig. 3.8 - 3.11), we can get magnitude and distance for significant earthquake corresponding to specified return period as a whole. The method employed here considers through the entire possible earthquakes that fall in the specified highest weight in the plot. Even though it is the highest, it may have just 10% or less weightage in overall hazard. Thus the bins other than highest weight have significant contributions. Few significant earthquakes lack to represent probabilistic earthquake for return period and simulate equivalent earthquake. Thus, it differs from other estimates which are based on significant or characteristic earthquakes. This method can be useful to estimate hazard where sufficient data are not available.

3.6 Conclusion

Earthquake ground motion histories are important for dynamic analyses. Though, many earthquakes have been reported in the history of Nepal, no accelerograms have been recorded. Thus, earthquake ground motions for the region where accelerograms are not available have been proposed. As a typical example, Pokhara city has been taken. Probabilistic spectra and deaggregation of hazard estimated in previous chapter were taken. Significant durations calculated for various distances and magnitudes were multiplied by weights of corresponding deaggregation and weighted average duration for specific return period was estimated. For the city, three separate probabilistic earthquakes were simulated. These earthquakes can be used for dynamic analyses for different life span structures. In usual practice, acceleration histories obtained from previous earthquakes are taken. However, they can not represent certain probability of exceedences. Same earthquake can not be used for varying life span structures. Thus, either new structures or existing structures, they are designed for specific life span. Thus these probabilistic earthquakes can be useful to design for new structures or retrofitting of existing structures.

Chapter 4

CHARACTERISTICS AND METHODOLOGIES FOR EVALUATION OF LSM HOUSES

4.1 Introduction

LSM houses are the oldest and most widely used in the world for past several thousand years and continue to be used for the days to come for its various advantages. Almost all historical buildings like churches, temples, shrine, pyramids etc. were built at the beginning of civilization fall under LSM category and have great importance from religious, historical and architectural aspects. These buildings were constructed before than any building regulation code emerged. So these houses had been built to take vertical loads and without consideration for seismic requirements. In every past earthquake, major damage has been occurred to public houses and monumental structures which have been built from low strength masonry and has been the major cause of loss of life (Yoshimura 2001, Jagadish 2003, Naeem 2005 and Hisada 2004). These poor quality houses have been the major earthquake problem in the world today. They account for thousands of deaths each year, from Greece the Mid East to Indonesia in the trans-Alpine Belt, in the Caribbean and along the entire west coast of Central and South America. However, it remains popular all over the world in engineering practice due to its simplicity, availability and cost effectiveness. Large numbers of LSM buildings are in stack in rural areas of developing countries and are the main threats for loss of lives. Recent Pakistan earthquake (Naeem 2005) shows that major loss of life and property is due to collapse of stone masonry, brick masonry and concrete block masonry buildings. Thus, the demand of strengthening of these houses has become increasingly stronger in the last few years. Moreover, based on modern design code, these buildings have to be upgraded. However, the question arises how these buildings can be strengthened efficiently and economically.

4.2 Types of LSM houses

LSM houses are made of brick, stone, wood, hollow blocks; and the units are joined by cementitious materials like mud, lime and cement etc. Placing of stones, composite blocks or bricks

units on top of other and bonding with various cementitious materials according to availability at particular locality is very successful technique due its simplicity in construction. The masonry buildings have been named separately in different locality of the world, the commonly used brick masonry can be classified as adobe (sun dried), confined masonry houses, reinforced masonry houses. Hollow block masonry and stone masonry houses are also in wide use.

4.3 Failure modes

Traditional LSM houses were designed only for vertical loads, when subjected to lateral loads by earthquakes or wind develop shear and flexure stresses. The internal friction between the units would be unable to resist the lateral force, thus, starts cracking, slip and separation between them. Due to increase in lateral force under earthquake excitation the walls undergo in plane shear force which causes shear failure in the form of tension cracks. Moreover, damages and major collapses occur due to out of plane failure (Jagadish 2003). Bruneau 1994 summarized the failures in unreinforced masonry are; lack of anchorage, anchorage failure, in plane failure, out of plane failure, combined in plane and out of plane effects and diaphragm related failure. Any kinds of failure occurred in masonry walls subjected to earthquake loadings governed by following three failure modes.

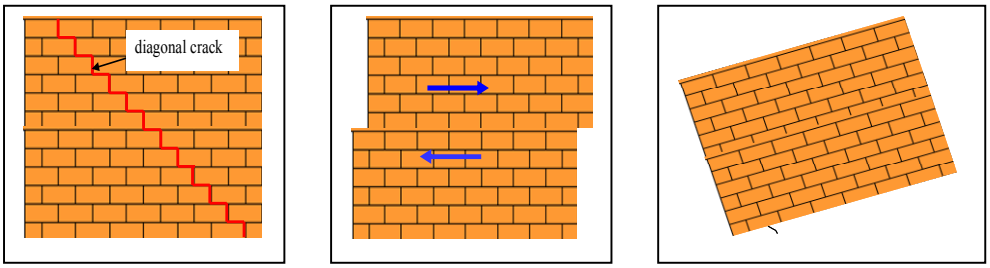

a. Shear b. Sliding c. Rocking

Fig. 4.1 Failure modes

Shear failure: It occurs when the principal tensile stress, which developed in wall as a resultant of horizontal and vertical stress, exceeds the tensile resistance of masonry. By the nature, brick is

strong and mortar is weak, the masonry fails at mortars and cracks propagate in wall along joints between the units in diagonal pattern (Fig.4.1a)

Sliding failure: In case of low vertical load and low friction at horizontal layers, crack forms at interface and slides between two layers occurs (Fig.4.1b).

Rocking failure: In case of high moment/shear ratio or highly improved shear condition, failure may occur due to overturning and crushing of compressed toe (Fig 4.1c).

These above mentioned masonry buildings are fairly better and walls act as a block. In case of vernacular construction such as stone masonry houses, stones units are not well joined by mortar and disintegrate when subjected to earthquake loadings and show following additional failure modes.

a. Corner cracking

b. Delamination into layers

c. Splitting into two layers

d. Racking shear failure

Fig.4.2 Various failure modes in vernacular houses (Desai 2001)

Corner cracks: All walls including interior walls are built one after another. Thus, their connections to each are very poor. When earthquake hits the building, crack propagation starts from corners (Fig. 4.2a)

Delamination: Stone walls lack through stones which are crucial for binding two inner and outer layers together. As a result two layers separate as the wall experienced shaking by earthquake (Fig. 4.2b).

Splitting: When walls experience earthquake, volume expansion occurs due to dilatational effect. As a result of which wall spilt out each other called budging failure (Fig.4.2c)

Racking shear: Like in brick and block masonry vernacular stone masonry also fails in shear (Fig. 4.2d).

4.4 Material used

Based on local availability, various materials such as wood, bamboo, burlap, rice and wheat straw, plastic sheets, steel rod and wire, rubber, polypropylene bands and fiber reinforced polymer have been used for strengthening the masonry structures in the form of strip, grids and fabrics. These reinforcing units are expected to increase the in plane and out of plane flexural and shear capacity of wall under lateral loads. Blonet et al used various industrial materials like PVC tube anchored to foundation, plastic mesh placed inside the mortar, steel reinforcement bars anchored to wall and geo-synthetic mesh externally fixed to wall to upgrade the masonry and investigated the performance. Kesner and Billington 2005 investigated the infill panel made from cementitious materials. However, various local materials can be used to upgrade the strength existing masonry, because of some difficulties associated to integrity to wall, less bonding, unavailability in sufficient quantities etc., most of local materials have limited capacity to increase the strength which might be insufficient according to prevailing design requirements. So, wood bond beams, steel bars and rods, polypropylene bands and fiber reinforced polymer have been found effective in strengthening of LSM.

4.4.1 Steel

Being steel as leading modern construction material, many investigations have been done to find effectiveness of steel (Arya 2000, Islam 2004) reinforcement in the form of bar and mesh applying single or both sides of masonry walls. Steel wire meshing consist of closely spaced multiple layer

of fine steel wire or rods embedded in a high strength cement sand mortar (Fig. 4.3) which is often called as ferro-cement (Scawthorn 1986 and Costa 2003). This type of mesh can be applied in both or single side of wall. The mechanical properties of ferro-cement depend upon strength of mortar, thickness of mortar and spacing of mesh units.

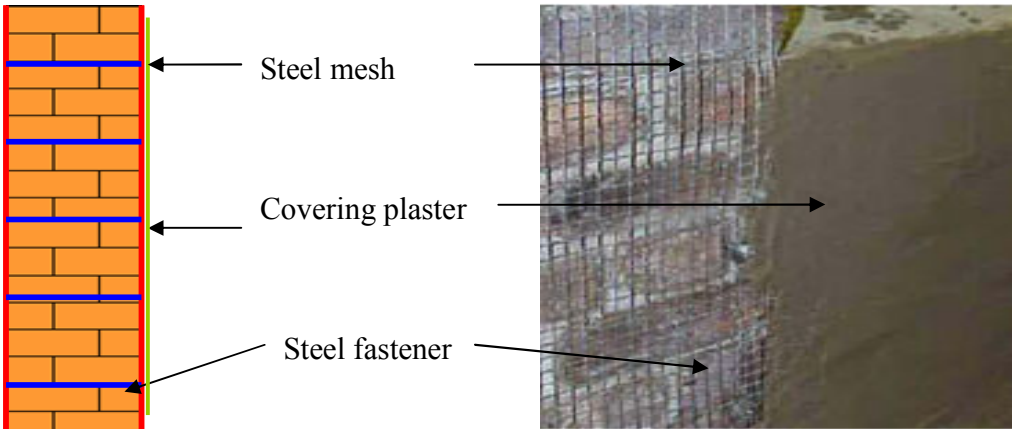

Fig. 4.3 Application of steel wire meshes; a) wall cross section steel fastener, b) Steel wire mesh in vertical wall and plaster

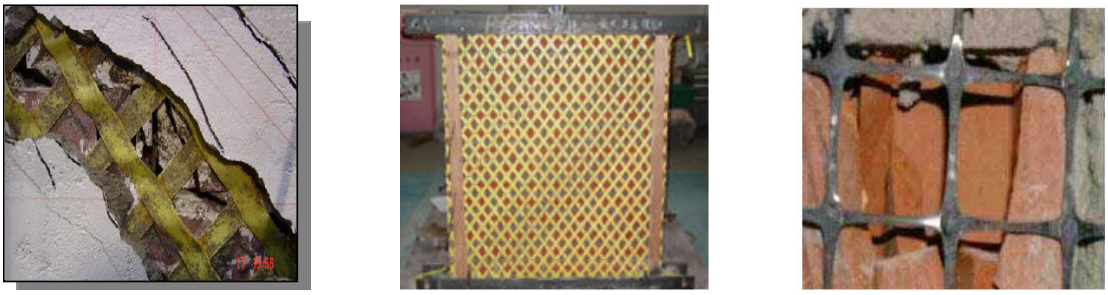

Fig. 4.4 PP bands in various patterns (Meguro 2004and Sofronie 2004)

4.4.2 PP bands

Strengthening of LSM against seismic loads by adding new structural members like frames or shear walls has been proved impractical in some cases. They have been either too costly, difficult to assemble or take working spaces. Meguro 2005 and Sofronie 2004 investigated the effectiveness of

Poplypropylene (PP) as an alternative which could be cost effective, easily available. PP band is commonly used in packing could be used as reinforcing material being cheap and easily available. PP- bands arranged in mesh fashion and embedded in mortar overlay. PP bands were installed on both sides of wall and wrap around the corner. The mesh was connected by steel wires passing previously drilled holes (Meguro 2004, Mayorca and Meguro 2004).The pitch and inclination of bands varies according to required earthquake resistance. However, because of low stiffness of PP-bands as compared to masonry, it did not increase the peak strength.

Sofronie 2004 investigated the performance of masonry strengthened with polymer grid formed from polypropylene sheets punched with precise and regular patterns of holes (Fig. 4.4c). The punched sheet were heated and stretched in pulling directions. Three techniques, inserting the polymer grids in the horizontal bed layers of mortar and bricks to improve the load transfer capacity between the brick units, coating outer surface of masonry by reinforced plaster to improve shear resistance of wall and confining the structural members with the same reinforced plaster to improve the compression and shear behavior of wall were applied. Testing was conducted to find the capacity of polymer grid to dissipate energy produced by shock and impact. The polymer grid was found as good as steel for retrofitting of masonry as a promising alternative.

4.4.3 Fiber Reinforced Polymer

Because of disadvantages associated with increased thickness due to added structural members and jacketing, high labor consumption, unavailability of skilled manpower, difficulty in inserting steel fasters through the wall led to researcher to explore an alternate material. At the same moment, due to rapid advancement in the construction material and technology in recent years, many new composite materials have explored in structural engineering. Fiber reinforced polymer (FRP) made from boron, aramid, carbon and glass have higher strength, higher stiffness and lower density were primarily used in aerospace and defense industries (Shrive 2006), are finding wider acceptance in conservative infrastructure construction industry also. FRP consists of high strength fiber bonded with polymeric resin matrix like epoxy. The fibers are commonly made of carbon (CFRP), glass (GFRP) and aramid (AFRP). FRP is many times strong in longitudinal direction but weak in lateral, have low weight and durable in adverse environment, available in strip, fabrics and tendons of unlimited lengths. The stress strain behavior can be taken as linear elastic and shows no ductility (Shrive 2006). Epoxy-bond FRP strip also have been applied to the surface of masonry in the

location of tensile and shear stress concentration (Triantafillou et al. 1998). Bakis et al 2002 summarized the commonly used strengthening techniques by FRP are prestressed strips, automated wrapping and curing, fusion bonded pin loaded straps, placement inside the slits and mechanically fashioned strips.

Because of high durability, light weight, easy application, FRP gained wide acceptance in construction industry, however, they have some disadvantages (Shrive 2006). It is susceptible under ultraviolet light. The resin slowly becomes brittle when exposed in sunlight for long time and FRP degrades under heat.

4.5 Conventional methods

Based on the availability of material, fund, expertise various methods have been adopted for strengthening LSM houses. Various strengthening measures such as surface treatment, confining by external reinforced concrete beam and columns, jacketing, addition of external element like walls and bracing base isolation are the very common methods to upgrade the masonry houses. Surface treatment is application of steel or FRP in the form of meshes or strips and covered by high strength cement sand mortar. The surface applications are attached to wall by means of nails and hooks embedded into high strength mortar.

Meli et al. 2004 found two effective methods of rehabilitation for rural areas of South American countries. One was the addition of steel welded wire meshes, either completely jacketing the wall or placed along selected portion of wall in the form of band. The other technique suggested was construction of reinforced concrete tie column and bond beam. From case studies, they, however, have indicated that extending confined masonry to existing adobe buildings with thick wall (400-600mm) has at least two shortcomings. First, because of wall thickness the confining element elements become too large and not economical. Second, because of their different coefficients of volumetric movement, the concrete and the adobe tend to separate. Verma 2000 proposed three methodologies to strengthen the adobe construction which had been applied in “Chapultepec Mex” of Mexico. Addition of reinforced concrete beam on the top of walls, steel mesh and cement mortar on both sides of walls and addition of tension, researches which have focused in experiments and steel bars were applied in meshes. However, addition of tension steel only is similar to reinforced

concrete beam it is easy to insert the steel rods than casting the beam. Addition of steel mesh and cement mortar at both sides was found most effective than other two techniques.

In northern India, after Chomoli M6.8 earthquake (Desai 2001), retrofitting program was launched for stone masonry houses. The program included various strengthening measures such as filling holes of wall with concrete, stitching the wall, application of ferro-cement belt around the wall, tightening of wooden element of floor and roof by diagonal steel bars, installation of steel bar at corners. Arya 2000 suggested to put vertical and horizontal and vertical seismic belts at the corner and wall junctions and stitch the outer and inner layer (wythes) of stone walls by steel rods. The seismic belts are steel meshes covered by cement sand mortar.

Addition of external beam, columns etc. or surface treatment enhances the capacity of structures. In a different way, instead of increasing the strength, idea of weakening the seismic forces by base isolation in structures has emerged as modern technique in reinforced concrete and steel buildings and bridges in recent years. However, it is difficult to put dampers to in old masonry structures; some researchers have investigated performance of masonry houses by base isolation (Kataoka et al. 2000, Luca et al. 2001 and Kawamata et al. 2004). Base isolation techniques by putting rubber bearings at the base of the building have been concluded as an effective alternative for retrofitting of existing old historical masonry buildings.

While strengthening masonry structures, attentions have given towards numerical analyses and experimental verifications to find stresses, strains, deformations, ductility and energy dissipation under static and dynamic loadings as indicators of measuring capacity. Certain guidelines have been developed to achieve the strength. Various in situ tests, full scale or nearly full scale pseudo-dynamic testing, scale down shaking table tests have been adopted to study the seismic responses of upgraded masonry. However, implementation of retrofitting program in wide region as disaster mitigation measures can not be successful until the user and the mason who build the houses fully understand the purpose of work and transfer the obtained knowledge in practice. In order to educate the general people and masons soft measure such as awareness rising is most important. In south America (Meli et al 2004) and Northen India (Desai 2001) have reported the implementation of retrofitting programs after launching the soft mitigation measures such as awareness raising for engineered and non engineered buildings. Five issues were discussed as disaster mitigation program

in engineered construction and they were: (1) evolution of earthquake engineering practice and code compliance; (2) reinforced concrete frame construction; (3) vulnerability of critical facilities; (4) compliance with codes standards and (5) vulnerability-reduction programs for existing buildings. For engineered construction the gap between complex and refined buildings standards and unimpressive level of knowledge and quality of practice of most of the practitioners was the key problem. The major vulnerability of buildings was attributed to insufficient transfer of knowledge, technology, and expertise to designers, contractors, and construction practitioners. To reduce the seismic vulnerability of engineered building the following recommendations were made

i. Promote structural systems like walls and braces rather than complex design and detailing
ii. Adopt technology which can be easily perceived by local expertise
iii. Develop specific design guidelines for critical facilities rather than adopting robust rehabilitation techniques
iv. Strengthen and improve the knowledge of expertise involved in local level

The non-engineered construction could be focused by addressing unreinforced, confined and reinforced masonry. To mitigate the seismic vulnerability of non engineered buildings, the following recommendations were made.

i. Encourage the participation of housing owners as stakeholders in different stages of vulnerability-reduction program, with emphasis on the construction process itself
ii. Promote the use of structural solutions akin to the local practice, but with superior performance based on their improved layout, materials and structural features.
iii. Develop training and educational programs for masons at local level and encourage the involvement of local universities
iv. Disseminate the case studies attained success in other areas

4.5.1 Numerical modeling

In civil engineering, as far as possible, every structural problem are primarily aimed to solve by numerical studies and later verified by tests. However, because of various difficulties in numerical modeling, some problems may require complicated experimental investigation to verify the results. To minimize the cost of big number of experiments and estimate the result of test, numerical analysis becomes necessary. However, various influencing factors such as anisotropy, dimension,

joint width, material properties of units (brick, stone, blocks etc.) and mortar, arrangement of header and stretcher, quality of workmanship etc make the modeling of masonry structures very difficult. Computational approach to investigate the strength of masonry have been conducted by large numbers of methods, ranging from simplified method to highly sophisticated method like using interface or joint element to define the possible failure. Researchers have modeled LSM houses especially by finite element and distinct element methods. The finite element analysis regarding the behavior of masonry ranges from very simple two dimensional continuum element which assumes the both mortar and masonry as single unit or type, to complicated three dimensional analyses which assumes mortar joints as the plane of weakness and brick as solid elements.

In existing masonry structures, various factors such as missing out geometric data, information about inner core and structural elements, mechanical properties of materials, variation of mechanical properties with age and workmanship, fatigue and strength degradation, accumulated damage due to loads such as wind and temperature, soil settlement and lack of understanding in structural behaviour create difficulty in modeling of masonry. Many researchers have sought the possibilities of these types of structures. Depending upon the level of accuracy and simplicity desired. Lourenco 2002 suggested three modeling strategies micro modeling, simplified micro modeling and macro modeling. In detailed micro modeling the units (brick or blocks) and mortar are represented by continuum element whereas unit-mortar interface is represented by discontinuum element. Young's modulus of elasticity, Poisson's ratio and inelastic properties of both unit and mortar are taken into account and mortar interface is assumed as the plane of failure, thus enables the combined effects of units and mortar. In simplified micro modeling expanded units are represented by continuum element whereas behaviour of mortar joint and unit-mortar interface are lumped as discontinuum element. The mortar and unit mortar interface is lumped into average properties and units are extended to keep the geometry unchanged, thus masonry is considered as elastic block connected by potential crack joint. It has lesser accuracy as compared to first method since Poisson's effect is not included. In macro modeling the units, mortars and unit-mortar interface are considered as homogeneous continuum element. It does not consider the individual behaviour of unit and interface and treats the masonry as homogeneous anisotropic continuum element. It is simple and easy, be applicable where compromises between accuracy and efficiency is needed.

4.5.2 Distinct element method

Distinct element which can be taken as simplified micro method in which structural system can be represented by assembly of blocks, interfaces of which is considered as discontinuities. The contact forces and displacements at the interfaces of stressed assembly of blocks are found through evaluation of equations obtained from Newton's law of motion which define movement of blocks. Papantonopoulos (2002) investigated the efficiency of DEM in predicting the earthquake response of classical monument by comparing the numerical results with experimental data. The dynamic response was calculated by time step algorithms assuming the velocities and accelerations are linear with in the interval. Both two and three dimensional analyses were performed. However, 2D analysis could not capture all the mode of failures together with it underestimate the response predicting the greater stability. They found this method could predict the earthquake response and found good compatibility with experimental data, however, small deviation in initial conditions and loading sequences can change the result by far. The value of joint parameters such as stiffness and friction were the important factors.

Alexandris et al (2004) investigated the collapses mechanism in non-engineered stone masonry houses subjected to severe earthquake excitations using distinct element method. Both two dimensional and three dimensional analyses of typical two types of buildings were performed. They found two dimensional analyses was failed to simulate the realistic response. The out of plane failure of long wall was found to be dominant mode of the failure mechanism in stone masonry. Response of wall using various strengthening techniques such as addition of concrete slab at floor level, bond beam on the top of wall, addition of steel ties at top of wall, addition of internal wall were studied. The first three strengthening methods found effective in decreasing the failure, while last one method changes the failure mechanism but does not decrease the possibility of collapse.

4.5.3 Finite element method

The response of masonry wall in earthquake loading depends upon the bonding of bricks with mortar. The mortar breaks first and relative movement starts between the layers. The analysis of this discontinuous system is governed by sliding and separation along the interfaces between adjacent blocks. An analysis, if it assumes perfect bonding at joints would over or under estimate the response of structure. So, dynamic behavior can be determined by non linear analysis that accounts the sliding and separation of joints. Three approaches, discrete crack approach, smeared crack

approach and interface element approach are best identified to model the cracks in the joist. The discrete crack approach requires monitoring of the response and modifying the mesh after exceeding the specified value of stress or strain at each state of loading. When stress or strain on node or average value of stress or strain in adjacent elements exceeds the specified value, the node is redefined two separate nodes which form crack. In smeared crack approach, the joints are modeled in average sense modifying the material properties of both units (brick and masonry). The formation of crack is similar to discrete element method. Both the discrete and smeared crack model approaches have limited capacity to model sharp discontinuities, for which joint element approach is more appropriate. Zienkiewicz et al (1970) proposed a joint element for laminar nature of material which is confined to narrow zone such as and old fault surface or joint. Beer (1985) investigated the interface between shell and solid using isoparametric joint element in two and three dimension. The stiffness matrix of joint element was formulated considering interface as separate isoparametric element with zero thickness. The non linear behaviour of joint was characterized by slip and separation taking place at the joint plane. The separation of joint was considered when it became tensile. Tzamtzis and Nath (1992) formulated three dimensional interface element which was designed to simulate time dependent sliding and separation along interfaces (in mortar joint) of brick masonry structures. Three dimensional finite element formulations was made by considering the relative displacements between the top and the bottom of the base elements and constitutive relationship, based on material properties containing shear and normal stiffness which could be found from stress displacement curves of mortar. Tzamtzis and Asteris(2002, 2004) further extended the finite element formulation in seismic loading. Non linear response by both Wilson theta and Newmark average acceleration methods were employed to find response and these results were found good compatible with the experimental results formed by previous researchers.

However, researches on analysis of masonry that can address the discontinuous behavior of joint also can be found, but, the researches have been least reported to date to analyze the response of retrofitted masonry structures considering the strength of retrofitting element, behavior of mortar, and masonry. For predicting the earthquake response of masonry structures, Cao and Watanabe (2004) developed a non linear finite element method considering the discontinuities at joints of masonry. In this method, brick was modeled by solid element and mortar was modeled by viscoelastic joint element which could simulate the opening and sliding behavior of joint. The building was first analyzed by without retrofitting and different failure modes (shear, tension crack

and out of plane failure) were identified. Then the building was retrofitted by wood frame and analyzed by same finite element method to predict the response of retrofitted building under El Centro earthquake loading. Use of wood fame found effective to control the failure to masonry.In an alternate approach, Islam and Watanabe (2004) investigated the adobe houses retrofitted with straw fiber. The material non linearity in finite element analysis was considered by equivalent linearization approach, however, authors themselves have pointed out to take the suitable interface element to account for separation of units.

A damaged masonry industrial building was strengthened (Mitroi and Olarn 2000) by using mixed steel brick connection. The authors took advantage of high tension bearing capacity of steel and compression resistance capacity of concrete. The steel were put in sides of wall as verticals, diagonals and horizontal manner with proper connectivity. It was found that the safety factor was increased four times than usual. Numerical analysis was done by finite element using equivalent element.

4.5.4 Experimental

Based on the cost, availability of materials and suitability of test, different testing methods such as in situ, pseudo-dynamic and shake table tests have been adopted. Some of the researches that have through experimental investigation have been summarized here;

Scawthorn (1986) carried out seismic analysis in proto type building considering the material as isotropic and elastic. In order to make appropriate strengthening measure three failure modes, tension or tearing failure at corners generated by out of plane inertial forces on the adjacent wall, in plane shear failure typically short occurred in short wall characterized by cracking and out of plane bending failure typically in long wall characterized by vertical cracks at corners, mid spans and openings were identified. Four alternatives, using bond at eave height of wall, a buttress at the mid-point of the long wall, 50% increase in wall thickness and a skin application to both faces of the walls were investigated to mitigate the above identified failure modes. The building was first analyzed by finite element method. Then the experimental investigations were performed in shaking table in approximately ¾ scale. Four types of models, no reinforcement, with bond beam, partial application (3 wall) of wire reinforcement and full application of wire reinforcement were tested.

Skin coat application stapled or fastened to base structure was found most efficient to enhance the existing low strength masonry.

Two storey 24 model buildings in 1:2 scales were tested by Benedetti 1998 in shaking tables in Italy and Greece to find the efficiency of various strengthening techniques and to understand and describe the mechanical and dynamic properties of the system as the damage increases. In the shake table, three components of base excitation for each shock were used. Seven model brick masonry and seven model stone buildings with wall thickness 45cm built.Several methods were employed to improve the connector between wall and slab to increase the resistance of wall. Primarily sealing of cracks was done. Steel network nailed to the slab, bent over surrounding of wall, connected to them and covered with cement plaster. In some cases steel network was placed at each storey level all around the wall covered with shallow cement plaster thus formed a bond beam. In some cases horizontal tendons and horizontal tie beams were applied at storey level. Curved steel plates at intrados of arches of door and windows were applied. Simultaneous base excitations acting two orthogonal directions and in vertical direction with peak acceleration in vertical direction was 70% of peak value of acceleration in horizontal was applied. Certain specified numbers of shocks were applied to each building.

A Full scale model of one storey stone building with two different combinations of retrofitting measures were tested by Shahi and Agrawal (2000) in shock table. The numerical evaluation using finite element method was good similarity with test results. Two different combinations were studied; the first one was provision of RC lintel plus grouting of wall, stitching of corner wall and putting steel wire mesh and the second was putting RC lintel band, corner jam steel, external binding of wire mesh and ties at sill level. The free vibration test result showed the frequency in longitudinal direction and transverse direction as 2.5 to 4.5 Hz. The damping ratio was found 3% to 4% in undamaged state and it was increased 50% to 100% at damaged state. That increase was due to energy dissipation in cracked stage. The authors had concluded that provision of lintel band, integration roof system with shear connection, bands at sill and lintel level and extra strengthening at corners and near openings could give good resistance in earthquake excitation.

Full scale lateral load tests on five samples, unreinforced and retrofitted, were tested by Verma and Miranda (2004). Two kinds of strengthening measures, applying confined reinforced beam and

hexagonal mesh of steel wire were adopted. The walls (2.3m* 2.3 m* 0.2m size) were tested in lateral reversible forces systems. Lateral load carrying capacity, ductility, and energy dissipation behaviors were investigated. Author concluded, the retrofitting measure by using confined reinforced concrete beam and column does not increase the lateral load carrying capacity of wall rather, increases the ductility and energy dissipation capacity. The steel ratio not play important role on the global performance, but the behavior could be improved by using superior quality of steel.

Costa (2002) implemented a rehabilitation program in Faial Island, Azores where buildings were damaged by 1998 earthquake. The buildings were made from stone masonry with two leaf double layer stone masonry wall having thickness 65 cm to 70 cm. Those walls were cleaned first and mortar slurry was poured into voids of walls. Then further strengthened by using steel wire mesh putting both sides of walls and plastering it. The wall and floor connectivity was strengthened by applying steel angle section. The steel mesh and base wall were interconnected by inserting the steel rods throughout the wall. The performance of retrofitted structures were verified by in situ tests

Six types of masonry wall strengthened with industrial materials (Blondet et al.) were tested to find the cost effective retrofitting method in rural area of Peru. Different test specimen applying plastic mesh, external strip of wire mesh, geosynthetic, single steel bar at each corners together with one unreinforced I shaped wall were tested. Load and displacement curve were plotted in each test specimen. Among the six alternatives, the wall retrofitted with steel wire mesh and covered with cement sand mortar was found most strong, however its post yielding failure is brittle. That wall, however, was not cheap in the local area. So investigators put geo synthetic mesh and tested it. That application was found most economical and effective to bear the lateral load.

Yamin et.al (2004), conducted shaking table tests and horizontal cyclic load tests in masonry walls strengthened by steel wire mesh and confining by wooden elements. The shaking table tests were conducted in reduced (1:5 scale) building with full scale wall, whereas, the horizontal cyclic tests were tested in nearly full (1:1.5) scale. In first stage, material properties of adobe and rammed earth wall in compression, diagonal tension and flexure were identified. Later, steel wire placed in horizontal and vertical direction in the critical zones of construction. The mesh was attached by nails which was applied both sides of walls. In addition steel anchors (8mm) were provided running

through the wall. Then the wire mesh was covered by lime mortar. Wooden elements were provided as second alternative in horizontal and vertical fashion and also applied at edges of doors and windows where cracks might occur. The horizontal and vertical elements were connected by bolts through previously drilled holes in walls, and later filled by cement mortar. The reinforcement based on boundary wooden element as better seismic behavior and presents advantages over other techniques. However, author suggested to the test validation by full scale shake table tests.

Paquette et al (2001) conducted out of plane shake table tests were conducted on three unreinforced masonry walls and wood backing assemblies extracted from and older existing residential building. One of three walls was tested in its existing condition, whereas other two were tested after applying retrofitting measures. The first retrofitting measure was use of anchors through out the wall connecting the masonry to the wood backing and additional two bolts that were used at mid height of the specimen. The second retrofitting measure was use of fiber glass strip which were glued to the side of masonry wall to increase its out of plane stiffness and strength. These wall specimens then were subjected shake table test in uniaxial earthquake simulator. All three walls were applied same seismic input of progressively increasing intensity expressed in terms of peak horizontal acceleration until structural was observed. Horizontal acceleration at different level, and horizontal and vertical were measured by accelerometers and displacement transducers. In between seismic excitation, low level impact test of walls were done by hammering the wall with bare fist to find the dynamic characteristics' in out of plane vibration. The experimental results were compared with the results of previous researchers. That test concluded that out of plane stiffness and strength can be increased significantly by using simple retrofitting methods. Use of fiber strips could be more effective than wood, however, the floor and wall connection is most essential.

Paquette and Bruneau (2003) A full scale one story URM building with flexible diaphragm was subjected pseudo-dynamic earthquake excitation. The building was rectangular with two wythes solid brick and flexible diaphragm was made by wooden joist and covered boards over it. The URM specimen was subjected to first series of tests under earthquake of progressively increasing intensity. The non linear elastic analyses were conducted to determine seismic input motion that would initiate pier rocking from the diaphragm. The selected seismic input was a synthetic ground motion with peak ground acceleration 0.453g. The earthquake input was produced by hydraulic actuator. The results were compared with predictions from existing seismic evaluation methodologies for

URM as the NEHRP handbook and Uniform building code. Four failure modes, rocking, bed joint sliding identified as deformation controlled diagonal tension and toe crushing identified as force controlled. The diaphragm found elastic through the tests. As author, to force the diaphragm in inelastic range and to find the effectiveness of repair, the walls were reinforced with fiberglass material and the specimens were tested with same input motion as before. The repaired wall showed the increased stiffness and was able to resist to peak ground acceleration 2.0g.

A.A. Hamid (2005) investigated the effect of orientation of mortar joint and layout of FRP laminates through experiments. Forty two unretrofitted and retrofitted masonry wall assemblages were tested under stress conditions. The highest increase in strength was found in direct joint shear assemblage with an average joint strength equals eight times that of their unretrofitted counterparts and least increase of strength found in compression.

K.M. Mosalam (2004) investigated the performance of GRP laminates applying one side of unreinforced masonry walls. Single wythe and triple wythe walls constructed using same types of bricks, but, with two types of mortar (strong and weak) which were aimed to represent the middle portion of unreinforced masonry was compressed diagonally. That stress created shear state inducing diagonal tension crack. From the experiment, the improved behavior of GFRP laminate URM in connection with wall thickness was sought. GFRP increased the capacity of single wythe wall by 50% but had minimum effect in ductility, whereas, triple wythe wall did not have significant increase in strength even after applying GFRP laminates.

C. Faella (2004) investigated the effectiveness of low density bidirectional carbon fiber tissue applied in stone masonry walls. Stone masonry wall was constructed, first thin coat of plaster was applied on the wall and then CFRP fabrics was stretched over the wall nailed with base wall and again second coat of plaster was applied. That specimen was tested on diagonal compression. Behavior of stone block, mortar and small stone masonry column in compression and bending were also investigated. Increase of wall strength due to application of FRP to single side and both side was investigated. Increase in shear strength in single side retrofitted wall was 70% where as both side retrofitted was 130% with respect to unreinforced masonry wall.

Candeias et al (2004) studied the different retrofitting alternatives applicable for high rise unreinforced masonry buildings stuck of Purtugal by shaking table tests. The prototype buildings

were selected from building typologies according to their percentage in housing stuck and level of vulnerability. Four storey high building with unreinforced masonry wall, 3.6m inter-storey height, wood frame floor and decking was identified as the most representative model. Two proto type(S and B) building were idealized considering the percentage opening in wall and size in plan. Depending upon the capacity of shaking table platform, the models were reduced in 1:3 scale following the Cauchy similitude law. While the constructing the test specimen buildings, simplified model having outer wall originally built by course rubble masonry was replaced by self compacting concrete to insure brittle behavior and low or almost null tensile strength and wood floor were built. In order control the out of plane collapse, to improve in plane capacity of wall and to control the generalized cracking in building, three retrofitting measures, were chosen based on simplicity and effectiveness which could be adequate for large scale risk mitigation. The first is wall to floor connection by steel connector and fiber glass strip glued with epoxy resin was applied at 3^{rd} and 4^{th} story level, the second is connection of opposing wall by steel ties at storey level of 3^{rd} and 4^{th} floor and last is strengthening of pier by fiber glass strips glued with epoxy resins and steel connector was applied. Reinforcement was put in full height and outside of the wall forming net in two directions. According to two proto type geometry and different patterns of retrofitting applications, eight tests were conducted. These specimens were subjected to time series loads in shaking table. Different failure modes were identified.

Velazquez and Eshani (2000) tested seven half scale URM wall constructed with clay bricks and low strength mortar. Two types of specimen; short wall (710 mm high and height/thickness ratio 14) and slender wall (1420 mm high and height/thickness ratio 28) with common width 1220mm were built. The specimens were strengthened with vertical glass fabric composite and subjected to static cyclic out of plane loading. All specimens were subjected to the same standard history pattern of static cyclic out of plane loading. The load was applied to the wall in two stages: A load controlled stage to observe uncracked behavior and displacement-controlled stage to monitor the stiffness degradation. No axial load was applied to the specimen. The specimen were simply supported at top and bottom and remained free along vertical edges. From this testing authors studied the tree flexure behavior corresponding to first visible crack propagation at bed, the first delamination and ultimate load. The main parameters investigated in this test were amount of composites, height to thickness ratio, the tensile strain in composites and failure modes of wall.

From the investigation linear elastic method was found best to analyze flexure behavior whereas ultimate strength method overestimated the flexure capacity and ultimate deflection of wall.

Albert et al. (2001) performed 13 tests in 10 wall subjected to out plane loads were conducted under monotonically increasing lateral out of plane loads. Different FRP materials; carbon plates, carbon sheets and glass sheets were applied in different patterns to strengthen the unreinforced walls. Three failure modes; mortar separation or slip, flexure and flexure were identified. Strength and ductility of FRP retrofitted walls were founded increased.

Ghobarah (2004) investigated the effects of openings like doors and windows, in out of plane performance enhancement of URM wall in five full scale wall specimen. CFRP laminates were applied to the tension side only to strengthen the walls in different patterns according to variation of size and location of openings. The wall specimens were subjected out of plane pressure by airbags. They found five times high lateral strength and ten times high ductility than that of existing URM wall whereas, opening reduces the load carrying capacity of wall and its size is important factor. Proper anchorage of CFRP was important for debonding failure.

Ehsani et al (1999) tested the three half scale URM specimens in out of plane loading. Five reinforcement ratio and two different glass fibre-reinforced polymer composites were investigated in cyclic out of plane loading. The test specimens were subjected prescribed out of plane load and displacement history by airbags. The ultimate flexure strength of retrofitted wall was significantly increased. The deflection as much as 2.5% of wall height was observed in wall reinforced with unidirectional fabrics and these walls deflected 14 times the maximum allowable deflection. Due stiffness degradation and delamination of both GFRP separate inelastic and brittle behaviors were observed.

Strong earthquake introduces severe in plane and out of plane forces to masonry walls which may lead to catastrophic collapse (Yoshimura et al., 2001, Jagadish et al. 2003 and Hisada et al. 2003 and Naeem et. al., 2005). However, majority of research conducted to date has been concentrated in out of plane behavior of URM strengthening by surface application especially by FRP. But out of plane failure may occur after the masonry unit became dislodged due to damage from in plane loading. Dakhakhni et al.(2006) tested URM specimen retrofitted with composites in compression in the direction normal and parallel to the bed joint, in diagonal tension and in shear to

investigate the effects of applying FRP laminates on the in plane behavior of URM assemblages present in masonry infill walls. The FRP laminates significantly increased the load carrying capacity of wall exhibiting shear failures along the mortar joint. The average joint shear strength of retrofitted wall found eight times that of unreinforced wall. The retrofitted wall prevented the brittle failure of masonry which occurs in ordinary masonry wall, and also prevents the catastrophic failure.

Triantafillou (2001) investigated the strength of masonry strengthened by externally bonded FRP laminates under in-plane bending and shear, and out of plane bending. Experimental tests in 12 specimens were conducted to validate the numerical results. They also concluded that if out of plane bending failure is dominant the FRP laminates could increase bending capacity substantially.

ElGawady et al (2005) tested upgraded URM walls by fiber reinforced polymer (FRP) under dynamic in plane loading. Five half scale walls having different patterns of FRP application with half scale brick-clay unit and upgraded one side only were built and studied in-plane capacity of upgraded wall. The masonry test specimens were built over shaking table with reinforced concrete base and a bond beam (reinforced concrete) at top. The superimposed load was simulated by two external post tensioning bars of 13 mm diameter. The displacement inputs were simulated in shaking table which is based on synthetic acceleration time histories compatible with Euro code 8(CEN 1994) with peak ground acceleration 1.6m/sec^2 for 14s. The FRP applied entire the wall and correctly anchored with base wall can help to control three types of failure; flexure, shear (sliding) and step cracking failure. However, the improvement in lateral drift was less significant and has low capacity of energy dissipation; they found the lateral load carrying capacity of wall can be increased by factor 1.3 to 2.9. No out of plane response of wall has been observed.

From this extensive shake table tests, some important conclusion were drawn. Lateral resistance of wall can be increased significantly by applying simple measure like, sealing of cracks and application of horizontal tendons. Application of horizontal ties found most effective to prevent collapse from separation of wall. The modal parameters like frequency, damping, mode participation factor etc., in different kinds of strengthening measures were found.

Ehsani et al (1997) studied the in plane shear behavior of unreinforced masonry wall upgraded with fiber reinforced polymer applied to exterior faces. The specimens were tested under static loading and strength and ductility could be significantly increased with the adopted strengthening

techniques. They also found that the orientation of angle of fiber with the plane of loading has major effect in stiffness of the retrofitted system but does not affect in ultimate strength.

Weng et al (1981) investigate in plane behavior in masonry through experimental test of 13 different masonry buildings strengthened with steel mesh covered with mortar layer, low and high strength GFRP under cyclic lateral load and axial load. The test found that GFRP could enhance the integrity of masonry, enhance the shear behavior, improve energy dissipating behavior and significantly increase the ductility and seismic resistance. Application of steel mesh with suitable anchorage length could also increase the integrity and lateral stiffness of wall.

4.5.5 Base Isolation

Kataoka et al (2000) used base isolation method to strengthen an old masonry school building. Base isolation was by combination of laminated natural rubber being and the red bar damper. Then non linear earthquake response analysis was carried to verify the earthquake resistant criteria to the severe ground motions. Three dimensional analysis using five different earthquake histories was done. The result of base isolation was verified by three tests; micro vibration test, human power vibration test and horizontal loading test and was confirmed to be verified to predicted values. Authors, so concluded, it could be a good alterative for retrofitting of old historical masonry buildings to which remolding of architectural appearance are not allowed.

A typical base isolation retrofitting suitable for masonry building was suggested by S. Kawamata et. al (2004). In this method, superstructure supported by rocking pillars encased in reinforced concrete caissons. The rocking pillars having spherical caps at both ends and mass produced from steel tube was filled with concrete. The caisson was put into dug hole and formed an isolation foundation. The houses on the foundation found very long vibration period which was determined from geometry of rocking pillar and independent of mass and free from torsion vibration. The building base isolated by this method, was tested in 1:4 scale in shake table which was subjected compressed (1/2 scale) El centro earthquake in one direction and two direction. The measure was found one of the effective methods of retrofitting.

Luca et al (2001) developed experimental testing program on full scale model which represents a sub-assemblage of the cloister faced of the Sao Vincente de for a monastery, a typical monument

of Lisbon, erected by the end of the 16th century and beginning of of the 18th century. The structural system composed by limestone block masonry column and arches, together with stone masonry bearing walls and ceramic domes. The test model is a plane structure consisting of three stone block columns, two complete arches, two external half arches and an upper part of the arcade made of stone masonry. Base isolation was done by high damping rubber bearing.

4.6 Conclusions

Review of literature show that a lot of efforts have been given to strengthening of LSM structures. Both analytical and experimental methods have been employed to estimate response of LSM under seismic loadings. But, only few literature have been reported in the area of non linear finite element analysis considering masonry as two phase material Depending upon cost, material availability, suitability of method, various innovative testing techniques such as, in situ tests, pseudo dynamic tests, shake table tests have been performed. Though, significant lateral strength can be increased by simple methods such as sealing of cracks by filling voids by grouting, stitching of large cracks and other weak zones with metallic or brick elements, it is still insufficient to resist the force produced in earthquake excitation. So variety of materials such as wood, steel, polypropylene, fiber reinforced polymer can be used to enhance the LSM structures in plane and out of plane failure. Among them steel wire mesh and fiber reinforced polymer were found most effective. Some application of base isolation method also performed in historical and school buildings, but, it still needs further research to make easy for the application of the method in massive retrofitting.

4.7 Further research

From extensive literature survey regarding the retrofitting by surface application, steel wire mesh and fiber reinforced polymer and addition of bond beams have been found effective. However, steel wire mesh, has been found even more effective if the lateral load resistance of wall is to be increased in far extent. However, steel reinforcements and polymers are also commercial materials and can not find at local sites. Wood is the material which can be available locally all over the world and can be good alternative over any other techniques of strengthening.

Chapter 5

EFFECTIVENESS OF WOODEN BOND BEAMS IN DRY STONE MASONRY HOUSES

5.1 Introduction

Stone has long been used as a building material for the construction of houses due to its availability and durability in the Alpine Himalalyan Belt (Pakistan, India, Nepal etc.) Large settlements of stone masonry buildings constructed with lime or earth mortar and even without mortar can be found in the area. Stone walls are built by stacking stones over stones normally in two leaves. Vertical joints are avoided as far as possible by placing various sized stones alternately. Corner stones are chisel dressed and mid span stones are hammer dressed. In cases where long stones are not available to break the vertical joints, wooden pieces are used. Roofing material may vary depending on location and can be corrugated galvanized iron sheet, slate or thick rammed earth laid over wooden joists and battons. One type of the dry stone masonry constructions using wood as bond beam called Hatil (Spence and Coburn 1992) in Turkey and Bhatar (Schacher 2007) in Pakistan (Fig.5.1) consists of single storey random rubble masonry with horizontal wood beams at specific intervals. Similar dry stone masonry houses fairly chisel dressed but without bond beams, are found in western Nepal also. Houses are generally one to two storeys and may have multiple rooms added at different stages of their history. Storey height is typically 2m and houses have small doors and windows and can therefore be dark inside even in day time. People use firewood to cook their meals, and stone built houses are highly fire resistant and durable against environmental degradation. Locally trained masons can build these houses easily and materials are locally available making these types of construction economical. If built correctly, they perform well under vertical loads. However, due to distinct directional properties of stone with its irregular shapes, it is difficult to make stone walls strong against lateral loads. Lateral strength depends upon friction between the stones and a very low cohesive strength of mortar if it is used. Thus, these houses have sustained heavy damages in historic earthquakes and have been the primary cause of fatalities. Usually, dry walls consist of two leaves of stones with total width of approximately 45 cm. The leaves have very weak bonding and interconnectivity and can become unstable even in minor

earthquakes. One possible methods of upgrading the wall could be to encourage the use of wooden elements as used Hatil (Spence and Coburn 1992) in Turkey and Bhatar (Schacher 2007) in Pakistan. Spence and Coburn 1992 found wooden elements to be effective in mitigating against failure in their experimental investigations. Cao and Watanabe 2004 analyzed brick masonry buildings by finite element methods considering bricks as solid elements and mortars as viscoelastic joint elements providing opening and sliding phenomenon. The buildings were analyzed before and after retrofitting by timber frame and they were found to be an effective way of preventing failure.

Wood bond beams have been found to be effective in resisting earthquake induced forces, hence these are known as seismic bands. However, the extents to which they contribute to preventing failures have yet to be investigated. There have only been a few studies testing with small dry walls examining these constructions (Lourenco et al. 2005 and Senthivel et al. 2006). Here, an attempt has been made to evaluate the performances of these houses in earthquakes. Two typical types of houses (one and two rooms) with and without applied wooden bond beams are modeled considering stones as elastic elements and interfaces between stones as inelastic joint elements. Subsequently, three dimensional dynamic analyses were carried out by applying various seismic accelerations obtained from past earthquakes and the results are discussed in the concluding part of this paper.

Fig.5.1 Contemporary Bhatar construction, Tarand-NWFP-Pakistan (Schacher 2007)

5.2 Numerical modeling

Even small masonry houses are made of thousands of pieces of stones and have joints at least three times that number. These joints are weak and are found to deform first under any kind of loading and govern the overall behaviour and failure mechanism of these structures. A large numbers of factors such as interior voids, irregular shaped units, varying properties of stone to stone,

quality of workmanship contribute to making the behaviour of these walls very complex. Computational approaches to investigate the strength of masonry have been conducted by various methods, ranging from simplified methods to highly sophisticated method which uses interface or joint element to define the possible failure. Analyses using distinct element method (DEM) which is also considered as a simplified micro method, model the wall as an assembly of small blocks and interfaces. The contact forces and displacements at the interfaces of stressed assembly of blocks are found through evaluation of equations obtained from Newton's law of motion which defines the movement of the blocks. There have been two recent pieces of work using DEM in examining the behavior of buildings: Papantonopoulos et al. 2002 investigated the efficiency of DEM to predict earthquake response of classical monuments by comparing the numerical results with experimental data. Alexandris et al. 2004 investigated collapse mechanisms of non-engineered stone masonry houses subjected to severe earthquake excitations using distinct element method. Two and three dimensional analyses of two types of buildings were studied. They concluded that two dimensional analyses were unable to simulate realistic responses. The out of plane failure of the long wall was found to be the dominant mode of the failure mechanism in stone masonry.

On the other hand, various investigators have utilized finite element method (FEM) which uses elastic and inelastic interfaces between units called discontinuities as having properties of sliding and separation. Zienkiewicz et. al. 1970 proposed a joint element for the laminar nature of a material which is confined by a narrow zone such as an old fault surface or joint in rocks. An isoparametric joint element in two and three dimension was introduced (Beer 1985) to represent the interface between shell and solid elements. The stiffness matrix of the joint element was formulated considering interface as separate isoparametric element with zero thickness. The non linear behaviours of joints were characterized by slip and separation taking place at the joint plane. Separation of joints was considered when it became tensile. Recently, this concept has also been used in modeling brick masonry (Tzamtzis and Nath 1992, Tzamtzis and Asteris 2002 and Tzamtzis and Asteris 2004) to simulate time dependent sliding and separation along mortar joints. Three dimensional finite element models were formulated by considering the relative displacements between the top and the bottom of base elements and the constitutive relationship, based on material properties containing shear and normal stiffness which can be found from stress displacement curves of the mortar. A brick masonry wall was analyzed in static and dynamic loadings and was found to be capable of predicting appropriate responses (Tzamtzis and Asteris 2004).

There have also been experimental investigations done in dry joint cut sawn stone masonry walls subjected to in plane and combined loadings(Lourenco 2005) and similar small walls have been investigated analytically in monotonic and reversed cyclic loadings (Senthivel 2006) considering multi-surface interface model (Lourenco 1997). From the literature review, we found that most researchers have followed the idea of modeling the units as solid elements and interfaces as zero thickness joint elements. Thus, the same approach considering stones as solid elements and their interfaces as joint elements has been employed here.

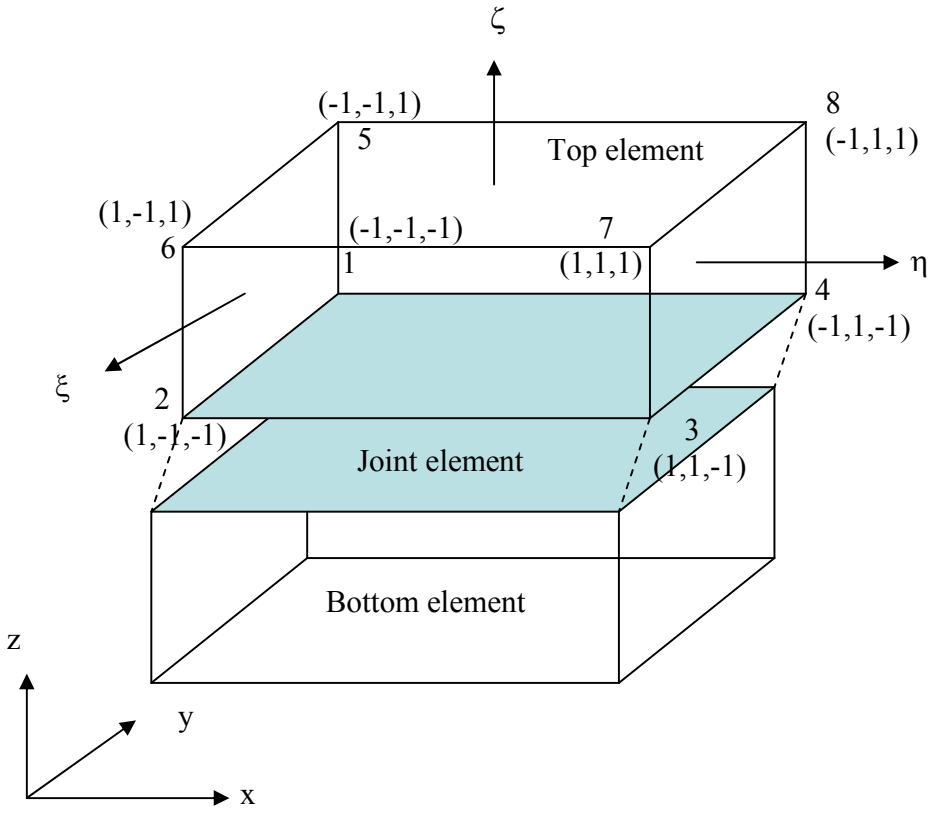

Fig. 5.2 Formulation of solid and joint elements

Generally, stone walls consist of a large numbers of irregular size stones, and modeling each individual stone and their interfaces in their as-built condition would be impossible. Thus a simplified numerical model has been developed making an equivalent group of eight node elastic solid elements for stones and eight node joint elements for their interfaces as shown in Fig. 5.2. In

the Fig., x, y and z are global axes and ξ, η and ζ are local axes. The ultimate objective of this dynamic analysis is to solve the widely known equation of motion:

$$[M]\{\ddot{u}\}+[C]\{\dot{u}\}+[K]\{u\}=-[M]\{\ddot{u}_g\} \quad 5.1$$

where, [M], [C], [K], are mass, damping and stiffness matrices, $\{\ddot{u}\}$, $\{\dot{u}\}$ and $\{u\}$, are acceleration, velocity and displacement responses respectively and $\{\ddot{u}_g\}$ is input ground acceleration. Modeling of stones and interfaces as built condition is impossible. Thus, numerical model is developed making equivalent 8 node elastic solid elements for stone and 8 node joint elements for interfaces between stones. The stiffness matrix for solid element shown in Fig.5.2 can be formulated (Chandrupatla and Belegundu 2002) through eqs. 5.2-5.26.

The displacement field can be represented as

$$u = N_1u_1 + N_2u_2 + N_3u_3 + N_4u_4 + N_5u_5 + N_6u_6 + N_7u_7 + N_8u_8 \quad 5.2$$

$$v = N_1v_1 + N_2v_2 + N_3v_3 + N_4v_4 + N_5v_5 + N_6v_6 + N_7v_7 + N_8v_8 \quad 5.3$$

$$w = N_1w_1 + N_2w_2 + N_3w_3 + N_4w_4 + N_5w_5 + N_6w_6 + N_7w_7 + N_8w_8 \quad 5.4$$

which can be written in matrix form,

$$\{u\}=[N]\{q\} \quad 5.5$$

or

$$\begin{Bmatrix} u \\ v \\ w \end{Bmatrix} = \begin{bmatrix} N_1 & 0 & 0 & N_2 & 0 & 0 & .. & .. & .. & N_8 & 0 & 0 \\ 0 & N_1 & 0 & 0 & N_2 & 0 & .. & .. & .. & 0 & N_8 & 0 \\ 0 & 0 & N_1 & 0 & 0 & N_2 & .. & .. & .. & 0 & 0 & N_8 \end{bmatrix} \begin{Bmatrix} u_1 \\ v_1 \\ w_1 \\ .. \\ .. \\ u_8 \\ v_8 \\ w_8 \end{Bmatrix} \quad 5.6$$

Where $\{u\}=\{u \quad v \quad w\}^T$ are global coordinates

$\{q\}=\{u_1 \quad v_1 \quad w_1 \quad .. \quad .. \quad u_8 \quad v_8 \quad w_8\}^T$ are local coordinates

$N=N_1,N_2,N_3\ldots. N_8$ are shape functions

The compact representation of equations is

$$N_i = \frac{1}{8}(1+\xi_i\xi)(1+\eta_i\eta)(1+\zeta_i\zeta) \quad 5.7$$

where, i=1 to 8 and ξ_i, η_i, ζ_i are local coordinates. In isoparametric representation, same shape functions can be used to express the nodal coordinates. Thus,

$$x = N_1x_1 + N_2x_2 + N_3x_3 + N_4x_4 + N_5x_5 + N_6x_6 + N_7x_7 + N_8x_8 \quad 5.8$$

$$y = N_1y_1 + N_2y_2 + N_3y_3 + N_4y_4 + N_5y_5 + N_6y_6 + N_7y_7 + N_8y_8 \quad 5.9$$

$$z = N_1z_1 + N_2z_2 + N_3z_3 + N_4z_4 + N_5z_5 + N_6z_6 + N_7z_7 + N_8z_8 \quad 5.10$$

Expressing the x, y and z in natural coordinate system,

$$f = f(x,y,z) \text{ and } f = f[x(\xi,\eta,\zeta), y(\xi,\eta,\zeta), z(\xi,\eta,\zeta)] \quad 5.11$$

Using chain rule

$$\frac{\partial f}{\partial \xi} = \frac{\partial f}{\partial x}\frac{\partial x}{\partial \xi} + \frac{\partial f}{\partial y}\frac{\partial y}{\partial \xi} + \frac{\partial f}{\partial z}\frac{\partial z}{\partial \xi} \quad 5.12$$

$$\frac{\partial f}{\partial \eta} = \frac{\partial f}{\partial x}\frac{\partial x}{\partial \eta} + \frac{\partial f}{\partial y}\frac{\partial y}{\partial \eta} + \frac{\partial f}{\partial z}\frac{\partial z}{\partial \eta} \quad 5.13$$

$$\frac{\partial f}{\partial \zeta} = \frac{\partial f}{\partial x}\frac{\partial x}{\partial \zeta} + \frac{\partial f}{\partial y}\frac{\partial y}{\partial \zeta} + \frac{\partial f}{\partial z}\frac{\partial z}{\partial \zeta} \quad 5.14$$

or,

$$\begin{Bmatrix} \frac{\partial f}{\partial \xi} \\ \frac{\partial f}{\partial \eta} \\ \frac{\partial f}{\partial \zeta} \end{Bmatrix} = [J] \begin{Bmatrix} \frac{\partial f}{\partial x} \\ \frac{\partial f}{\partial y} \\ \frac{\partial f}{\partial z} \end{Bmatrix} \quad 5.15$$

Where [J] is Jacobian matrix

$$[J] = \begin{bmatrix} \frac{\partial x}{\partial \xi} & \frac{\partial y}{\partial \xi} & \frac{\partial z}{\partial \xi} \\ \frac{\partial x}{\partial \eta} & \frac{\partial y}{\partial \eta} & \frac{\partial z}{\partial \eta} \\ \frac{\partial x}{\partial \zeta} & \frac{\partial y}{\partial \zeta} & \frac{\partial z}{\partial \zeta} \end{bmatrix} = \begin{bmatrix} J_{11} & J_{12} & J_{13} \\ J_{21} & J_{22} & J_{23} \\ J_{31} & J_{32} & J_{33} \end{bmatrix} \quad 5.16$$

The strain displacement relation can be written as

$$\{\varepsilon\} = \left\{ \frac{\partial u}{\partial x} \quad \frac{\partial v}{\partial y} \quad \frac{\partial w}{\partial z} \quad \frac{\partial v}{\partial z} + \frac{\partial u}{\partial y} \quad \frac{\partial w}{\partial x} + \frac{\partial u}{\partial z} \quad \frac{\partial u}{\partial y} + \frac{\partial v}{\partial x} \right\}^T \tag{5.17}$$

After some mathematical manipulation strain can be written as

$$\{\varepsilon\} = [B]\{q\}, \text{ where } [B] = [G][H] \tag{5.18}$$

Where,

$$[H]\{q\} = \left\{ \frac{\partial u}{\partial \xi} \quad \frac{\partial u}{\partial \eta} \quad \frac{\partial u}{\partial \varsigma} \quad \frac{\partial v}{\partial \xi} \quad \frac{\partial v}{\partial \eta} \quad \frac{\partial v}{\partial \varsigma} \quad \frac{\partial w}{\partial \xi} \quad \frac{\partial w}{\partial \eta} \quad \frac{\partial w}{\partial \varsigma} \right\}^T \tag{5.19}$$

$$[G] = \begin{bmatrix} J_{11}^{'} & J_{12}^{'} & J_{13}^{'} & 0 & 0 & 0 & 0 & 0 & 0 \\ 0 & 0 & 0 & J_{21}^{'} & J_{22}^{'} & J_{23}^{'} & 0 & 0 & 0 \\ 0 & 0 & 0 & 0 & 0 & 0 & J_{31}^{'} & J_{32}^{'} & J_{33}^{'} \\ 0 & 0 & 0 & J_{31}^{'} & J_{32}^{'} & J_{33}^{'} & J_{21}^{'} & J_{22}^{'} & J_{23}^{'} \\ J_{31}^{'} & J_{32}^{'} & J_{33}^{'} & 0 & 0 & 0 & J_{11}^{'} & J_{12}^{'} & J_{13}^{'} \\ J_{21}^{'} & J_{22}^{'} & J_{23}^{'} & J_{11}^{'} & J_{12}^{'} & J_{13}^{'} & 0 & 0 & 0 \end{bmatrix} \tag{5.20}$$

Superscript of J indicates components of inverse of Jacobin matrix.

Stress can be calculated from, $[\sigma] = [D][B]\{q\}$, where, [D] constitutive matrix is given by

$$[D] = \frac{E}{(1+\nu)(1-2\nu)} \begin{bmatrix} 1-\nu & \nu & \nu & 0 & 0 & 0 \\ \nu & 1-\nu & \nu & 0 & 0 & 0 \\ \nu & \nu & 1-\nu & 0 & 0 & 0 \\ 0 & 0 & 0 & 0.5-\nu & 0 & 0 \\ 0 & 0 & 0 & 0 & 0.5-\nu & 0 \\ 0 & 0 & 0 & 0 & 0 & 0.5-\nu \end{bmatrix} \tag{5.21}$$

Where, E is modulus of elasticity and ν is Poisson's ratio.

Strain energy stored in element can be calculated from

$$U = \int_V \frac{1}{2} [\sigma]^T \{\varepsilon\} dV \tag{5.22}$$

or, $$U = \int_V \frac{1}{2} ([D][B]\{q\})^T [B]\{q\} dx dy dz \tag{5.23}$$

$$\text{or, } U = \sum_e \frac{1}{2}\{q\}^T \left[\int_{-1}^{1}\int_{-1}^{1}\int_{-1}^{1} [B]^T [D][B] \det[J] d\xi d\eta d\zeta \right] \{q\} \quad 5.24$$

where $dxdydz = \det[J] d\xi d\eta d\zeta$

$$\text{or, } U = \sum_e \frac{1}{2}\{q\}^T [K]_s^e \{q\} \quad 5.25$$

Then element stiffness matrix for solid element is given by

$$[K]_s^e = \left[\int_{-1}^{1}\int_{-1}^{1}\int_{-1}^{1} [B]^T [D][B] \det[J] d\xi d\eta d\zeta \right] \quad 5.26$$

The displacement of joint element depends upon relative movement of top and bottom solid elements (Fig. 5.2), and corresponding stiffness matrix for zero thickness joint elements is formulated (Zienkiewicz et al. 1970, Beer 1985 and Tzamtzis and Asteris 2004) through eqs. 5.27-5.32.

$$N_i = \frac{1}{4}(1+\xi_i\xi)(1+\eta_i\eta) \quad 5.27$$

Relative difference can be obtained from deducting bottom displacement from top

$$\{u\} = \{u\}_{TOP} - \{u\}_{BOTTOM} \quad 5.28$$

$$\text{Or, } \{u\} = ([N]\{q\})_{TOP} - ([N]\{q\})_{BOTTOM} = [N]\{q\} \quad 5.29$$

$$\text{or, } \begin{Bmatrix} u \\ v \\ w \end{Bmatrix} = \begin{bmatrix} -N_1 & 0 & 0 & -N_2 & 0 & 0 & .. & .. & N_4 & 0 & 0 \\ 0 & -N_1 & 0 & 0 & -N_2 & 0 & .. & .. & 0 & N_4 & 0 \\ 0 & 0 & -N_1 & 0 & 0 & -N_2 & .. & .. & 0 & 0 & N_4 \end{bmatrix} \begin{Bmatrix} u_1 \\ v_1 \\ w_1 \\ .. \\ .. \\ u_8 \\ v_8 \\ w_8 \end{Bmatrix} \quad 5.30$$

$$[K]_j^e = \left[\int_{-1}^{1}\int_{-1}^{1} [N]^T [k][N] \det[J] d\xi d\eta \right] \quad 5.31$$

$$[k]=\begin{bmatrix} k_{sx} & 0 & 0 \\ 0 & k_{sy} & 0 \\ 0 & 0 & k_n \end{bmatrix} \quad 5.32$$

where, k_{sx}, k_{sy} and k_{sn} are components (shear stiffness along x direction, shear stiffness along y direction and normal stiffness) of material property matrix [k] of joint, [N] and [J] are shape function, and Jacobian matrices, and ξ and η are local coordinates. Normal and shear stiffness are calculated by regarding the wall as a series of two vertical springs, one representing the stone unit and the other representing the joint which leads to the following Lourenco 2005.

$$k_n = \frac{1}{h\left(\frac{1}{E_{wall}} - \frac{1}{E_{unit}}\right)} \quad 5.33$$

$$k_s = \frac{k_n}{2(1+\nu)} \quad 5.34$$

where k_n is normal stiffness of joint, k_s is shear stiffness of joint, h is height of unit (average height of stone unit), E_{wall} is Young's modulus of elasticity of wall, E_{unit} is Young's modulus of elasticity of unit and is taken equal to 15,500N/mm^2, and υ is Poisson's ratio (assumed equal to 0.2).

The modulus of elasticity is dependent on many factors such as type of stone, workmanship, void inside the wall etc. A wide range of values have been proposed in literature (Ref. 69) varying from 200-1000 N/mm^2. In situ tests were carried out in Faial Island, Azores (Costa 2002), and the modulus of elasticity of random rubble stone masonry wall was found to be 200N/mm^2. This value corresponds to 1.3% of the modulus of elasticity of stone and has been used in this study.

In order to get the damping matrix (eq. 5.35), the mass and stiffness proportional to Rayleigh damping has been used.

$$[C]=\alpha[M]+\beta[K] \quad 5.35$$

where, α and β are coefficients selected to control the damping ratios of the lowest and highest modes expected to contribute significantly to the response.

Unfortunately, there is a sever lack of data available on damping parameters in linear solid mechanics problems, and even less information is available on damping in non linear dynamic analysis. Tzamtzis and Asteris 2004 did dynamic analysis of brick masonry wall by using quite high damping coefficients and found that the numerical simulation was matching with experimental results. At multiple modes of vibrations, damping ratios change with natural frequencies because of different mass participation factors at different modes (Tzamtzis and Asteris 2002). For the problem under consideration the coefficients α and β have been taken as 0.0555 and 0.0105 respectively so as to maintain initial value of damping (Tzamtzis and Asteris 2002 and Costa 2002) 6% and maximum value 10% considering dry masonry constructions are highly deformable.

5.3 Constitutive relationship

The joint is characterized as fully elastic, perfectly plastic and incapable of taking any tensile forces. The idealized constitutive relationship shown in Fig. 5.3 has been used to denote the sliding and opening of joint. Separation occurs when the normal strain is greater than zero and since the joint cannot take any tensile stress and both act in the normal direction, the shear stiffness has also been set to zero. Contact occurs when normal strain is less than zero, and normal forces are assumed to be restored corresponding to the normal stiffness of the joint. Sliding occurs when the shear at joints exceeds the value given by the Mohr-Coulomb yield criterion (eq. 5.36).

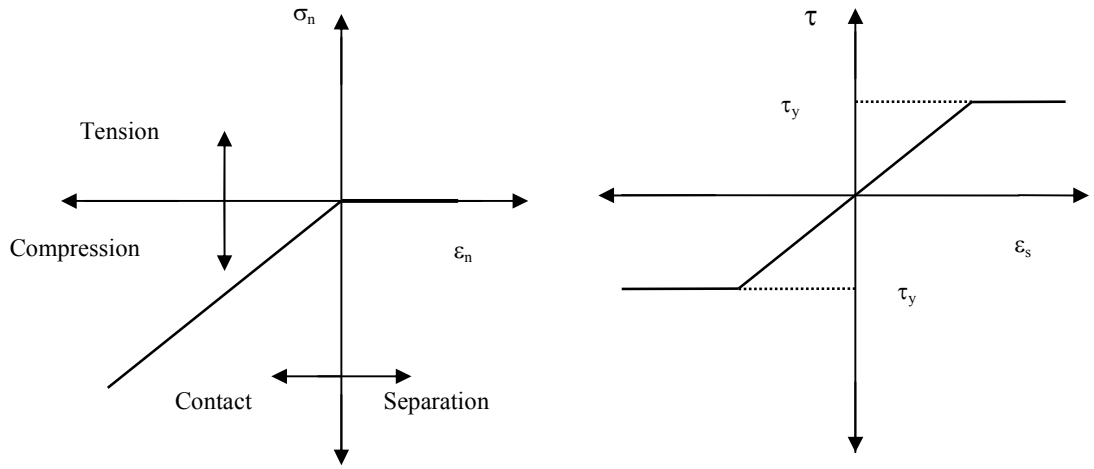

Fig. 5.3 Constitutive relationships for joints in normal (left) and shear (right)

$$\tau_y = c + \sigma_n \tan\phi \quad 5.36$$

where, τ_y is yield shear stress, c is cohesion (equal to zero being mortar less joint), σ_n is normal stress and tanϕ is coefficient of friction.

5.4 Calibration of parameters

Stiffness parameters represent the strength of the joint. In the case of brick masonry, it is calculated from the relationship between wall thicknesses, mortar thickness and the modulus of elasticity of bricks (Tzamtzis and Nath 1992). In the case of dry stone masonry there is no material between the two stones, therefore the stiffness of joint can be zero to infinity depending upon the way of thinking. In order to investigate this, a small experiment was done with wooden blocks.

Wooden blocks were cut into pieces and a dry wall (0.40mx0.08mx0.26m) was constructed as shown in Fig. 5.4. The wall was shook manually on a small table using a handle. The acceleration at the base was measured by means of an acceleration sensor and the final displacement was measured. The unit weight of wood was 4.47 KN/m^3, the modulus of elasticity (Green et al.) was taken as 8100000 KN/m^2 and Poisson's ratio as 0.3. The stiffness (k_n=2883430 KN/m^3, k_s=1201430 KN/m^3) were calculated using equations 5.33 and 5.34 assuming the modulus of wall was 1.3% of the unit. The dry wall structure is a discontinuous, highly deformable system and is similar to dry stone masonry houses, therefore the same Rayleigh damping coefficients (α=0.0555, β=0.0105) were assumed. The coefficient of friction was simply measured by putting a block over flat base and raising the base gradually. When the block started to move angle was noted and average of tangent of values was found 0.3. Our ultimate goal is to analyze the LSM house, thus parameters have been taken focusing appropriateness for stone masonry houses. Purpose of calibration analysis is to see the suitability of parameters itself. Finally, a finite element model of the wall considering the wooden blocks as solid and interfaces as joint elements was made.

Using the above mentioned parameters and an acceleration time history (Fig. 5.5) obtained from a previous shaking test, a dynamic analysis was carried out. The displacements obtained from the experiment (Fig. 5.6) and numerical simulations (Fig. 5.7) were plotted. A comparison of displacements measured along height of the model wall has been plotted as shown in Fig. 5.8. Due

to the inconsistent friction between elements and possibly human error, this is considered inevitable. However, the average displacements obtained in the experiment of the two edges are in good agreement with the numerical result. The numerical simulation gives 3.4 cm displacement at the top and the average (left edge and right edge) displacement of the experimental wall was also 3.5 cm.

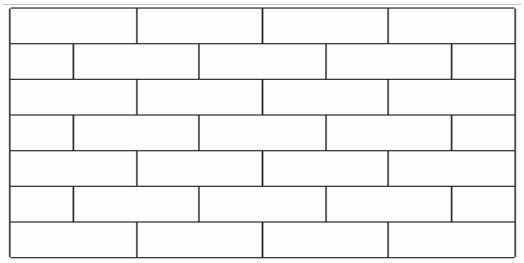

Fig. 5.4 Wood block wall (0.40mx0.08mx0.26m)

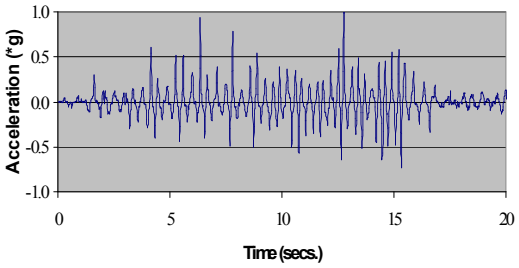

Fig. 5.5 Measured acceleration at the base of wall

Fig. 5.6 deformed wood wall after experiment

In discontinuous systems, behaviour of individual element affects the overall response. However, measured residual deformation at the end of the test is consistent with numerical result though

positions of individual elements are not consistent. That is because of different frictional values among the elements. But in numerical analysis, same friction coefficient was employed for all elements. Though movement of individual elements and energy dissipation at each time step have effects in overall response, it is not practical for big models which may have thousands of elements like stone masonry house which are dealing here. So, the deformations of individual elements have not been measured at each time step.

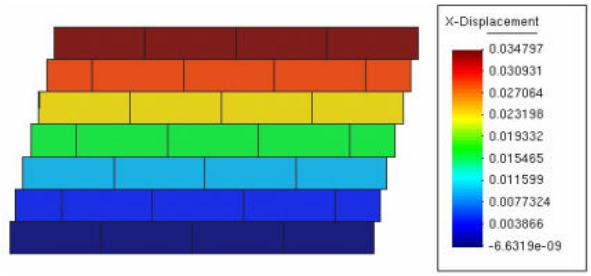

Fig. 5.7 Simulated displacement of wooden wall

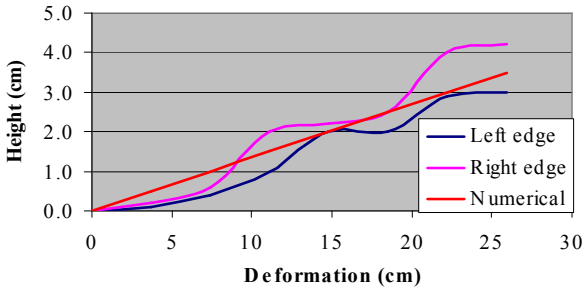

Fig. 5.8 Comparison of displacements

5.5 Description of model houses and analyses

Two typical types of single storey houses, one with a single room with an internal size 4.05mx3.15m and the other with two rooms of equal internal sizes of 3.15mx3.60m, and both with wall thickness 0.45m were modeled. The roof load depends on what type of roofing is used. Approximate calculations suggest a roof load equal to 1.5KN/m^2 which represents a thin slate roof, would be a good average considering roofs could also be made of thicker slate, corrugated galvanized iron (C.G.I) sheets or thick rammed earth. The stone walls were divided into small solid elements considering joint elements between the elements. In reality, there are thousands of stone

elements of varying sizes and tens of thousands of joints in wall. For, exact representation of houses in models, these elements either units or joints should be considered separately in equal numbers. However, modeling all the stones and interfaces as built condition is very impractical, thus equivalent solid elements having length and width equal to width of wall and thickness is approximately half of the length has been taken for this study. The interfaces formed between the equivalent solid elements are considered as joint elements. For the upgraded models houses (Fig. 5.10), wooden beams are also modeled as sold elements taking the properties of wood. At the corners, the joints are rigid and considered as continuous elements. The lengths of the elements are equal to neighboring stone made solid element to identify the joint element between them. Joint elements are assigned between the wood and stone elements interfaces. Properties of joints such as normal and shear stiffness are calculated from the equation 5.33 and 5.34. They depend upon the properties and thickness of neighboring elements. Both houses were analyzed twice with and without applying wood bond beams and subjected to different ground motions. At first, static analyses were run considering self weight and roof loads. The stresses and strains obtained from static analyses were used as initial values for dynamic analyses. In dynamic analyses, roof loads were converted into masses by dividing acceleration due to gravity and allocated as lumped masses at the top nodes of walls. Material properties for wooden bond beams and coefficient of friction were taken same as used in calibration analysis. The primary purpose of the analyses is to judge the appropriateness of method to evaluate the behavior low strength masonry structures such as stone masonry houses under earthquake loadings regardless the properties of ground motion and local site effects. Once the method is found realistic, site specific earthquakes motions are considered. Thus, Kobe 1955 and El Centro 1940 earthquakes were taken. Peak accelerations of the three components of the time histories for the Kobe earthquake of 1995 and the 1940 El Centro earthquake are given in Table 5.1. The aim of this analysis is to see whether these houses can sustain large deformations. Therefore, solid elements have been assumed linear and the focus is in the non linear deformation at joints. The properties of the solid and joint elements are shown in Table 5.2 and Figs. 5.9-5.10.

Table 5.1 Peak accelerations

Earthquake	Kobe, 1995			El Centro, 1940		
Peak acceleration	X	Y	Z	X	Y	Z
(m/sec^2)	8.06	5.87	3.36	2.63	2.62	2.63

Table 5.2 Various models

SN	Description	Elements
1	One room dry stone house Element size 0.45mx0.45mx0.30m	Stone:328 Joint:586 Total:914
2	One room dry stone house with wooden bond beams Stone element :0.45mx0.45mx0.26m Wood element :0.45mx0.45mx0.08m	Stone:328 Wood:170 Joint:766 Total:1264
3	Two room dry stone house Element size:0.45mx0.45mx0.30m	Stone:524 Joint:951 Total:1475
4	Two room dry stone house with wooden bond beams Stone element: 0.45mx0.45mx0.26m Wood element :0.45mx0.45mx0.08m	Stone:524 Wood:272 Joint:1238 Total:2034

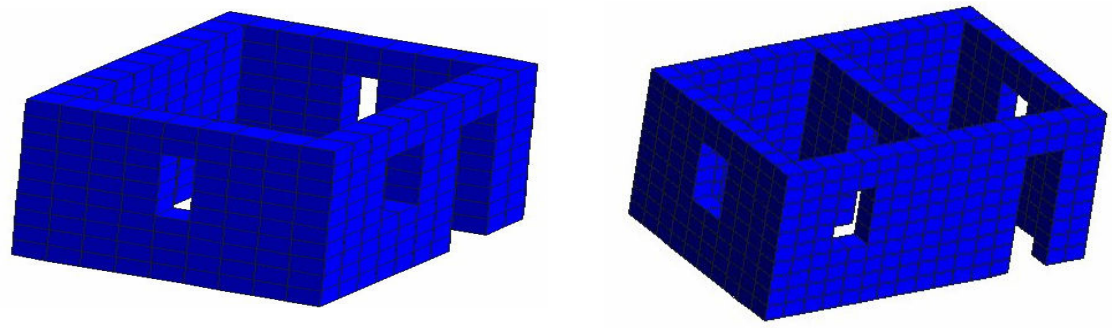

Fig.5. 9 Model houses (single room –left and two room- right) without bond beams

Four different models with varying sizes of elements, numbers of rooms and material used were prepared:

1. Model 1 is single storey, one room house with a lintel beam over the opening. The lintel beam is assumed to have the same properties of as the stone.
2. Model 2 is similar to model 1 but has horizontal wood bond beams at 0.52m interval.

3. Model 3 is single storey, two room house with lintel beam above opening.
4. Model 4 is the same as model 3 but has wood bond beams added at 0.52 m intervals.

The details of the numbers of elements, sizes etc. are shown in Table 5.2. The model houses are shown in Figs. 5.9 and 5.10 in which the pink colored continuous elements represent the wood bond beams and the blue elements are stone elements and vertical and horizontal lines are joints.

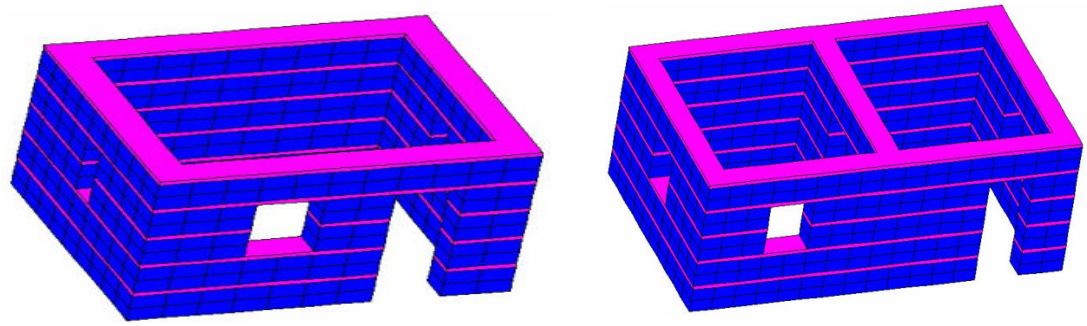

Fig. 5.10 Model houses (single room-left and two room - right) with wood bond beam

5.6 Discussion

The four models for the two houses described above were analyzed using various ground motions and their deformations and stresses are plotted in Figs. 5.11-5.16. The various colors in the Figs. have shown the deformations and stresses at the walls. The values related to various colors are shown in box at the right side of the corresponding Figs. Initially, model 2 was analyzed using the Kobe earthquake time history. The acceleration was too high for the masonry building and the house produced large deformations (Fig. 5.11) within 8 secs. The reason why displacements were much larger along the x direction as compared to the y direction was due to the large accelerations in that direction (Table 5.1).

In all of the analyses, when deformation exceeded 30 cm, the program automatically stopped due to the large deformations. The limit 30cm is arbitrarily assumed value. It can be less or more. Even if it is not assigned the program runs to final step. It can simulate beyond this limit also, however, as the displacement increase the nonlinear iterations also increase and it directly elongates the

computation time. The stone masonry houses are very weak and cracks are formed and become unserviceable even in few centimeters residual deformations. Average length of random rubble stone used in masonry house is less than 20cm. If residual deformation exceeds 30cm, most of the stones are dislocated from its original position and the house is no more usable. Our aim is not to look whole collapse process. If we are looking for effectiveness of wood bond beam, the deformation of such houses under seismic loadings should be less than the few centimeters.

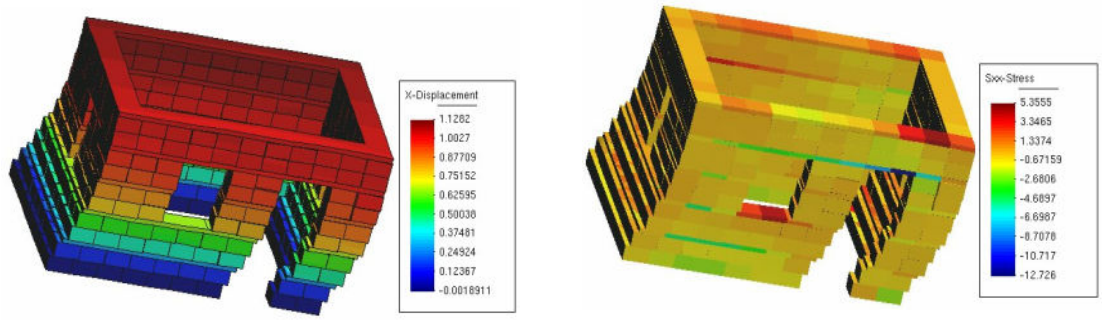

Fig. 5.11 Response of model 2 house in Kobe earthquake (deformations-left and stresses-right)

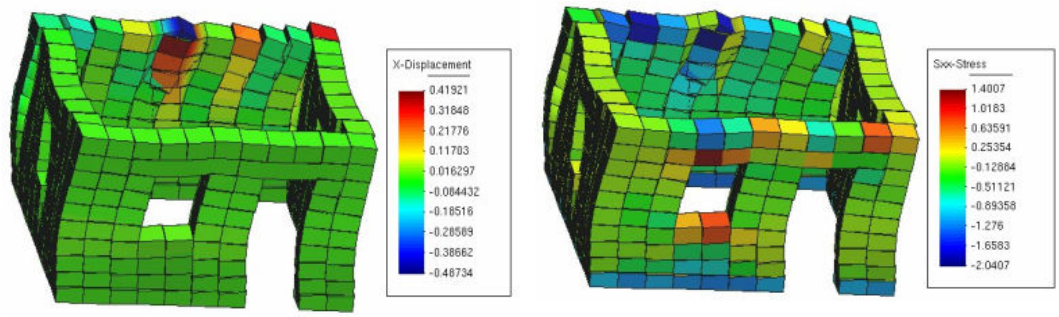

Fig. 5.12 Response of model 1 house in El Centro earthquake (deformations-left and stresses-right)

The stresses in all Figs. are in ton/m^2 and displacements are in meters. Model 1 does not have any seismic band and is weaker than model 2, thus it will be meaningless to analyze using the input motions of the Kobe earthquake. Therefore, model 1 was analyzed in El Centro earthquake. The deformations and stresses are shown in Fig. 5.12. It sustained large deformations quickly. In Fig. 5.12, we can see deformations were higher in the back wall than in the front. This is because rigid lintel beams were placed over the openings, which did not deform and strengthened the walls and

eventually, the house failed due to the separation of the weaker wall. In model 2, which was analyzed with the El Centro ground motion, the structure was found to perform well as shown in Fig. 5.13. In order to test the performance limit, model 2 was analyzed again with an amplification of 2 of the El Centro ground motion; this deformed with large displacements (Fig. 5.14). Subsequently, the response of the two room house as represented by model 3 was analyzed subjected to the El Centro earthquake ground motion.

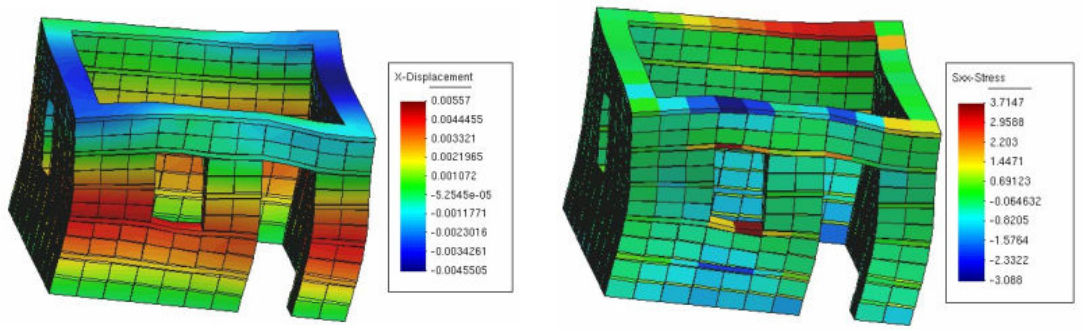

Fig. 5.13 Response of model 2 house in El Centro earthquake (deformations-left and stresses-right)

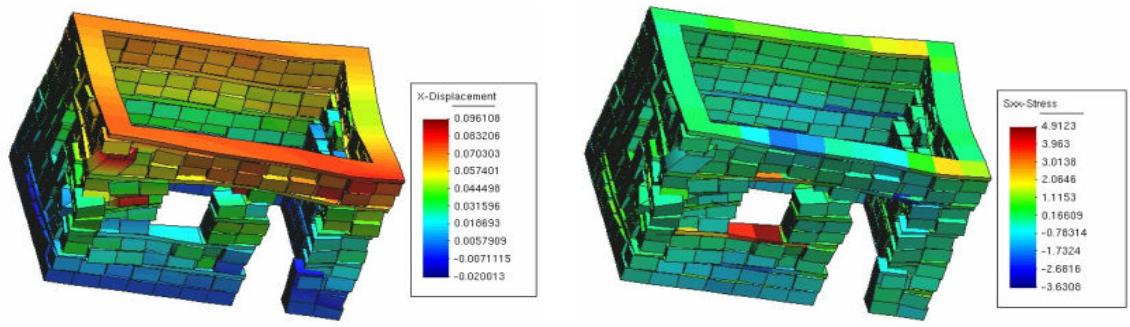

Fig. 5.14 Model 2 house in 200% El Centro earthquake (deformations-left and stresses-right)

To examine the response of a two-room house, model 3 was analyzed using the El Centro earthquake motion. Like in model 1, model 3 also sustained large deformations and failed due to separation of the back wall (Fig. 5.15). Model 4 building was analyzed using the same input motion and was found to perform well (Fig. 5.16) like model 2. In conclusion, both model 2 and model 4 houses which had been strengthened by wood bond beam deformed less than 6mm and showed good performance under earthquake loading.

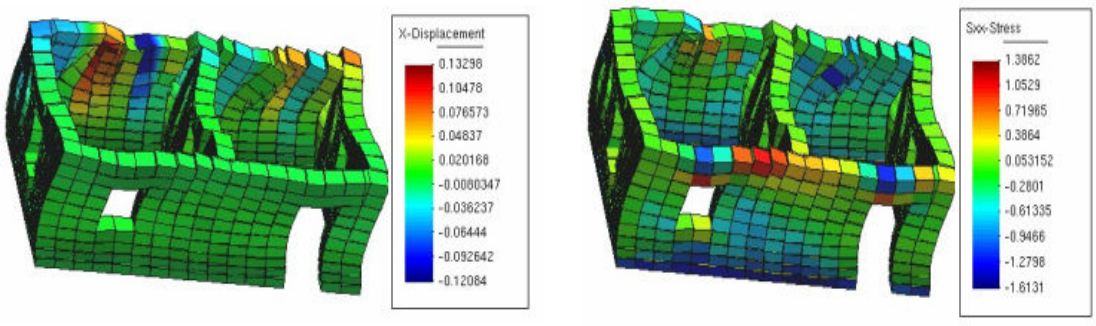

Fig. 5.15 Response of model 3 house in El Centro earthquake (deformations-left and stresses-right)

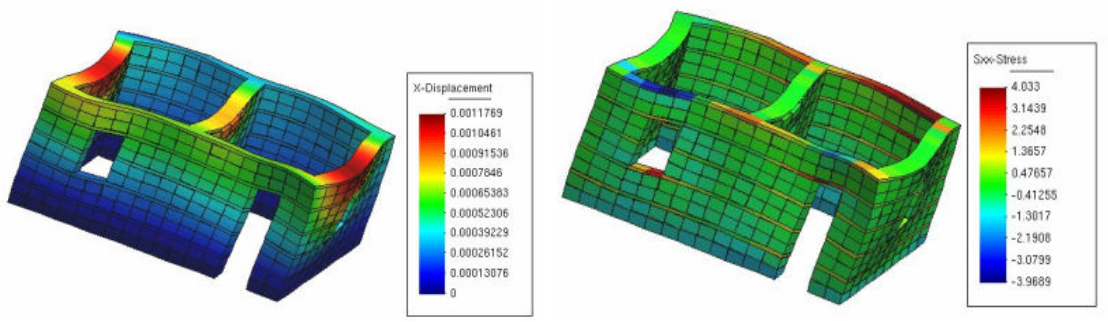

Fig. 5.16 Response of model 4 house in El Centro earthquake (deformations-left and stresses-right)

Stone blocks considered in the numerical analysis consist of equivalent block of many different sized stones. If the stone sizes vary each other, moduli of elasticity of walls also vary. It directly affects the value of stiffness constants. As irregular sized stones increase, wall becomes weaker and spring constants are less than that of regular sized stone wall. However, blocks should be as small as the average size of stone in the wall. In these simulations, the wall was divided making the length and breadth of the element equal to the width of the wall and the height equal to nearly half of the length. Width of wall has been taken as the reference for size of elements. In order to see size effect, the elements were further subdivided and analyzed. The differences of deformations are negligible but computation time increased by far. However, even a small house consists of thousand of units; and each unit will possess different properties and shapes and therefore show different behaviour. In this regard this model may be still too generic. If the elements are again further divided into small elements, computation time would be too long and is therefore governed by the level of accuracy required. Thus, size of elements considering the width of wall can give reasonable response.

Four models from two typical types of houses were analyzed under various ground motions. If a stronger earthquake such as the Kobe earthquake is expected, wooden bond beam alone would not be able to resist the collapse of these houses. Under slightly lower acceleration levels, such as when the houses experienced an acceleration level twice that of the El Centro event, the houses still sustained very large deformations and failed. In the El Centro earthquake, the peak acceleration was about 0.31g and testing under this input ground motion, the houses without wooden bond beams still failed, but houses constructed with the additional wooden beam did not.

The main possible failure mechanism for stone masonry houses are skin splitting, vertical cracking at corners, separation of wall, wedge shape failure and diagonal cracking. If we looked at the figures we can find most of them in this study also. In Fig. 5.11, houses failed in shear and swept to collapse. Kobe 1995 earthquake's acceleration is so high that LSM house can not resist. In usual practice, lintel beams (Figs. 5.12 and 5.15) are often provided over the openings even in unreinforced LSM houses. Lintel beam is not provided at back side wall and it is the weakest one. Thus corner cracking starts at the junction of two walls leading to large deformation. This may be reasonable as more than forty percent houses had damaged in El Centro earthquake. In Fig. 5.14, two times amplified El Centro 1940 was given, corner and diagonal cracks have formed near openings leading to collapse, which is quite natural since area around openings are the weakest zones. Both one and two roomed wooden beam reinforced houses (Figs. 5.13 and 5.16) performed well under El Centro 1940 earthquake. The key point here is that the coefficient of friction was taken as 0.3 and the peak acceleration was 0.31g. Theoretically, sliding should not occur until 0.3g therefore the question arises as to why model 1 failed since it had equal friction. One possible explanation is that the house in model 1 experienced tension first, which the caused separation and there was nothing between the stones to control the tension leading ultimately to failure, even though it still had spare shear capacity. The wood bond beams modeled here assume rigid connections at their edges, where elements are linear and have negligible deformation which in turn confines the wall and the stone elements. Forces at the joints develop where there are relative displacements. Wood beams break vertical joints, hold the corners effectively and join the two wythes which are responsible for diagonal cracks, separation of wall and forming vertical cracks at corners and splitting of wall into two folds respectively. A single wood beam connects many stone elements and is therefore responsible for controlling the deformation of many joints.

Displacements generated by models 2 and 4 were low. There are 3 possible explanations for this:

1. Firstly, there are no precise and predetermined values of permissible displacements or drift for these types of houses to define a credible failure mechanism. Very small tensile forces could lead to collapse of these structures because of bulging, which is the prominent failure mode of double-leaved stone masonry walls. There is no bonding between the elements and although the presence of a wood beam could reduce the deformation substantially, the rest of the wall not attached to the wood beam could still fail due to tensile forces at the joints.
2. Secondly, this may be due to the method of modeling. In a real wall, there are many stone blocks between the two beams but in this model there are only two blocks along vertical direction. Therefore, each block would be in contact with the wooden beam, either at the top or the underside. The faces of the joint in contact with wood would deform less. Thus, the model may underestimate deformation as only one joint is free to move in the numerical analysis which is not true in the case of a real wall. If the houses are modeled with thousands of elements and joints the computation time is very long.
3. Lastly, in this analysis solid elements have been assumed linear and only large deformations at interfaces have been examined. Non linear deformation in solid elements can be significant in small deformations when the wall is confined by the wood bond beam.

To the authors' best knowledge; this was the first attempt at analyzing this type of dry stone masonry house in detail. Using similar method, few studies (Cao and Watanabe 2004 and Tzamtzis and Nath 1992) have been done in brick masonry. They are bonded by cement sand mortar and dry stone masonry houses are quite different from brick masonry. This method has been implemented in Pakistan (Schacher 2007) as disaster mitigation measure, but nobody has investigated dry stone houses analytically, numerically and experimentally. Does it resist any earthquakes? How much peak acceleration can be resisted when wood bond beams are used? These questions have been addressed here, following the numerical methods that can be found in open literatures. However, the problem which we dealt is totally new and investigation presented here is novel.

5.7 Conclusion

The behaviors of two types of dry stone masonry houses under various ground motions were investigated through detailed dynamic analyses. From these analyses, it was clear that dry stone masonry houses strengthened by applying wood bond beams would not be able to resist strong

earthquakes such as Kobe 1995. However, it can be an effective technique in confining the walls under smaller ground motions similar to the El Centro earthquake of 1940. The small deformation obtained from the analyses shows that sufficient cracks could develop and make the houses inhabitable after earthquakes; however, the wood bond beams would prevent complete collapses of the dry stone masonry houses which would ensure life safety in low intensity earthquakes Thus, this could be an appropriate upgrading technique in low seismicity zones along the Alpine Himalayan Belt where these houses are common and frequent but low acceleration earthquakes are expected. Since wood can be locally available, it is the only most economical solution for upgrading these kinds of vernacular houses.

Chapter 6

EVALUATION OF MUD BONDED STONE MASONRY HOUSES AND MITIGATION

6.1 Introduction

Stone masonry houses bonded with clay or mud mortar are very common in Himalayan region across Nepal, India, Pakistan and Tibet. Typical stone masonry house s that are very common in Himalayan region are shown in Fig.6.1. Houses are generally one to two storeys and may have multiple rooms added at different stages of their history. Roofing material may vary depending on location and can be dry grass, corrugated galvanized iron sheet, slate or thick rammed earth laid over wooden joists and battons. Stone walls are built by stacking stones over stones normally in two leaves. Locally available earth mixed with water is used as bonding material between the stones. All materials are locally available and thus, the houses are very cheap. They are aimed to take vertical loads only. Thus, they may experience severe damages during earthquakes. Large numbers of population in the region are living in these kinds of houses (Desai 2001). So, there is urgent need to investigate performances of these constructions under seismic loadings. Some researchers (Spence and Coburn 1992) have given attempt to find behavior of these structures by experiments. Because of economical consequences, stone masonry houses can not be tested in lab and even it is almost impossible to do full scale. So, developments of appropriate numerical analyses are most necessary. Numerical investigations of similar constructions have been done by finite element Zienkiewicz et al. 1970, Beer 1985, Tzamtzis and Nath 1992, Tzamtzis and Asteris 2002 and Tzamtzis and Asteris 2004) and discrete element (Alexandris et al. 2004 and Papantonopoulos 2002) methods. In both methods, stones are considered as solid elements and interfaces between two stones as joint elements. However, parameters required for numerical analyses are unknown and, so far, parameters such as coefficient of friction, stiffness constants and damping etc. have been estimated by theoretical formulae (Lourenco et al. 2005, Tzamtzis and Asteris 2004 and Lourenco et al. 1997).

In order to get more precise results from numerical analyses good numerical formulations as well as appropriate parameters are necessary. A three dimensional finite element models for typical two

types of houses are made. Required parameters are estimated from shaking table tests and from theoretical formulae used by previous researchers. Using these parameters, houses are analyzed under site specific acceleration histories simulated for Pokhara City of Nepal in chapter 3. Possibility of strengthening of these houses using locally available wood bond beam are investigated. Numerical model for two kinds of buildings were made using same numerical formulation and constitutive relationship as used in chapter 5. In the previous chapter, parameters were calculated from theoretical formulae. Here, these are investigated through shaking table tests.

Fig.6.1 Typical stone masonry houses in Nepal

6.2 Investigation of parameters

6.2.1 Experimental setup

Experiments were done on the shaking table available in Katsura, Campus, Kyoto University, Japan (Fig. 6.2). It is one directional 1.5m square table and can move up to 10cm. Forcing frequencies can be given from 0.5Hz to 30 Hz and acceleration of table can go up to 2000gal. Arbitrary seismic excitation also can be applied as long as its maximum and minimum limits of frequencies, accelerations and displacements are maintained. The shaking table is controlled by hydraulic system. Inputs for the table are given as history of displacements. Two stones having size 0.30mx0.30mx0.065m were laid one over other. Bottom stone was fixed and top was made free to move. Weight of upper stone was measured 16.5kg. Two types of experiments were performed. First set of experiments were performed without any mortar between two stones (Fig.6.3) and second sets of experiments were performed with clay mortar between joints (Fig.6.4). Two accelerometers; one for table and other is for top of specimen as shown in Figs. 6.3 and 6.4 were installed to read the acceleration history of the table and specimen. Three laser sensors; one for table, other two for left and right sides of top edges of specimens were attached at 30 cm distance

from the edges of specimen on the frame installed around the table to measure the displacement of the specimen and table. The displacement history for input is given by eq.6.1

$$u(t) = u_0 \sin(2\pi f t) \tag{6.1}$$

$$\ddot{u}(t) = -(2\pi f)^2 u_0 \sin(2\pi f t) \tag{6.2}$$

$$u_0 = \frac{\ddot{u}_{\max}}{(2\pi f)^2} \tag{6.3}$$

where $u(t)$, $\ddot{u}(t)$, $\ddot{u}_{\max}$, u_0 ,f and t are displacement history, acceleration history, maximum acceleration, displacement amplitude, forcing frequency and time respectively.

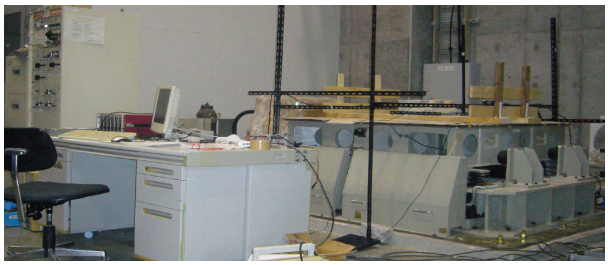

Fig. 6.2 Experimental set up

Fig. 6.3 Two stones without mortar

Fig. 6.4 Two stone with clay mortar

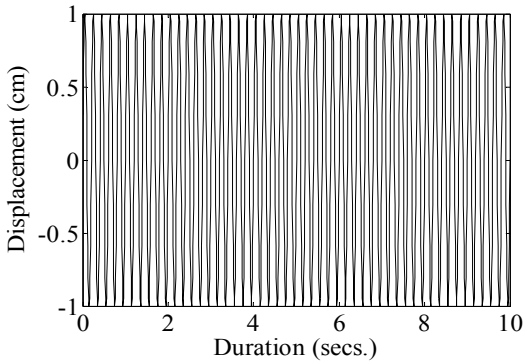

Fig 6.5 Sinusoidal wave for f=5Hz and A=1cm

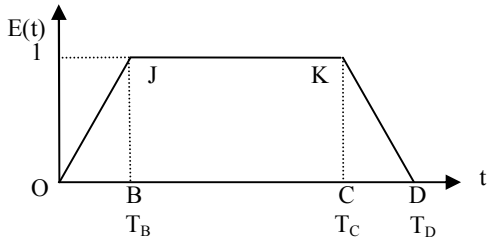

Fig. 6.6 Envelope function

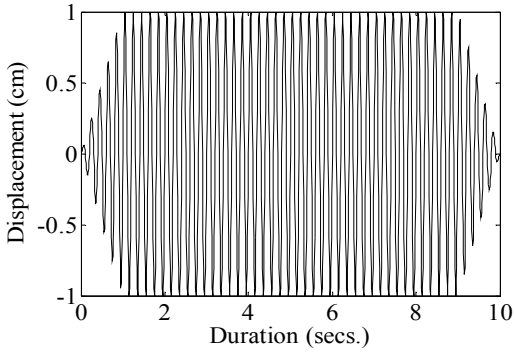

Fig. 6.7 Input wave for f=5Hz and A=1cm

The total duration is taken 10 seconds and time step is taken 0.01 sec. The experiments are aimed to increasing frequency gradually. If frequency increases, the wave attains its peak value quickly and this makes the shaking table start and stop suddenly (Fig. 6.5). Thus to avoid this situation, an envelope function was made as shown in Fig.6.4. Durations between O to B and C to D were assumed 10% of total duration and lines OJ and KD were drawn by linear interpolation. When multiplied the Fig.6.5 by envelope (Fig.6.6) the input wave becomes as shown in Fig. 6.7.

6.2.2 Coefficient of friction

Shaking experiment on dry joint stones was started taking initial frequency at 5Hz arbitrarily. Acceleration was assumed 400 gal and this value was put in eq. 6.3 which gives displacement amplitude. Then obtained displacement amplitude was substituted in eq. 6.1 to get acceleration history. As explained above, obtained history was multiplied by envelope function (Fig. 6.6) gives final wave that is applied in to the shaking table through computerized system. When table shakes, acceleration of table and upper stone were measured by accelerometers. Displacement of table and upper stones were measured by laser sensors. No relative displacements obtained between two stones. Reason behind it is friction force is strong enough to resist induced force by applied acceleration. Thus, keeping frequency constant, maximum acceleration was increased until there is relative displacement. Small relative displacement obtained when acceleration exceeded 650gal. Thus we can say that the coefficient of friction for stones is 0.65. This value is quite similar to the value 0.62 used by Lourenco et al 2005. High value of friction may be the reason that old stone made monument structures survived in great earthquakes.

6.2.3 Damping estimation

The process by which free vibration of a body diminishes its amplitude is called damping. It is measure of energy dissipation when the body is in motion. Energy dissipation occurs by several mechanisms such as friction, heat generation, plastic yielding etc. One of the methods of representing energy dissipation is equivalent viscous damping. Ntural frequency and the equivalent viscous damping for friction governing phenomenon can be estimated (eqs. 6.4 and 6.5) from hysteresis loop with maximum friction force F at displacement u_0, forcing frequency f and natural frequency f_n (Chopra 1995).

$$\xi_{eq} = \frac{2}{\pi \frac{f}{f_n}} \frac{F}{k u_0} \qquad 6.4$$

$$f_n = \frac{1}{2\pi} \sqrt{k/m} \qquad 6.5$$

where, k is stiffness and m is mass. There is nothing between the stones and stiffness of the joint can be taken as zero to infinity depending upon way of thinking. Stiffness is force per unit displacement. The experimental specimen has two stones; one is without bonding and other is with very weak mud (clay) mortar bonding between them. There are no theoretical formulae that can

estimate exact stiffness of the joint in dynamic loadings. Thus, stiffness at each step is calculated as force which is obtained by mass of stone multiplied with measured acceleration divided by relative displacement. Then maximum stiffness during effective time steps T_B to T_C is noted and natural frequency is calculated using eq. 6.5. To get clear picture of relative displacements, maximum acceleration was increased to 850 gal and the specimen was shaken giving input motion histories as explained above at frequencies 4.5Hz and 5.0Hz and obtained force per displacement and calculated frequencies are shown Table 6.1.

Table 6.1 Comparison of applied and obtained frequencies for unbonded stones

S.N	Input frequency (Hz)	Stiffness (KN/m)	Calculated frequency (Hz)
1	5.0	1162	42.3
2	5.0	1327	45.1
3	5.0	1468	47.5
4	5.0	1566	49.0
5	5.0	1134	41.7
6	4.5	1132	41.7
7	4.5	1268	44. 1
8	4.5	1433	46.9
9	4.5	1140	41.8
10	4.5	1322	45.1
Average stiffness		1295	

Similarly, other model which has two stones bonded clay mortar was also tested at frequency 5Hz and input acceleration around 900gal. At first it was not cracked and deformed very small. As experiments were repeated four-five times, stiffness was found decreasing. It is quite natural that the mortar cracks and starts to slip gradually. In five steps it was fully cracked. The results are shown in table 6.2. In order to see differences between behaviors of dry joint stones and cracked bonded stones, experiments were continued at different frequencies and at same maximum acceleration 850gal as in dry stones. The experimental results are shown in Table 6.3. The average value of stiffness obtained from the experiments on dry stones and the experiments on cracked bonded stones are similar. In existing masonry structures, though they might be bonded by earth

mortar, cracks are formed at the beginning of earthquakes tremors and behave as dry joint masonry houses.

Table 6.2 Comparison of applied and obtained frequencies for bonded stones

S.N	Input frequency (Hz)	Stiffness (KN/m)	Calculated frequency (Hz)
1	5.0	3170	69.9
2	5.0	2475	61.7
3	5.0	2242	58.7
4	5.0	2053	55.2
Maximum		3170	69.9

Table 6.3 Comparison of applied and obtained frequencies for cracked bonded stones

S.N	Input frequency (Hz)	Stiffness (KN/m)	Calculated Frequency (Hz)
1	20.0	1141	41.8
2	13.0	1470	47.5
3	12.0	1875	53.7
4	11.0	1789	52.4
5	10.0	1558	48.9
6	9.0	1490	4.65
7	8.0	1027	39.7
8	7.0	1038	39.9
9	6.0	1173	41.3
10	5.5	1176	42.5
11	5.0	1095	41.0
12	4.5	1231	43.5
13	4.0	1057	40.3
14	4.0	1265	44.1
15	4.0	1047	40.0
16	4.0	1325	45.0
17	4.0	1057	40.0
18	3.5	1024	39.7
Average		1269	

Average stiffness of Table 6.1 and Table 6.3 are almost similar. In table 6.2, difference of applied frequency is 0.5Hz while calculated frequency difference is about 7Hz. In Table 6.3, applied frequency ranges from 3.5Hz to 20Hz while calculated frequency ranges from 40Hz to 53Hz. The difference of calculated frequency is less than difference of applied frequency. In both cases calculated frequencies are almost similar. The relative displacement is totally governed by friction.

Five hysteresis curves at frequency 4.5Hz for dry joint have been plotted (Fig. 6.8-6.12). The plots show that there are irregularities in paths followed by the stone while moving under given loading. Theoretically, hysteresis loop for friction should be rectangular. However, in practical, because of irregularities of friction on sliding surfaces, the loop has been found like rhombus. In order to find maximum force (F) and its corresponding displacement (u_0) simplified loop (green line on figs. 6.8-6.12) following the paths that most of cycles were moved were drawn in all hysteresis loops. For purely rectangular, force corresponding to positive or negative displacement remains same. However, from simplified loop, we can find two values of forces. Thus, minimum force corresponding to maximum displacement is taken in order to avoid over estimation of damping. Since the phenomenon is governed by friction, stone does not move until the external force exceeds frictional force. So we can see few cycles have path near zero. As applied force exceeds friction force, then stones moves and relative displacement occurs. Relative displacements are approximately 3.5mm

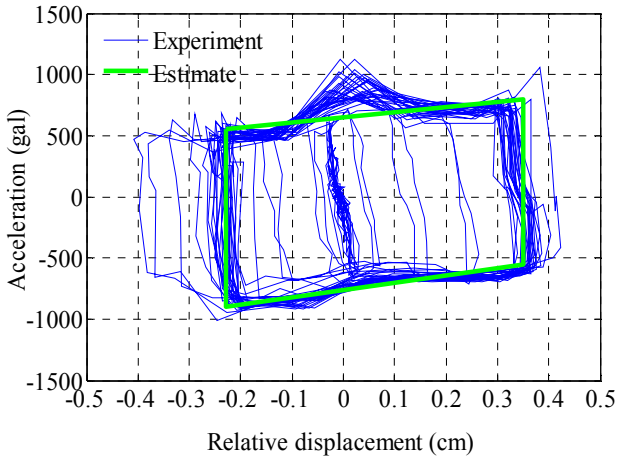

Fig. 6.8 Hysteresis curve for model 1 at f=4.5Hz and f_n=41.7Hz

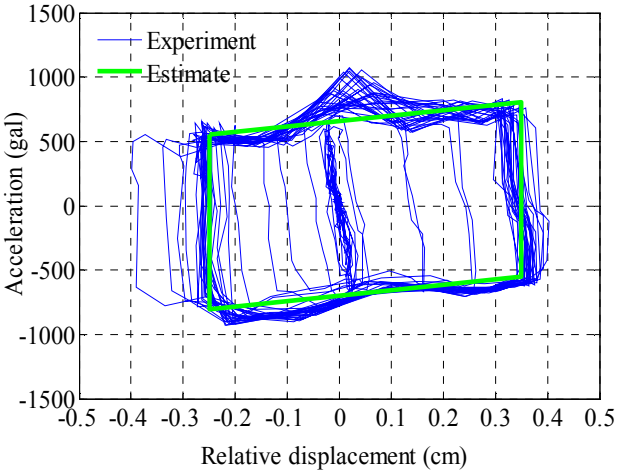

Fig. 6.9 Hysteresis curve for model 1 at f=4.5Hz and f_n=44.1Hz

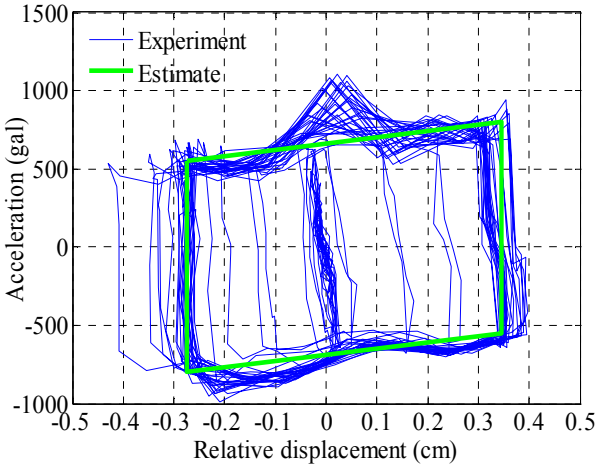

Fig. 6.10 Hysteresis curve for model 1 at f=4.5Hz and f_n=46.9Hz

The hysteresis curves (Figs. 6.8 -6.12) look very irregular and rough. The reason behind it is the unequal friction at the contact surfaces. However, at most of time steps, paths are same and have formed dark line which can be seen in the figs. 6.8-6.12. Equivalent viscous damping was calculated and shown in Table 6.4. Average damping is 12.6%. In order to get damping matrix this damping should be changed into Rayleigh coefficients. For the problem under consideration corresponding coefficients α and β have been taken as 0.05549 and 0.0105 respectively (Chowdary et al. 2003).

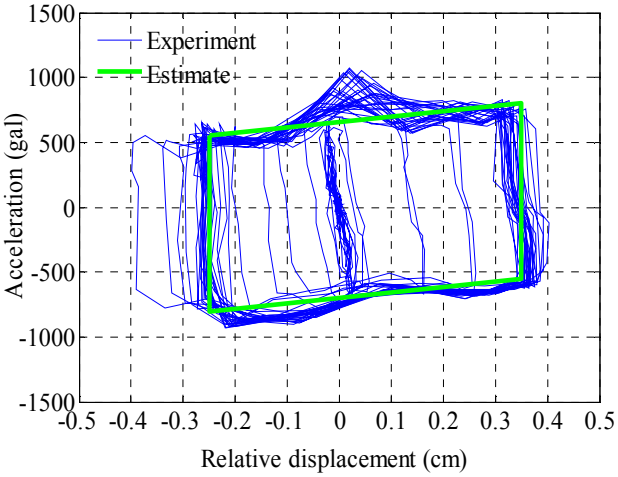

Fig. 6.11 Hysteresis curve for model 1 at f=4.5Hz and f_n=41.8Hz

The hysteresis curves look very irregular and rough. The reason behind it is the unequal friction at the contact surfaces. However, at most of time steps, paths are same and have formed dark line which can be seen in the figs. 6.8-6.12. Equivalent viscous damping was calculated and shown in Table 6.4. Average damping is 12.6%. In order to get damping matrix this damping should be changed into Rayleigh coefficients. For the problem under consideration corresponding coefficients α and β have been taken as 0.05549 and 0.0105 respectively (Chowdary et al. 2003).

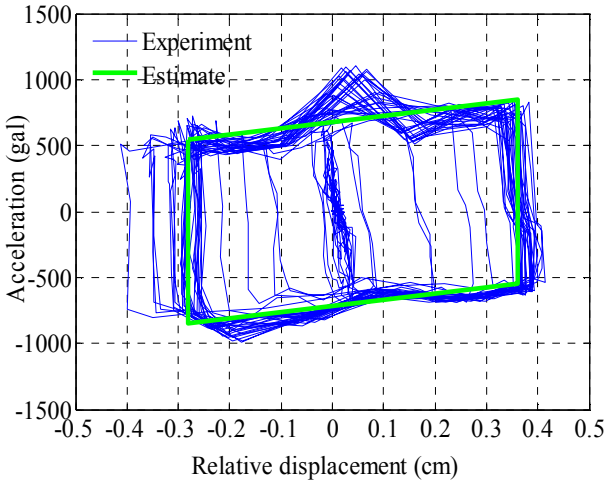

Fig. 6.12 Hysteresis curve for model 1 at f=4.5Hz and f_n=45.1Hz

Table 6.4 Damping estimate

Estimate	1	2	3	4	5
F (KN)	0.089	0.089	0.089	0.089	0.089
u_0 (cm)	0.350	0.350	0.345	0.350	0.360
f (Hz)	4.5	4.5	4.5	4.5	4.5
f_n (Hz)	41.7	44.14	46.9	41.8	45.1
k (KN/m)	1132	1268	1433	1141	1322
ξ_{eq} (%)	13.2	12.5	11.9	13.2	11.9
Average equivalent viscous damping (%)					12.6

6.2.4 Stiffness, modulus of elasticity and Poison's ratio

Stiffness coefficients for material property matrices (eq. 5.31-5.31) are calculated from the equations 5.33 and 5.34 as explained in previous chapter. Young's modulus of elasticity of stone and is taken equal to 15,500N/mm^2 and Poison's ratio is equal to 0.2 (Lourenco et al. 2005).The modulus of elasticity of wall is dependent on many factors such as type of stone, workmanship, void inside the wall etc. A wide range of values have been proposed in literatures varying from 200-1000 N/mm^2. In situ tests were carried out in Faial Island, Azores (Costa 2002), and the modulus of elasticity and unit weight of random rubble stone masonry wall was found to be 200N/mm^2 and 17KN/m^3 respectively. This value corresponds to 1.3% of the modulus of elasticity of stone and has been used in this study. The unit weight of wood was 4.47 KN/m^3, the modulus of elasticity (Green et al.) and Poison's ratio were taken was taken 8100000 KN/m^2 and 0.3 respectively.

6.3 Modeling of stone masonry houses

Two typical representative houses are modeled. Model 1 is single room two storeys house (Fig. 6.13). It represents the house that people live and cook their meals on lower storey and store agriculture products such as rice wheat millet etc. at upper storeys. Some people use the upper storey as bed room also. Model 2 is similar to model 1 but it has big opening in the front side of lower storey (Fig. 6.14). This house is called 'Dhansar' in local language. The word 'Dhansar' comes from the house to store rice. Thus, people use upper storey as store of agriculture products or as bed room according to their desires and needs. Size of houses may vary according to people's

need. Here, houses with an average internal size 4.05mx4.05m have been analyzed. Wall thickness is 0.45m. The walls are descretized into small elements. These elements are considered as eight node solid elements and the interfaces between them are joint elements. Descretized stone wall element size is 0.45mx0.0.45x0.12m. For these elements, using eqs. 5.33 and 5.34, normal and shear stiffness are 1,701,283 KN/m^3 and 708,868 KN/m^3 were obtained.

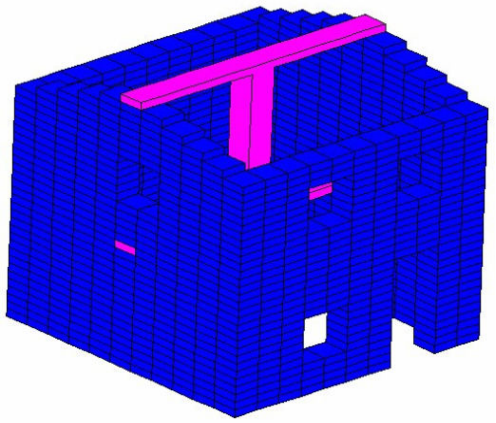

Fig. 6.13 Two storey single room house (model 1)

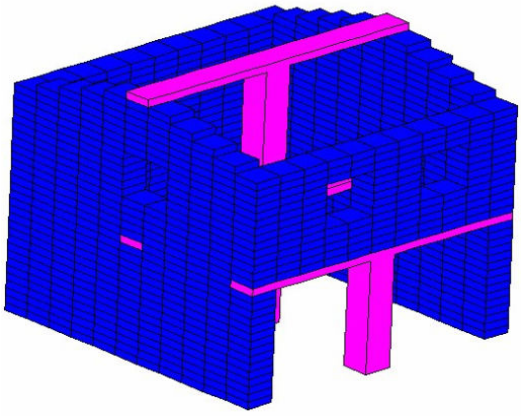

Fig. 6.14 Two storey single room house with opening (Model 2)

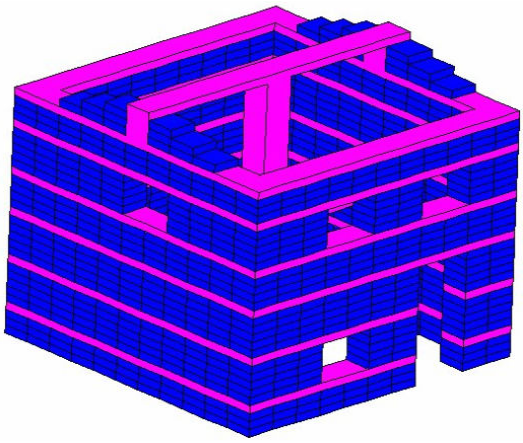

Fig. 6.15 Mitigation of model 1house with bond beams (Model 3)

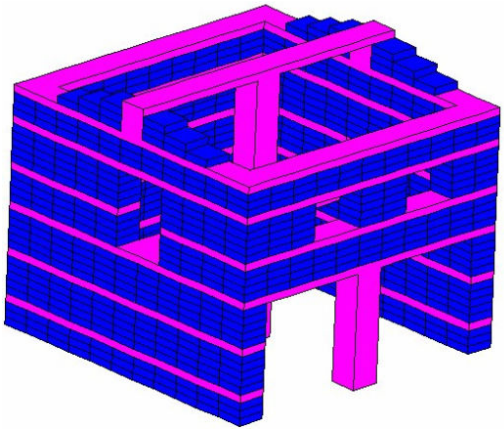

Fig. 6.16 Mitigation of model 2 house with bond beams (Model 4)

Wooden beams are also descretized in similar way as stone walls to make joint detection easy. Wooden columns are descretized according to their width and thickness of the elements are maintained same as stone elements. The roof load depends on what type of roofing is used. Approximate calculations suggest a roof load equal to 1.5KN/m^2 which represents a thin slate roof, would be a good average considering roofs could also be made of thicker slate, corrugated galvanized iron (C.G.I) sheets or thick rammed earth. Since these houses are very weak, as mitigation measure or alternative, locally available wooden bond beams are added at different heights. Thus, model 3 (Fig.6.15) is mitigation for model 1 house and model 4 (Fig.6.16) is mitigation for model 2 house have been proposed. Details of elements present in all models are shown in Table 6.5.

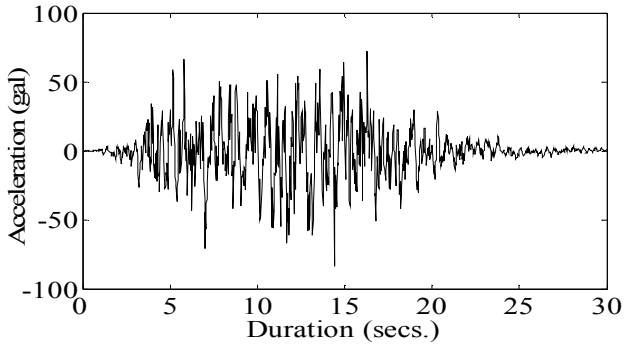

Fig. 6.17 40% in 50 years earthquake ground motion

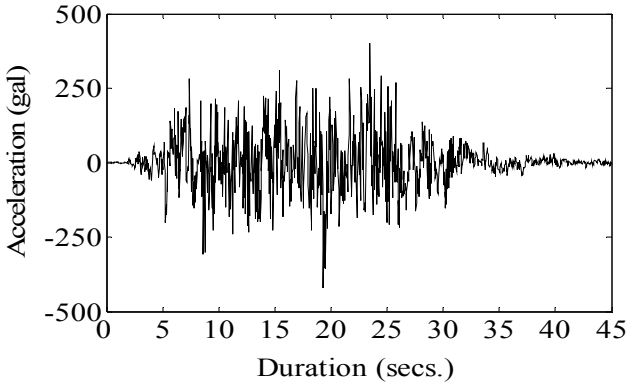

Fig. 6.17 10% in 50 years earthquake ground motion

Table 6.5, Details of various models

Model	Elements			
	Stone	Wood	Joint	Total
1	1170	55	2252	3477
2	1064	81	2059	3204
3	958	295	2071	3324
4	861	292	1856	3009

6.4 Results and discussion

FEM model was prepared considering linear solid and non linear joint for stone and interfaces respectively. At first model 1 and model 2 (Figs. 6.13 and 6.14) houses were analyzed subjected to 40% in 50 years (98 yrs RT) earthquake ground motions (Fig. 6.17) for the region taking time increment 0.01sec. Prior to dynamic analysis, static analyses were run considering self weight and roof loads. The stresses and strains obtained from static analyses were used as initial values for dynamic analyses. In dynamic analyses, roof loads were converted into masses by dividing acceleration due to gravity and allocated as lumped masses at the top nodes of walls. The deformations and stresses on houses have shown in Figs. 6.19-6.30 in various colors. The weights of colors have been shown in the box right side of all Figs. The Both houses performed weak (Figs. 6.19 and 6.20). The residual deformations exceeded 5cm which mean that the houses may have big cracks making unserviceable. Higher deformations are found near the openings and at top elements. Then proposed mitigated houses, model 3 and 4 (Figs. 6.15 and 6.18) were analyzed under same earthquake ground motion and found well performed (Fig. 6.21 and 6.22). The deformations are less than 2mm. Thus, the proposed mitigation measure is quite enough to resist the 40% in 50 years (98 yrs RT) earthquake ground motion. Then, in order to find out the capacity of wooden bond beams added houses, model 3 and 4 houses were analyzed under 10% in 50 years (475 yrs RT) earthquake ground motion (Fig. 6.18). Both houses were sustained very large deformations after 20 secs. (Figs. 6.23 and 6.24).When the residual deformations exceed 20cm, the elements are displaced about half of their length. In actual case, length of stones is less than 20cm. Thus, 20cm displacement means stones are totally dislocated from their positions. In this case, houses are certain to collapse or sustain sever damages. The analyses beyond this deformation are meaningless. Thus, program was made to stop. This analyses show that mud bonded stone masonry houses are

very weak and can not resist the very frequent and low acceleration earthquakes also. The peak accelerations of 98 and 475 yrs RT earthquake ground motion are 90gal and 450gal respectively. The durations are 30 and 45 secs. for 98 and 475 yrs RT earthquake ground motions respectively.

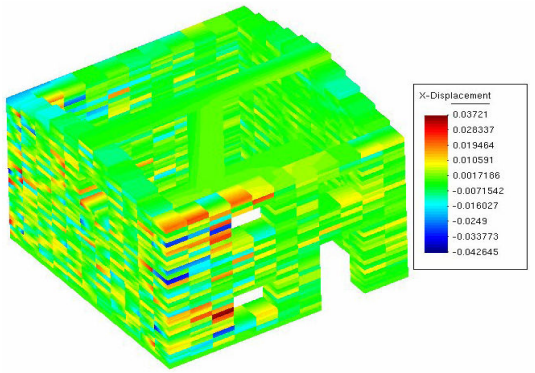

Fig. 6.19 Deformations in model 1 under 98 yrs RT earthquake

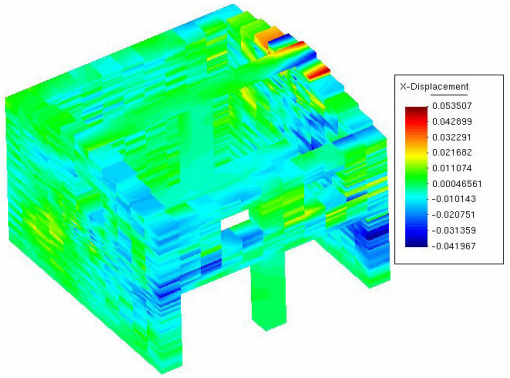

Fig. 6.20 Deformations in model 2 under 98 yrs RT earthquake

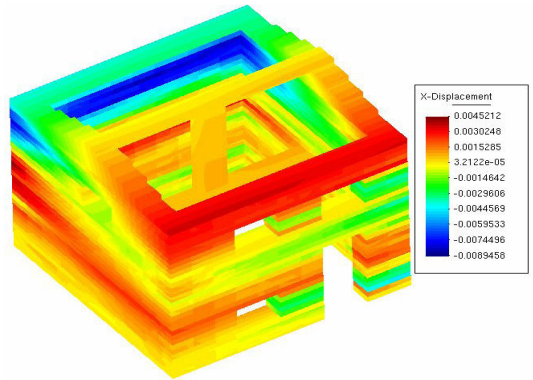

Fig. 6.21 Deformations in model 3 under 98 yrs RT earthquake

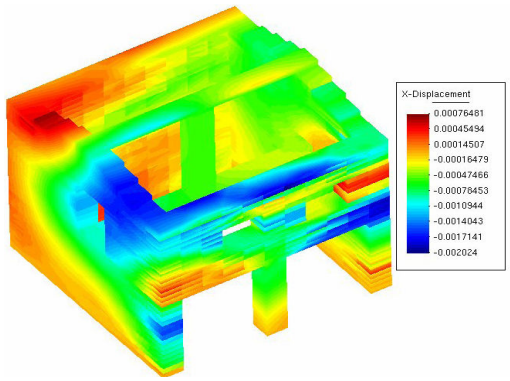

Fig. 6.22 Deformations in model 4 under 98 yrs RT earthquake

The mitigated houses were experienced severe deformation after 20 secs. under 475 RT earthquake ground motion. It means that wooden bond beams added houses can not resist peak ground acceleration 450gal and more. There are approximately 350 gal and 377 years differences between two motions. They can resist earthquakes less than 475 years return period. To find more reliable period of years that these houses can resist, more analyses using acceleration histories for other periods of years are necessary. However, mitigated houses can resist frequent earthquakes.

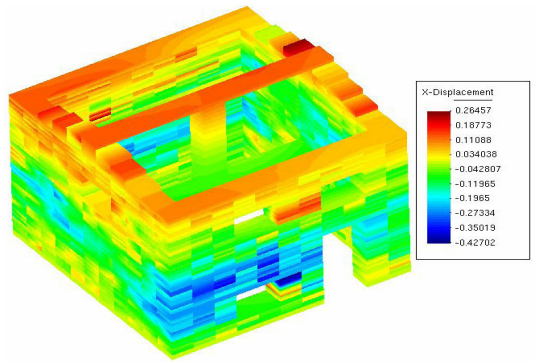

Fig. 6.23 Deformations in model 3 under 475 yrs RT earthquake

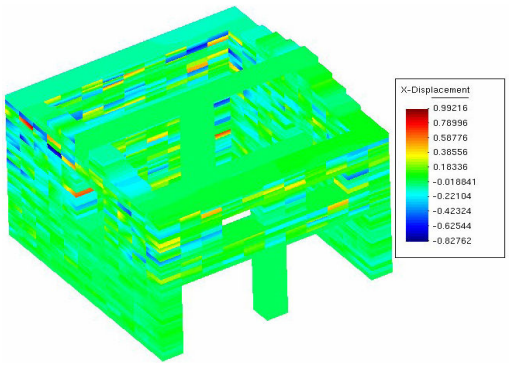

Fig. 6.24 Deformations in model 4 under 475 yrs RT earthquake

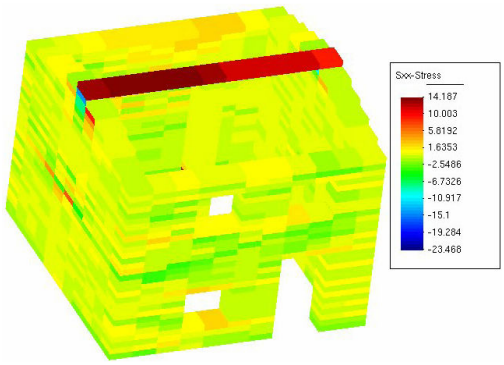

Fig. 6.25 Stresses in model 1 under 98 yrs RT earthquake

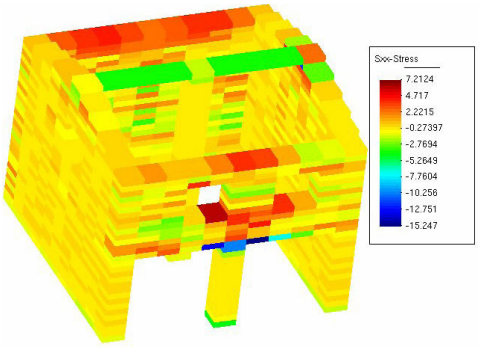

Fig. 6.26 Stresses in model 2 under 98 yrs RT earthquake

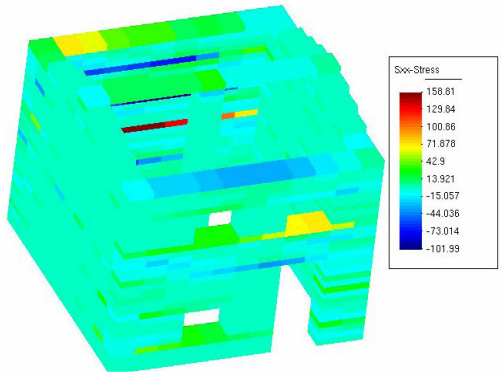

Fig. 6.27 Stresses in model 3 under 98 yrs RT earthquake

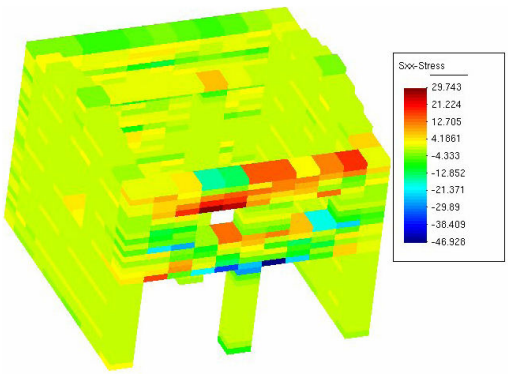

Fig. 6.28 Stresses in model 4 under 98 yrs RT earthquake

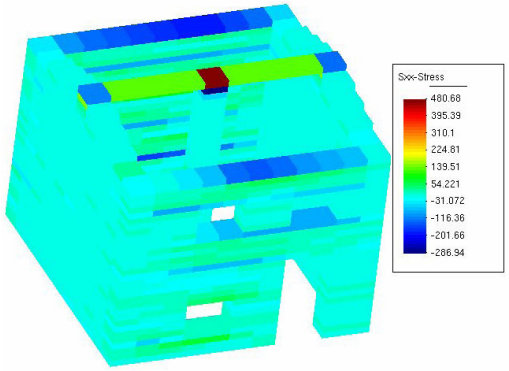

Fig. 6.29 Stresses in model 3 under 475 yrs RT earthquake

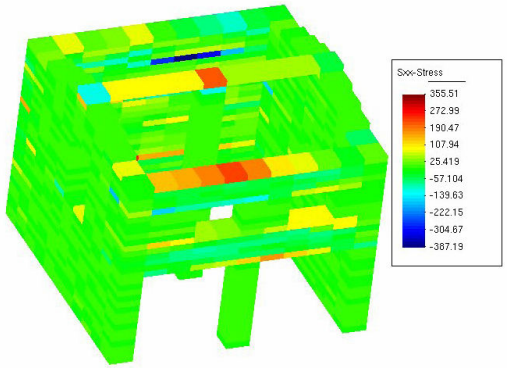

Fig. 6.30 Stresses in model 4 under 475 yrs RT earthquake

In the Figs. 6.25 and 6.26, the houses have deformed without developing big stresses. This is because of separation and slips, while, in the Figs. 6.27-6.28, houses have been have stressed which have been taken by wooden bonds beams so that their deformations have been ten times less than the unmitigated houses. However, under 475 years return period earthquakes, stresses and deformations are too much and they can not resist such acceleration and more (Figs. 6.29-6.30).

Parameters especially stiffness required for material property matrix constants were calculated buy theoretical formulae (Laurence et al. 2005) and damping and coefficient of friction were estimated experimentally. From experiments, damping was found higher than previous estimate for similar houses (Costa 2002) and phenomenon was governed by friction. This is because of discontinuity present between the elements. Because of discontinuity (joint) much energy dissipates resulting high damping. This investigation makes further clarification of what was done in previous chapter.

In recent years, many investigations have been performed regarding retrofitting of various kinds of LSM houses. However, most of the knowledge have been focused at application of steel (Costa 2002), polypropylene (Meguro 2005) and fiber reinforced polymers (Sofronie 2004) various patterns. They all are commercial materials and can be available in local rural areas. They also need trained manpower to apply. Therefore, most easy and economical solution is to use indigenous materials such as wood. The stone masonry houses are made in cheap cost. People are making and dismantling these houses frequently. Wooden beam added houses were found effective from

analysis and can also be most easy and economical solution for mitigating against frequent earthquakes from practically also. Thus, it is only the most easy and economical solution.

6.5 Conclusion

Finite element models of two typical types of mud mortar bonded stone masonry houses that can be found in Himalayan region were prepared considering stones as linear elastic solids and interfaces between the stones as non linear joint elements. Some parameters such as damping and coefficient of friction required for analysis were investigated through shaking table experiments. From the experiments, coefficient of friction was obtained 0.65 and damping for the dry stone masonry was found 12.5%. It shows that much energy dissipates at joints.

Non linear dynamic analyses using site specific acceleration histories were done. These houses were found very weak in frequent and low accelerations earthquakes also. As mitigation measure same houses were modified by using wooden bond beams and analyzed under same loadings. These mitigated houses were found effective. However, wooden bond beam used houses can not resist less frequent earthquakes such as 475 years return period earthquakes and greater. Wood is locally available and cheap also. Locally trained mason can built the houses easily. Thus, this method is the most economical solution over any other means of retrofitting measures.

Chapter 7

SUMMARY AND CONCLUSIONS

7.1 Summary

In this study, there are basic two parts; one is simulation of seismic input through probabilistic seismic hazard analysis and other is application of obtained input to dynamic analysis of stone masonry houses. Nepal and its major cities - Kathmandu and Pokhara, have been taken as study site. Three thrust (MCT, MBT, and HFT) fault systems pass throughout the length of Nepal and many small faults near Kathmandu show high seismicity in the region. Available earthquake data is not sufficient to justify the current slip rate of Himalaya. As an alternate approach, magnitude frequency relation was developed using available earthquake data, then taking slope of the fit as constant, it's other coefficient was calculated considering 50% slip rate which closely satisfies the rate of occurrences of big events and small events which are almost complete. Since no attenuation equations have been developed for the region, an attenuation equation formulated by Atkinson and Boore in 2003 which was developed for subduction zone taking worldwide earthquakes data was selected. Two different approaches; one dividing the whole region into small area sources and other using Bayesian approach to combine the occurrences from directly historical earthquakes data and digitized faults, were utilized. Assuming the occurrence of earthquakes as Poisson's process, mean rate of exceedences of horizontal ground acceleration and spectral acceleration at various natural periods were obtained. Hazard curve for the city Kathmandu, was plotted from both methods. Hazard estimate obtained from areal sources is higher than historical earthquakes and faults. Sensitivity analysis regarding the maximum magnitude was also investigated. Probabilistic seismic hazard estimate taking minimum magnitude M5, maximum magnitude M8.8, 50% intra-plate slip and area sources can give better estimate results. From this approach, probabilistic response spectra for, Kathmandu city corresponding to three return periods were plotted. This method was extended to whole Nepal to estimate hazard of the region. Contour maps showing peak ground acceleration for three various probabilities of excedences in 50 years were plotted. Significant earthquakes for the two major cities Kathmandu and Pokhara, were estimated on the basis of deaggregation of hazard for peak ground accelerations. Magnitude and distance of significant earthquakes were

found from highest weight of deaggregated hazard plot. Typically, for Pokhara city, significant durations calculated for various distances and magnitudes are multiplied by weight of corresponding to deaggregation and weighted duration for response acceleration corresponding to various natural periods were calculated. Weighted average duration for specific return period was estimated by summing up all weighted durations corresponding to various response accelerations that fall in same return period. For the city, design earthquake ground motions for three probabilities of exceedences (40%, 10% and 5%) in 50 years, were simulated.

In second phase, stone masonry houses were analyzed by giving real earthquakes and simulated acceleration histories. Two types of stone masonry houses; one is stone houses without any bonding and other is stone houses bonded with locally available soil. Because of environmental effects cracks are formed at joints and mud bonded houses also behave like dry stone masonry houses. These masonry houses are the most common type of construction in the Alpine Himalayan Belt across Pakistan, India and Nepal. They perform well under vertical loads. However, the seismic resistance of these houses is highly questionable if constructed without any form of lateral support. Since the problem is discontinuous system, a finite element model considering the stones as equivalent solid elements and discontinuities present at interfaces of elements are joint elements was made. The joints are allowed to open and close, and separation and re-contact satisfying the Mohr-Coulomb criteria. Using the program, effectiveness of wooden bond beams as a retrofit solution was examined. To calibrate the values used in the numerical modeling an experiment using a small scale wall made of wooden blocks was shaken in small custom made table. The corresponding parameters which showed good agreement with experimental results were taken as inputs for the non linear dynamic analyses of four dry stone masonry model houses under real earthquakes (Kobe 1995 and El Centro 1940). Two models were two types of houses; one room and two rooms, single storey. Other two models are same houses with addition of bond beams at various heights. Differences between with and without bond beams were investigated. The results showed that wooden bond beams can be an effective technique for upgrading low strength masonry houses in low seismicity regions

Using same methodology, mud mortar bonded stone masonry houses also were analyzed. Parameters required for the analysis were estimated both from theoretical formulae and shaking table test. Two representative houses were modeled by finite element method and analyzed under

site specific earthquake ground motions simulated for Pokhara city. The model houses performed very poor even in 98 years return period earthquakes. As a mitigation measure, modified model houses by adding wooden bond beams were run under same earthquake ground motion as they were run before. Analyses show locally available wooden bond beams can be good mitigation measure.

7.2 Conclusions

From the study through seismic hazard assessment, simulation of probabilistic earthquake ground motions (design earthquakes) and analyses of stone masonry houses giving real earthquakes and simulated design earthquakes, following conclusions are drawn. These are the new points learned from the study.

1. Available earthquake data does not satisfy the intra-plate slip of Nepal Himalayan faults. Smaller events such as less than M5 are complete. Three great events have been already recorded, great earthquakes are unlikely to miss and can be assumed as complete. Thus, taking magnitude frequency relation developed using available earthquake data is constant, other coefficient, when calculated, considering 50% slip rate satisfies closely with the rate of occurrences of big events and small events which are almost complete.
2. The hazard analysis based on latest information of earthquake records and attenuation laws is much higher than previous hazard estimate done by BECA 1993. BECA 1993 hazard estimate is also basis for building code requirements. To make civil structures safe against future earthquake, there is urgent need to revise the existing estimates incorporating the latest developments in earthquake engineering.
3. Civil structures are made for various life spans and they have various natural periods. Same earthquake time history can not be suitable for all life span structures. Thus, the method to simulate probabilistic earthquake ground motions has been developed through deaggregated hazard which can be used all structures that may have different natural periods but same life span. This method is applicable for zone where earthquake data are not available.
4. In the second part of the study, finite element numerical model considering discontinuities at the joints of dry joint stone masonry with and without added bond beams was formulated. Various model houses were analyzed under Kobe 1995 and El Centro 1940 earthquakes.

Horizontal wooden bond beam added at various layers of house was found effective in low acceleration earthquakes such as El Centro 1940.

5. Mud bonded houses were analyzed under simulated earthquakes for two return periods; 98 and 475 years return period. They are very weak and may collapse if the earthquake occurs with peak acceleration more 100 gal. However, these houses when modified with wooden bond beams can resist frequent earthquakes such as 98 years return period.

In both cases; dry stone masonry houses and mud bonded houses, wooden bond beam are effective to confine the wall so that it can resist the future earthquakes. Wood can be found locally and is cheaper than any other strengthening materials such as steel, FRP, PP bands etc. Thus, it is the most and the only one cost effective solution for strengthening these kinds of vernacular houses.

REFERENCES

1. Abrahamson, N.A., Silva and W.J. (1997). "Empirical response spectral attenuation relations for shallow crustal earthquakes." *Seismological Research Letters*, **68**(1), 94-126.
2. Albert M. L, Elwi A. E., Cheng J. J. R. (2001). "Strengthening of unreinforced masonry" *J. Compos. for Constr.* 5, 76.
3. Alexandris, A., Protopapa, E., Psycharis, I. (2004). "Collaspe mechanism of masonry buildings derived by the distinct element method", *13th World Conference on Earthquake Engineering*, Vancouver B.C., Canada, August 1-6, Paper No. 548.
4. Ambraseys, N.N. and Douglas, J. (2004). "Magnitude calibration of north Indian earthquakes." *Geophysics. J. Int*., **159**, 165-206.
5. Ambraseys, N.N. and Jackson, D. (2003). "A note on early earthquakes in northern India and southern Tibet." *Current science,* **84** (4), 570-582.
6. Atkinson, G.M. and Boore, D.M. (2003). "Empirical ground-motion relations for subduction-zone earthquakes and their application to Cascadia and other regions." *Bull. Seismol. Soc. Am*., **93** (4), 1703-1729.
7. Atkinson, G.M. and Boore, D.M.(1995). "New ground motion relations for eastern North America." *Bull. Seismol. Soc. Am*., **85** (4), 17-30.
8. Arya A. S. (2000), "Nonengineered construction in the developing countries: An approach toward earthquake risk reduction", *12th world conference on Earthquake Engineering*, Auckland, New Zealand, Index 2824, Vol 1
9. Avouac, J.P. (2003). "Mountain building, erosion, and the seismic cycle in the Nepal Himalaya." *Advances in Geophysics, Elsevier Inc*, **46**.
10. Bakis C. E., Bank L.C., Brown V. L., Cosenza E., Davalos J.F, Lesko J.J., Machida A., Rizkalla S.H., Triantafillou T.C. (2002). "Fiber-reinforced polymer composites for construction-State-of-the-art- Review", *J. Compos. for Constr.* 6, 73.
11. Bazzurro P., Cornell C.A. (1999). "Deaggregation of seismic hazard." *Bull. Seismol. Soc. Am.*, **89** (2), 501-520.
12. Beer, G., (1985). "An isoparametric joint /interface element for finite element analysis", *International Journal for Numerical methods in engineering*, (21), 585-600.
13. Benjamin, J.R. and Cornell, C.A. (1970). "Probability, Statistics, and Decision for Civil Engineers." *McGraw-Hill Book Company.*

14. Benedetti P. C. and Pezzoli P. (1998). "Shaking Table Tests on 24 simple masonry buildings", Earthquake engineering and Structural Dynamics", Vol 27:67-90.
15. Bilham, R. (1995). "Location and magnitude of the 1833 Nepal earthquake and its relation to the rupture zones contiguous great Himalayan earthquakes." *Current science,* **69** (2), 155-187.
16. Bilham, R., and Ambraseys, N. (2005). "Apparent Himalayan slip deficit from the summation of seismic moments for Himalayan earthquakes, 1500-2000." *Current science,* **88** (10), 1658-1663.
17. Bilham, R., Gaur, V. K. and Molnar, P. (2001). "Himalayan seismic hazard." Science, *www.sciencemag.org*, **293**, 1442-1444.
18. Bilham, R., Larson, K., and Freymueller, J. (1997). "GPS measurement of present-day convergence across the Nepal Himalaya." *Nature*, **386**(6).
19. BECA World International (New Zealand) in association with SILT Consultants (P.) Ltd. (Nepal), TAEC Consult (P.) Ltd. (Nepal), Golder Associates (Canada) and Urban Regional Research (USA), (1993). "Seismic Hazard Mapping and Risk Assessment for Nepal."
20. Blondet, D. Torrealva, G. Villa Garcia, F. Ginocchio, I. Madueno, "Using Industrial materials for the construction of safe adobe houses in seismic areas", Catholic University of Peru
21. Boore, D.M., Joyner, W.B., and Fumal, T.E. (1997). "Equations for estimating horizontal response spectra and peak acceleration from western North American earthquakes: A summary of recent work." *Seismological Research Letters*, **68** (1), 128-153.
22. Bruneau M (1994), "Performance of unreinforced masonry buildings", *ASCE, Journal of structural engineering*, Vol 120, No 1.
23. Campbell, K. W. (1997). "Empirical near-source attenuation relationships for horizontal and vertical components of peak ground acceleration, peak ground velocity, and pseudo-absolute acceleration response spectra." *Seismological Research Letters*, **68** (1), 154-177.
24. Campbell, K. W. (2003). "Prediction of strong ground motion using the hybrid empirical method and its use in the development of ground-motion (attenuation) relation in eastern North America." *Bull. Seismol. Soc. Am*., **93** (3), 1012-1033.
25. Campbell, K. W., and Bozorgnia, Y. (2003). "Updated near-source ground motion (attenuation) relations for the horizontal and vertical components of peak ground acceleration and acceleration response spectra." *Bull. Seismol. Soc. Am*., **93** (1), 314-331.

26. Candeias P., Costa A. C., Coelho E. (2004), "Shaking table tests of 1:3 reduced scale models of four story unreinforced masonry buildings", *13th world conference on Earthquake Engineering*, Vancouver B.C., Canada, Paper No. 2199.
27. CAO, Z., Watanabe, H. (2004). "Earthquake response prediction and retrofitting techniques of adobe structures", *13th world conference on Earthquake Engineering*, Vancouver B.C., Canada, No. 2394.
28. Chapman, M.C. (1995). "A probabilistic approach for ground motion selection for engineering design." *Bull. Seismol. Soc. Am.* **85**, 937-942.
29. Crouse, C.B. (1991). "Ground-motion attenuation equations for earthquakes on the Cascadia Subduction" zone, *Earthquake Spectra*, **7,** 201.
30. Chandrupatla, T. R. and Belegundu, A.D. (2002). *Introduction to finite element methods in engineering*, PEARSON Education.
31. Chen, Y., Liu, J., Chen, L., Chen, Q. and Chan, L.S. (1998). "Global seismic hazard assessment based on area source model and seismicity data." *Natural Hazards, Kluwer Academic Publishers*, **17**, 251-267
32. Chowdary, I. and Dasgupta, S.P. (2003), "Compulation of Rayleigh damping for large system", http://www.ejge.com/2003/Ppr0318/Ppr0318.pdf
33. Cornell, C.A. (1968). "Engineering seismic risk analysis." *Bull. Seismol. Soc. Am.*, **58** (5), 1583-1606.
34. Costa A. (2002). "Determination of mechanical properties of traditional masonry walls in dwelling of Faial Island, Azores", *Earthquake engineering and structural dynamics*, (31), 1361-1382.
35. Das S., Gupta, I.D., and Gupta, V.K. (2006). "A probabilistic seismic hazard analysis of northeast India" *Earthquake spectra*, **22**(1), 1-27.
36. Desai R. (2001). "Upgrading vernacular building system for enhanced earthquake resistance", *workshop on collaborative open source design of appropriate technologies*, MIT, Cambridge, MA, USA.
37. Dobry, R., Borcherdt, R., Crouse, C. B., Idriss, I. M., Joyner, W.B., Martin, G. R., Power, M. S., Rinne, E. E., Seed, R. B. (2000). "New site coefficients and site classification system used in recent building seismic code provisions" *Earthquake Spectra,* **16**, 41-67.
38. Ehsani M. R., Sandatmanesh H., and Al-Saidy A. (1997). "Shear behavior of URM retrofitted with FRP overlays", *Journal of composites for construction*, Vol. 1, No.173.

39. Ehsani M. R., Sandatmanesh H., and Velazquez-Dimas J. I. (1999), "Behaviour of retrofitted URM walls under simulated earthquake loading", *Journal of composites for construction*, Vol 3, No. 3.
40. El-Dakhakhni W. W, Hamid A. A., Hakam Z. H. R. and Elgaaly M. (2006) "Hazard mitigation and strengthening of unreinforced masonry walls using composites"**,** *Composite Structures*, Volume 73, Issue 4, Pages 458-477.
41. ElGawady M. A., Lestuzzi P., and Badoux M. (2005). "In-Plane Seismic Response of URM Walls Upgraded with FRP", J. Compos. for Constr. **9**, 524.Faella C., Martinelli E., Nigro E., Paciello S. (2004). 'Tuff masonry walls strengthened with a new kind of CFRP sheet: Experimental tests and analysis, *13th world conference on Earthquake Engineering*, Vancouver B.C., Canada, Paper No. 923.
42. Feldl, N., and Bilham, R. (2006). "Great Himalayan earthquakes and the Tibetan plateau." *Nature Publishing Group*, 444(9), 165-170.
43. Ghobarah K. and El Mandooh Galal (2004). "Out of plane strengthening of unreinforced masonry walls with openings", *J. Compos. for Constr.* 8, 298.
44. Green, D.W., Winandy, J.E., Kretschmann, D.E., "Mechanical properties of wood", http://www.fpl.fs.fed.us/documnts/fplgtr/fplgtr113/ch04.pdf
45. Hamid A. A., El-Dakhakhni W. W., Hakam Z. H. R., Elgaaly M. (2005). "Behaviour of composite unreinforced masonry-fiber reinforced polymer wall assemblages under in-plane loading", *J. Compos. for Constr.* 9, 73.
46. Hank, T.C., and Kanamori, H. (1979). "A moment magnitude scale." *Journal of Geophysics Res*., **84**, 2348-2350.
47. Harmsen, S., Perkins, D., and Frankel, A. (1999). "Deaggregation of probabilistic ground motions in central and eastern United States." *Bull. Seismol. Soc. Am*., **89** (1), 1-13.
48. Harmsen, S. (2001). "Mean and Modal ε in the deaggregation of probabilistic ground motions." *Seismol. Soc. Am*., **91**, (6), 1537-1552.
49. Haraguchi Y., Kiyono J., Scawthorn C. (2004). "House collapse simulation by use of 3D distinct element method", *The seventeenth KKCNN Symposium on Civil Engineering*, Dec. 13-15, Thailand.
50. Hisada Y., Shibaya A. and Ghayamghamian M. R. (2004). "Damage and Seismic Intensity in Bam City from Bam, Iran, Earthquake", *Buletin, Earthq. Res.Inst*. Univ. of Tokyo, vol 79:81-93

51. Imitiyaz, A.P. and Avadh, R. (1999). "Probabilistic assessment of earthquake hazards in the Indian subcontinent." *Pure applied geophysics*, **154**, 23-40
52. Islam S, Watanabe H, and Agrawal P. (2004)., "FEM simulation of behaviour of adobe structures", *13th world conference on Earthquake Engineering*, Vancouver B.C., Canada, Paper No. 1310.
53. Jaiswal, K., and Sinha, R. (2007). "Probabilistic seismic hazard estimation for peninsular India." *Bull. Seismol. Soc. Am*. **97** (1b), 318-330
54. Jagadish, K.S., Raghunath, S., and Narjunda Rao, K.S. (2003). "Behaviour of masonry structures during Bhuj earthquake of January 2001." *Proc. Indian Acad. Sci. (Earth Planet. Sci.)*, **112**, (3), 431-440.
55. Jouanne, F., Mugnier J. L., Gamond, J.F., Le Fort, P., Pandey, M.R., Bollinger, L., Flouzat, M., Avounac, J.P. (2004). "Current Shortening across the Himalayas of Nepal." *Geophysics. J. Int.*, **157**, 1-14
56. Katayama, T. (1982). "An engineering prediction of acceleration response spectra and its application to seismic hazard mapping." *Earthquake Engineering and Structural Dynamics*, **10**, 149-163.
57. Kawashima, K., Aizawa, K. and Takahashi, K. (1984). "Acceleration of peak ground motion and absolute acceleration response spectra." *Proc. Eight World Conference on Earthquake engineering, San Francisco*, **2**, 257-264.
58. Kawamata S. , Funaki N., Hori N., Fujita T., Inoue N., "Base Isolation system suitable for masonry houses", *13th World Conference in Earthquake Engineering*, Vancouver B.C., Canada, Paper No. 668.
59. Kataoka K., Seki M., Miyazaki M., Tsuneki Y. (2000). "A masonry school building retrofitted by base isolation technology", *12th world conference on Earthquake Engineering*, Auckland, New Zealand, Idex 1118, vol 10.
60. Kesner K. and Billington S. L. (2005). "Investigation of infill panels made from engineered cementitious composites for seismic strengthening and retrofit", *Journal of structural engineering*, *ASCE,* vol 131, No. 11.
61. Kiyono, J., Sato, T. (1992). "Risk spectrum taking into account fault rupture mechanisms." *10th World Conference on Earthquake Engineering*, *Madrid*

62. Kiyono J. and Furukawa A. (2002). "Casualty occurrence mechanism in the collapse of timber-frame houses during an earthquake", *Earthquake engineering and structural dynamics*, Issue 33, page 1233-1248.
63. Kramer, S.L. (1996). "Geotechnical earthquake engineering." *Prentice-Hall International series in Civil Engineering and Engineering Mechanics*
64. Kumar, S., Wesnousky, S.G., Rockwell, K.T., Briggs, R.W., Thakur, V.C, and Jayangondapernumal R. (2006). "Paleoseismic evidence of great surface-rupture earthquakes along the Indian Himalaya." *Journal of Geophysical research*, **111.**
65. Lave, J., Yule, D., Sapkota, S., Basnet, K., Madan, C., Attal, M., and Pandey, R. (2005). "Evidence for a great medieval earthquake (1100 A.D.) in the central Himalayas." Nepal, *Science www.sciencemag.org,* **307**
66. Lourenco, P.B. Oliveira, D.V., Roca, P., Orduna, A. (2005) "Dry joint stone masonry walls subjected to in plane combined loading", *Journal of Structural Engineering Mechanics*, ASCE, Vol. 131 (11).
67. Lourenco, P.B. and Rots, J.G. (1997), "Multisurface interface model for analysis of masonry structures", *Journal of Engineering Mechanics*, ASCE, Vol. 123 (7).
68. Lourenco P. B. (2002). "Computations on historic masonry structures", *Prog. Struct. Engng. Mater.*, 4:301-319.
69. Low rise residential construction detailing to resist earthquakes, *http://www.staff.city.ac.uk/earthquakes/Repairstrengthening/RSStoneMasonry.htm#Third%20link*
70. Luca A. D., Mele E., Molina J., Verzeletti G., Pinto A. V. (2001). "Base isolation for historic buildings: Evaluation of seismic performance through experimental investigation", *Earthquake engineering and structural dynamics,* Issue 30, page 1125-1145.
71. Maskey, P.N., Datta, T.K. (2004). "Risk consistent response spectrum and hazard curve for a typical location of Kathmandu valley." *13th world conference on earthquake engineering, Vancouver, B.C., Canada*, Aug.1-6, **3124.**
72. Mayorca P., and Meguro K. (2004). "Proposal of an efficient technique for retrofitting unreinforced masonry dwellings", *13th World Conference in Earthquake Engineering*, Vancouver B.C., Canada, Paper No. 2431.
73. Mcguire, R.K. (1995). "Probabilistic hazard analysis and design earthquakes: Closing the loop." *Bull. Seismol. Soc. Am.*, **85**, (5), 1275-1284.

74. Mcguire, R. K. (2004). "Seismic hazard and risk analysis." *Earthquake Engineering Research Institute, MNO-10*
75. Meguro K. (2005). "Economic And Efficient Method for Strengthening Unreinforced Masonry/Adobe Structures In Developing Countries", *Disaster reduction technology list on implementation strategy*, Kobe-Hyogo.
76. Meli R. and Sergio M. A. (2004). "Implementation of structural earthquake-disaster mitigation programs in developing countries", *Natural Hazard Review, ASCE*.
77. Mishra, H. K. (2004). "Attenuation of ground motion for the region." *Master's thesis, TU, IOE, Pulchowk Campus, Nepal.*
78. Mitroi C. C. and Olarn D. R. (2000). "Mixed steel-brick strengthening system for damaged masonry structures", *12th world conference on Earthquake Engineering*, Auckland, New Zealand, Idex 1124, Vol 10.
79. Mosalam K. M (2004). "Retrofitting of unreinforced masonry walls using glass fiber reinforced polymer laminates", *International conference*, Cairo Egypt 20-22.
80. Molas, G.L., and Yamazaki, F. (1995). "Attenuation of earthquake ground motion in Japan including Deep focus events." *Bull. Seismol. Soc. Am*., **85**, 1343-1358.
81. Molnar, P. (1984), "Structures and tectonics of Himalaya: Constraints and implication of geophysical data." *Ann. Rev. Earth Planet Sci*. **I2**, 489-518.
82. Naeem S., Ali Q., Javed M., Hussain Z., Naseer A., Ali, S.M., Ahmed I. and M. Ashraf (2005). "A Summary Report on Muzaffarabad Earthquake", Pakistan, Earthquake Engineering Centre at Department of Civil Engineering, N-W.F.P. University of Engineering and Technology, Peshawar, Pakistan.
83. Nath, S.K., Vyas, M., Pal, I., and Sengupta P. (2005). "A seismic hazard scenario in the Sikkim Himalaya from seismotectonics, spectral amplification, source parameterization, and spectral attenuation equations using strong motion seismometry." *Journal of Geophysical Research*, **110.**
84. Osaki Y. (1994). "Introductory book for spectral analysis of earthquakes motion", *Kajima Institute of Publishing Co. Ltd.* in Japanese (大崎順彦　1994. 新・地震動のスペクトル解析入門　鹿島出版会)
85. Parajuli, H. R. (2002). "Seismic risk assessment of a reinforced concrete framed building." *Master's thesis,* TU, IOE, Pulchowk Campus, Nepal.

86. Parajuli, H., Kiyono, J., Scawthorn, C. (2007). "Probabilistic seismic hazard assessment of Kathmandu", *Proceedings of twentieth KKCNN symposium on civil engineering*, Jeju, Korea
87. Papantonopoulos, P., Psycharis, I.N., Papantonopoulos, D.Y., Lemos, J.V., Mouzakis, H.P., (2002). "Numerical prediction of the earthquake response of classical columns using the distinct element method", *Earthquake engineering and structural dynamics*, (31), page 1699-1717.
88. Paquette J., Bruneau M., Filiatrault A. (2001). "Out of plane seismic evaluation and retrofit of turn of the century North American masonry walls", *Journal of structural engineering*, *ASCE* Vol. 127, no. 5.
89. Paquette J. and Bruneau M. (2003). "Pesudo- dynamic testing of unreinforced masonry building with flexible diaphragm", ASCE, Journal of structural engineering, Vol. 129, no. 6.
90. Portugal, A., Kiyono, J., and Miura, F. (1995). "Seismic risk analysis for the Yamaguchi prefecture." *Annual conference of the institute of social safety science*, (5)
91. Sato, T., Kiyono, J. (1989). "Estimation of seismic intensity of ground motion during the 21 August 1988 earthquake in the Nepal-India border region." *Journal of Natural Disaster Science*, **11**, (2), 21-36
92. Scawthorn C. (1986). "Strengthening of low-strength masonry buildings: Analytical and shaking table results", *Middle and Mediterranean regional conference on earthen and low-strength masonry buildings in seismic areas*.
93. Schacher, T., (2007). "Bhatar construction, Timber reinforced masonry", *Guidebook prepared by Awiss Agency for Development and Cooperation SDC and French Red Cross FRC, in collaboration with Belgian Red Cross Architectural and Development, UN Habitat, NESPAK*.
94. Shahi T. and , Agarwal P. (2000), "Seismic evaluation of earthquake resistant and retrofitting measures of stone masonry houses", *12th world conference on Earthquake Engineering*, Auckland, New Zealand, Index 0110, vol 8.
95. Senthivel, R., Lourenco, P.B. and Vasconcelos, G. (2006), "Analytical modeling of dry stone masonry wall under monotonic and reversed cyclic loading", *Structural Analysis of Historical Constructions*, New Delhi.
96. Shrive N. G. (2006). "The use of fibre reinforced polymers to improve seismic resistance of masonry", *Construction and Building Materials*, Volume 20, Issue 4, Pages 269-277.
97. Sofronie R. A. (2004). "Performances in seismic strengthening of masonry", *13th world conference on Earthquake Engineering*, Vancouver B.C., Canada, Paper No. 182

98. Spence, R., Coburn, A. (1992). "Strengthening buildings of stone masonry to resist earthquakes", *Kluwer Academic Publishers*, Printed in the Netherlands.
99. Spudich, P., Fletcher, J.B., Hellweg, M., Boatwright, J., Sullivan, C., Joyner, W.B., Hanks T.C., Boore, D.M, McGarr, A., Baker, L.M and Lindh, A.G. (1997). "SEA96-A new predictive relation for earthquake ground motions in extensional tectonic regimes." *Seismological Research Letters*, **68**, (1), 190-198.
100. Stepp, J.C. (1972). "Analysis of completeness of the earthquake sample in the Pudet Sound area and its effect on statistical estimates of earthquake hazard." *Proceedings of the first microzonation conference, Seattle, WA*, 897-909.
101. Toki, K., Sato, T., Kiyono, J., and Fujimura, K. (1991). "Seismic risk analysis for the Kinki district based on the historical earthquake and active fault data." *Annual, Disaster Prev., Res. Inst.,* Kyoto Univ., **34** , (B-2).
102. Tomazevic M. (1999). "Earthquake-Resistant Design of Masonry Buildings, series on Innovation in Structures and construction", *editors A.S. Elnashai & P.J. Dowling, Imperial Collage Press*, London Vol. 1.
103. Triantafillou T. C. (1998). "Strengthening of masonry structures using epoxy-bonded FRP laminates", *Journal of Composites for Construction, ASCE*, Vol 2, No 2.
104. Triantafillou T. C. (2001). "Seismic retrofitting of structures with fibre-reinforced polymers", *Progress in Structural Engineering and Materials*, Vol. 3, Issue 1, Pages: 57-65.
105. Tzamtzis, A.D. and Nath B., (1992). "Application of three-dimensional interface element to non -linear static and dynamic finite element analysis of discontinuous systems", PD-Vol. 47-1, *Engineering System Design and Analysis*, (1), ASME.
106. Tzamtzis, A.D., Asteris P.G., (2002). "A 3D model for non-linear microscopic FE analysis of masonry structures", *Proceeding of the sixth international masonry conference*, London, (9), pp.493-497.
107. Tzamtzis, A.D., Asteris P.G., (2004). "FE analysis of complex discontinues and jointed structural systems", *Electronic Journal of Structural Engineering*, (1).
108. USGS:*http://pubs.usgs.gov/gip/dynamic/understanding.html*,*http://earthquake.usgs.gov/regional/world/world_deaths.php*
109. Velazquez-Dimas J. I. and Ehsani M. R. (2000). "Modeling out of plane behavior of urm walls retrofitted with fiber components", *Journal of Composites for construction, ASCE*.

110. Verma R., Albiter A., Miranda S. (1981). "Seismic capacity evaluation and retrofitting of adobe constructions" *12th world conference on Earthquake Engineering, Auckland, New Zealand*, 2000 Index , vol 1.

111. Verma R. and Miranda S. (2004). "Experimental study of retrofitting techniques for adobe walls', *13th World Conference in Earthquake Engineering*, Vancouver B.C., Canada, Paper No. 2861.

112. Wells, D.L. and Copersmith, K.J. (1994). "New empirical relationships among magnitude, rupture length, rupture width, rupture area, and surface displacement." *Bull. Seismol. Soc. Am*., **84**, (4), 974-1002.

113. Wesnousky, S.G., Scholz, C.H., Shimazaki, K., and Mastsuda, T. (1983). "Earthquake frequency distribution and mechanics of faulting", *Journal of Geophysics Res*.,**88**, (B11), 9331-9340.

114. Weng D., Lu X., Zhou C., Kubo T., Li K. (2004), "Experimental study on seismic retrofitting of masonry walls using GFRP", *13th world conference on Earthquake Engineering*, Vancouver B.C., Canada, Paper No. 1981.

115. Woo, W. (1996). "Kernel estimation methods for seismic hazard area source modeling." *Bull. Seismol. Soc. Am*., **86 (2)**, 353-362

116. Yamin L. E, Phillips C. A., Reyes J. C and Ruiz D. M. (2004). "Seismic behavior and rehabilitation alternatives for adobe and rammed earth buildings", *13th World Conference in Earthquake Engineering*, Vancouver B.C., Canada, Paper No. 2942.

117. Yoshimura K. and Kuroki M. (2001). "Damage of masonry buildings caused by El Salvador earthquake of January 13, 2001", *Journal of Natural Disaster Science*, Vol. 23, Nov. 2, page 53-63.

118. Youngs, R.R, Chiou, S.J, Silva, W.J and Humhrey, J.R. (1997). "Strong ground motion attenuation relationships for subduction zone earthquakes." *Seismological Research Letters*, **68** (1)**,** 58-73.

119. Zienkiewicz, O.C., Best, B., Dullage, C., Stagg, K.G. (1970). "Analysis of non linear problems in rock mechanics with particular reference to jointed rock systems"*, Proceedings of 2nd International conference,* Society of Rock Mechanics, pp501-509, Belgrade, (3).